# ETHIOPIAN MANGOES, THE RESOURCEFUL RAW MATERIAL FOR THE MANGO SEED KERNEL OIL PRODUCTION

Mustefa Kemal[1], Anuradha Jabasingh S[1,*], Abubeker Yimam[1]
[1]Process Engineering Division, School of Chemical and Bio Engineering,
Addis Ababa Institute of Technology, Addis Ababa University, Ethiopia
*Corresponding author's E-mail: anu3480@gmail.com

## ABSTRACT

*Oil extracted from the mango seed kernel, one of the byproducts of juice processing industry, have application in the cosmetics industry, due to its antioxidant, skin whitening and anti-wrinkle properties. The main aim of this research is to determine the optimum operating condition for the extraction of oil from the mango seed kernel. A general factorial design was applied to investigate the effect of process variables on the oil yield. The optimum operating conditions for the extraction were a particle size range of 0.25-0.5 mm and extraction time of 6 h. At these conditions, the maximum oil yield with hexane as solvent was 84.81% and the minimum yield was 57.41%. The maximum and minimum yield for the same operating conditions, when petroleum ether was used as solvent was found 83.33% and 61.48%, respectively, while ethanol as solvent results a maximum yield of 57.04% and minimum yield of 23.70%. The physicochemical properties of the mango oil were determined and the results guarantee the use of mango kernel oil for cosmetic application.*

**Keywords:** Extraction, Hexane, Mango seed kernel, Oil, Petroleum Ether, Yield.

## INTRODUCTION

Natural oils are used in a wide variety of cosmetic products including personal care as well as makeover products. They consist of ethereal salts of glycerin with a large number of organic acids such as citric acid, oleic acid, and palmitic acid. They are excellent emollients and are derived from a variety of plants [1]. Food and Drug Administration (FDA) defines cosmetics as intended to be applied to the human body for cleansing, beautifying, promoting attractiveness, or altering the appearance without affecting the body's structure or functions [2]. The total value of the cosmetics market in Ethiopia reached $25milion up to June 2012, according to figures from the country's Ministry of Trade and Industry, with the average growth rate over the last three years at 10%. Imported products account for around 90% of the market, with the remaining 10% sourced from domestic manufacturers. Mango seed kernel oil has been used as an ingredient in soaps, shampoos and lotions as it is a good source of phenolic compounds [3]. Presence of high unsaponifiable matter guarantees the use of mango kernel oil in cosmetics industry [4]. It also has a protective effect against the harmful UV radiations [5].

The high content of stearic acid allows its application as a preservative. Hence, it has wide applications, especially in the stearin manufacturing, confectionery and soap industry [6]. To start with the study, the world's top ten mango producers with their main varieties were identified and provided in Table.1. In the context of Ethiopia, mango is produced in the southern and western parts of the country. The total production of mango in Ethiopia is 72,187 tons in 2013/14 [8]. This accounts for 7219 tons of mango seed kernel, annually. The production of mango at Arba Minch and Zuria Woreda is 126,800 qt with total area coverage of 634 hectares. Mango farmsteads in Asossa produce an average of 13,500 mangoes per farmstead [9].

**Table 1.** World's top ten mango producers, 2015 [7]

| No. | Country | Variety | Production (tons/year) |
|---|---|---|---|
| 1 | India | Alphonso, Badami, Chaunsa, Dasheri, Kesar, Jauhari, Lucknowi, Fazli, Totapuri, Banganapalli, Sindhuri, Kalmi, Neelam, Langra | 16,337,400 |
| 2 | China | Zillate, Mallika, Deshehari,Edward, Saigon, R2E2, Spooner, Bambaroo | 4,351,593 |
| 3 | Thailand | Brahm Kai Meu | 2,550,600 |
| 4 | Pakistan | Anwar Ratol, Langra , Sindhri, Chaunsa, Fajri, Samar Bahist, Dasehri, Saroli | 1784,300 |
| 5 | Mexico | Ataulfo, Haden, Tommy Atkins, Kent, Keitt | 1,632,650 |
| 6 | Indonesia | Arumanis, Gedong | 1,313,540 |
| 7 | Brazil | Espada, Rosa, Bourbon, Uba | 1,188,910 |
| 8 | Bangladesh | Gopalbhog, Himsagar, Khirsapat, Langra, Fasli, Ashwina, Amropali | 1,047,850 |
| 9 | Philippine | Champagne mangoes | 823,576 |
| 10 | Nigeria | Kerosene, Sherri | 790,200 |

The Ethiopian government has a plan to expand mango production by distributing high yielding varieties for small scale farmers, especially, in the Southern region and Oromia region, by grafting mangos of known and high yielding varieties. In Ethiopia, there are many large and small scale mango juices processing industry [10]. During mango processing, peel and kernel constitute about 17-22% of the fruit. The production of oil from the mango seed kernel could be an efficient method of utilizing the waste seed kernels. The operating conditions, including the particle size, extraction time, and solvent type, solid to solvent ratio, temperature and moisture content were proved to have an effect on the oil yield. This research aims to find optimum operating conditions to maximize the oil yield for the production of oil from the mango seed kernel.

## MATERIALS AND METHODS

### Materials

Asossa mango varieties were purchased from Kenuma and Akea juice processing house, Addis Ababa. Hexane, Petroleum ether, Ethanol, Sodium hydroxide, potassium hydroxide, hydrochloric acid, Folin Ciocalteu reagent, Gallic acid, Sodium carbonate, acetone, and phenolphthalein were procured from Merck, Germany.

### Deseeding and processing

The mangoes were peeled and deseeded. The seeds were sun dried for five days. The hard cover of the seed was decorticated manually to obtain the seed kernel. The seed kernel was dried in the oven at 50°C for 18 h. The dried mango seed kernel was milled in centrifugal miller with a sieve size of 4 mm. Then the sample was sieved using a vibrating shaker for 15 min.

**Moisture content of the kernel**

Seven samples of the kernel were randomly weighed and dried in an oven at 105°C and the weight was measured every 2 h. The procedure was repeated until a constant weight was obtained. The percentage moisture content of the kernel was calculated using the following formula.

$$Moisture\ content\ (\%) = \frac{w1 - w2}{w1}\ \mathrm{x}\ 100 \qquad (1)$$

w1 and w2 are the weight of the sample before drying and after drying respectively.

**Mango oil extraction**

The experimental work was conducted using soxhlet extractor in triplicate with three different solvents: hexane, petroleum ether and ethanol. 75 g mango seed kernel at three different particle sizes (3-1.5mm, 1.5-0.5mm and 0.5-0.25mm) were extracted using Soxhlet extracter with 300 mL solvents with varying treatment times (2 h, 4 h and 6 h).

The resulting extracts, were purified by simple distillation. The obtained fractions were weighed and physicochemical properties determined. Mango seed kernel had an oil content of 12%. Hence this was used for the calculation of yield. The percentage yield was calculated as follows

$$\%\ Oil\ yield = \frac{(Mass\ of\ oil)x100}{(0.12 \times Mass\ of\ the\ sample)} \qquad (2)$$

$$\%\ Extraction\ yield = \frac{(Mass\ of\ oil)x100}{(Mass\ of\ the\ sample)} \qquad (3)$$

**Physical and chemical characterization**

Physical properties including the moisture content, volatile matter, specific gravity, viscosity, pH value, refractive index and chemical properties including the saponification value, un saponifiable matter, iodine value, acid value, peroxide value and total phenolic content were determined.

***Moisture and volatile matter of oil***

5 g of oil was weighed and dried in an oven at 105 °C for 1 h. The dish was removed from the oven, cooled in a dissector and weighed. The process was repeated until a constant weight was observed. The moisture and volatile matter was calculated using the following formula.

$$Moisture\ and\ volatile\ matter = \frac{W_1}{W}x100 \qquad (4)$$

Where w1 and w, are the reduction in the weight of the dried sample and the initial weight of the sample in g.

***Specific gravity***

The density of oil was determined using a specific gravity bottle. A clean and dry density bottle of 25 mL capacity at 30°C was weighed, filled with water and extracted oil, separately and weighed again. The specific gravity was calculated using the following formula.

$$Specific\ gravity\ at\ 30°\mathrm{C} = \frac{(A - B)}{(C - B)} \qquad (5)$$

Where A, B and C are the weights of the specific gravity bottle with oil, empty specific gravity bottle and empty specific gravity bottle with water at 30°C.

***Kinematic viscosity***

Kinematic viscosity of the oil was measured using Vibro viscometer. 35 mL oil sample was heated to 30°C and fed to the sample holder. The sensor of the viscometer was immersed into the oil, which measures the dynamic viscosity of oil. The kinematic viscosity is calculated using

$$\nu = \frac{\mu}{\rho} \qquad (6)$$

Where, μ and ρ are the dynamic viscosity and density of oil respectively.

***Determination of pH***

2 g of the oil sample was added to 25 mL beaker and 13 mL of hot distilled water was added to the sample in the beaker and stirred slowly. It was cooled in a cold water bath to 25°C. The pH electrode was standardized with a buffer solution and immersed into the sample [11].

***Saponification value***

2 g of sample was added to 250 mL flask. 25 mL of alcoholic potassium hydroxide solution was added and the flask was connected to reflux condenser, kept on the water bath and boiled gently for 1 h. After cooling, the condenser was washed with 10 mL of hot ethyl alcohol. Few drops of phenolphthalein indictor were added and excess potassium hydroxide was titrated with 0.5 N HCl until the disappearance of the pink color [12]. The saponification value, expressed as the number of milligrams of KOH required to saponify 1 g of fat is calculated using

$$Saponification\ value = \frac{56.1(B-S)N}{W} \qquad (7)$$

Where, B, S, N, W are the volume of standard hydrochloric acid required for the blank, volume of standard hydrochloric acid required for the sample in mL, normality of hydrochloric acid and weight of oil taken initially in g respectively.

***Unsaponifiable matter***

5 g of the sample was added to 250 mL conical flask. 50 mL of alcoholic potassium hydroxide solution was added and the content was boiled under a reflux condenser for 1 h. The condenser was washed with 10 mL of ethyl alcohol. The saponified mixture was transferred to separating funnel and allowed to cool until 25°C.

After the addition of 50 mL of petroleum ether, the separating funnel was shaken vigorously, to allow the layers to separate. The lower soap layer was transferred into another separating funnel and the extraction was repeated three times using 50 mL portion of petroleum ether. To insure the ether extract was free of alkali, the combined ether extract was washed three times with 50 mL aqueous alcohol followed by 25 mL distilled water. The ether solution was transferred to 250 Ml beaker and the ether was evaporated. When all the ether is evaporated, 3 mL of acetone was added, followed by drying at 100°C for 30 min [12]. The residue was dissolved in 50 mL of warm ethanol and titrated with 0.02 N sodium hydroxide. The amount of unsaponifiable matter was determined as follows,

$$Unsaponifiable\ matter = \frac{100(A-B)}{W} \qquad (8)$$

$$where, \quad B = 0.282VN$$

Where, A, B, N,V, W are the weight of the residue, weight of free fatty acids in the extract as oleic acid in g, normality of standard sodium hydroxide solution, volume of standard sodium hydroxide solution in mL and initial weight of the sample in g.

***Acid value***

2.510 g of the sample was added to 250 mL conical flask and 50 mL of hot ethyl alcohol was added. A few drops of phenolphthalein was added to the mixture and boiled for 5 min and titrated with 0.5 N sodium hydroxide solutions.

$$Acid\ value = \frac{56.1VN}{W} \qquad (9)$$

Where, V, N, W are the volume of standard sodium hydroxide solution in mL, Normality of sodium hydroxide solution, and initial weight of sample in g. The free fatty acid can be calculated as follows

$$Percent\ free\ fatty\ acid\ = \frac{AV}{1.99} \qquad (10)$$

***Total phenolic content***

The phenolic compounds concentration in mango seed kernel oil ethanoic, hexanoic, and petroleum ether extracts was determined using Folin Ciocalteu method [13]. 0.4 mL of mango kernel oil were mixed with 2 mL of 10% Folin ciocalteu reagent and 1.6 mL of 7.5% $Na_2CO_3$ and left in a dark room for 30 min and measured spectrophotometrically at 965 nm. A blank sample consisting of water and reagent was used as a reference. The results were expressed as mg of galic acid equivalents per g the sample (mg GAE/g sample) by reference to galic acid calibration curve. Total phenolic content (TPC) expressed as mg of galic acid equivalent per g of sample is calculated using Equation 11.

$$TPC = \frac{CV}{M} \qquad (11)$$

Where, C, V and M are the concentration of the oil sample in garlic acid equivalent, volume of oil sample and mass of the sample respectively.

***Peroxide value, iodine value and refractive index***

The Peroxide value, iodine value and refractive index value of the sample was determined at JIJE Analytical testing service laboratory [12].

**Experimental design**

Regression model were established for the dependent variables to fit the experimental data for the response using Design expert 7.0.0 software.

**Table 2. Factors and corresponding ranges and levels**

| Factors | Levels | | |
|---|---|---|---|
| | Low (-1) | Medium (0) | High (+1) |
| A:Particle size(mm) | 0.25-0.5 | 0.5-1.5 | 1.5-3.0 |
| B:Time (h) | 2 | 4 | 6 |
| C: Solvent | Hexane | Ethanol | Petroleum ether |

Factorial design is used to test the effect of each factor. (Table 2) In the factorial experiments all the possible combinations of the factor levels were tested [14]. The analysis has performed by Design Expert software using the general factorial design method [15].

## RESULTS AND DISCUSSION

**Moisture content of the seed kernel**

The moisture content of the seed kernel with 11.6, 16.2, 10.5, 10.4, 9.5, 4.9, and 3.5 g was 46.6, 46.9, 49.0, 47.6, 52.6, 51.0 and 51.4 %, respectively. The mean plus the standard deviation of the seven samples gives 49.3% ± 2.47.

**Yield of Extraction**

The oil extraction was carried out in a Soxhlet apparatus using three different solvents (Fig.1). The oil yield and extraction yield were calculated and summarized in Table 3.

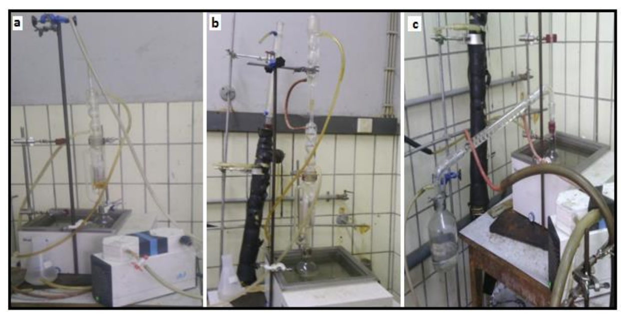


Fig.1. Apparatus for Extraction (a) Hexane and Ethanol (b) Petroleum ether (c) Apparatus for oil separation and purification

Maximum percentage oil yield was 84.81±1.7 (equivalent to 10.18±0.2 percentage extraction yield) for the particle size range of 0.25-0.5 mm, extraction time of 6 h and hexane as the solvent. Minimum percentage oil yield was 18.89±1.11 (equivalent to 2.27±0.13 percentage extraction yield) for the particle size range of 0.5-1.5 mm, extraction time 2 h and ethanol as solvent. Previous reports presented an extraction yield of 8.46±0.1% (equivalent to 70.5±0.83 % oil yield)

[16] with hexane as a solvent for an extraction time of 6 h. Saipraha and Goswami-Giri, 2011 [17] reported an yield of 10.2% (85% oil yield) using hexane as solvent and with extraction time of 5 h.

**Effect of process parameters on percentage oil yield**

The effect of particle size on oil yield for hexane as a solvent is shown in Fig. 2a. The particle size plays a great role on yield of mango seed kernel oil.The percentage oil yield was inversely related to the particle size i.e smaller particle size gave a high yield while larger particle size resulted in a lower yield. For 2 h, 4 h and 6 h, as a particle size decreases, the oil yield increases from 42.22% to 57.41%, 45.57% to 82.22% and 64.07% to 84.81% for the particle sizes in the range 0.25-0.50, 0.50-1.50, 1.50-3.0 respectively [18]. However, when the particle size is too small or very fine the oil yield decreases even though, the surface area of contact is increased. The reason may be due to agglomeration of fine particle which reduces the contact surface area. Effect of extraction time on percentage oil yield is shown in Fig 2b. The percentage oil yield was directly related to extraction time. The yield increased as extraction time increased. A similar kind of trend was reported earlier [19]. The oil yield increased by 24.81% as the extraction time increased from 2 h to 4 h and it increased by 2.59%, as the time increased from 4 h to 6 h. However, for larger particle size, the yield was lower at the beginning of the extraction and increased gradually as the extraction time increased. The yield increased by 3.35% as the time increased from 2 h to 4 h and by 18.50% as the extraction time increased from 4 h to 6 h. Maximum oil yield is obtained at lower particle size. And the optimum extraction time is 4 h, since 97% of the maximum yield was obtained at this time. The effect of solvent type on percentage oil yield is shown in the Fig. 2c. The maximum oil yield was obtained when hexane is used as a solvent. However, for larger particle size, the yield was lower at the beginning of the extraction and increased gradually as the extraction time increased. The yield increased by 3.35% as the time increased from 2 h to 4 h and by 18.50% as the extraction time increased from 4 h to 6 h. Maximum oil yield is obtained at lower particle size. And the optimum extraction time is 4 h, since 97% of the maximum yield was obtained at this time. The effect of solvent type on percentage oil yield is shown in the Fig. 2c. The maximum oil yield was obtained when hexane is used as a solvent.

The maximum oil yield was 84.81% at extraction time of 6 h and the minimum yield was 57.41% at extraction time. The maximum and minimum yield for the same operating conditions, when petroleum ether was used as solvent was found 83.33% and 61.48%, respectively, while ethanol as solvent resulted in a maximum yield of 57.04% and minimum yield of 23.70%. According to the result obtained in this study the maximum percentage oil yield of petroleum ether (83.33%) was almost equal to that of hexane (84.81%). The boiling point range of petroleum ether (40°C – 60°C) is lower than that of hexane (65°C -69°C) so as to avoid thermal degradation of bioactive components. It is preferable to use petroleum ether than hexane. In comparison to hexane and petroleum ether, the yield obtained from ethanol was the lowest. Hexane and petroleum ether are non-polar organic solvents that have high capacity to dissolve non polar compounds while ethanol can extract non-oil components due to the presence of OH bond (polar). However, currently both hexane and petroleum ether have been identified as air pollutants and can react with other pollutants to produce ozone and photochemical oxidants [20,21].

Table 3. Oil yield and extraction yield of Mango seed kernel oil using full factorial design

| Run | Factors | | | Oil yield (%) | | | | Extraction yield (%) |
|---|---|---|---|---|---|---|---|---|
| | A (mm) | B (h) | C (type) | Replicate 1 | Replicate 2 | Replicate 3 | Mean±SD | |
| 1 | 0.25-0.5 | 2 | Hexane | 57.78 | 60.0 | 54.44 | 57.41±2.8 | 6.89±0.34 |
| 2 | 0.5-1.5 | 2 | Hexane | 43.33 | 45.56 | 44.44 | 44.44±1.1 | 5.33± 0.13 |
| 3 | 1.5-3 | 2 | Hexane | 42.22 | 40.0 | 44.44 | 42.22±2.2 | 5.07±0.27 |
| 4 | 0.25-0.5 | 4 | Hexane | 82.22 | 83.33 | 81.11 | 82.22±1.1 | 9.87±0.13 |
| 5 | 0.5-1.5 | 4 | Hexane | 58.89 | 57.78 | 58.89 | 58.52±0.6 | 7.02±0.08 |
| 6 | 1.5-3 | 4 | Hexane | 45.56 | 43.33 | 5.73 | 45.57±2.2 | 5.47±0.27 |
| 7 | 0.25-0.5 | 6 | Hexane | 84.44 | 86.67 | 83.33 | 84.81±1.7 | 10.18±0.2 |
| 8 | 0.5-1.5 | 6 | Hexane | 68.89 | 70.0 | 71.11 | 70.0±1.11 | 8.4±0.13 |
| 9 | 1.5-3 | 6 | Hexane | 64.44 | 64.44 | 63.33 | 64.07±0.6 | 7.69±0.08 |
| 10 | 0.25-0.5 | 2 | Ethanol | 23.33 | 22.22 | 25.56 | 23.70±1.7 | 2.84±0.20 |
| 11 | 0.5-1.5 | 2 | Ethanol | 21.11 | 20.0 | 20.0 | 20.37±0.6 | 2.44±0.08 |
| 12 | 1.5-3 | 2 | Ethanol | 17.78 | 20.0 | 18.89 | 18.89±1.1 | 2.27±0.13 |
| 13 | 0.25-0.5 | 4 | Ethanol | 48.89 | 47.78 | 50.0 | 48.89±1.1 | 5.87±0.13 |
| 14 | 0.5-1.5 | 4 | Ethanol | 40.0 | 42.22 | 41.11 | 41.11±1.1 | 4.93±0.13 |
| 15 | 1.5-3 | 4 | Ethanol | 30.0 | 30.0 | 31.11 | 30.37±0.6 | 3.64±0.08 |
| 16 | 0.25-0.5 | 6 | Ethanol | 56.67 | 55.57 | 58.89 | 57.04±1.6 | 6.84±0.20 |
| 17 | 0.5-1.5 | 6 | Ethanol | 46.67 | 46.67 | 47.78 | 47.04±0.6 | 5.64±0.08 |
| 18 | 1.5-3 | 6 | Ethanol | 43.33 | 44.44 | 47.78 | 45.18±2.3 | 5.42±0.28 |
| 19 | 0.25-0.5 | 2 | Petroleum ether | 62.22 | 61.11 | 61.11 | 61.48±0.6 | 7.38±0.03 |
| 20 | 0.5-1.5 | 2 | Petroleum ether | 38.89 | 40.0 | 36.67 | 38.52±1.7 | 4.62±0.20 |
| 21 | 1.5-3 | 2 | Petroleum ether | 40.0 | 40.0 | 40.0 | 40.0±0 | 4.8±0 |
| 22 | 0.25-0.5 | 4 | Petroleum ether | 73.33 | 75.56 | 73.33 | 74.07±1.2 | 8.89±0.15 |
| 23 | 0.5-1.5 | 4 | Petroleum ether | 56.61 | 56.67 | 57.78 | 57.02±0.6 | 6.84±0.08 |
| 24 | 1.5-3 | 4 | Petroleum ether | 44.44 | 42.22 | 45.57 | 44.08±1.7 | 5.29±0.20 |
| 25 | 0.25-0.5 | 6 | Petroleum ether | 83.33 | 82.22 | 84.44 | 83.33±1.1 | 10.0±0.13 |
| 26 | 0.5-1.5 | 6 | Petroleum ether | 68.89 | 71.11 | 67.78 | 69.26±1.7 | 8.31±0.20 |
| 27 | 1.5-3 | 6 | Petroleum ether | 61.11 | 60.0 | 63.33 | 61.48±1.7 | 7.38±0.20 |

Therefore, even if the yield obtained from ethanol was the lowest, from the health and environmental point of view, it is suggested for this extraction process. Table 4 shows the analysis of variance (ANOVA) result. The model F- value of 35.57 implies the model is significant. Value of probe>F less than 0.05 indicates the terms are significant. In this case, A-particle size, B-extraction time, C-solvent type and $A^2$-square of particle size are significant model terms. Values greater than 0.1000 indicates the model terms are not significant. Hence AB-interaction between particle size and time, AC-interaction between particle size and solvent type, BC-interaction between time and solvent type and $B^2$-the square of time are not significant model terms [22]. The model terms A, B, C and $A^2$ were significant model terms, whereas interaction model terms AB, AC, BC and $B^2$ are not significant model terms. Often we think about removing non-significant model terms or factors from a model, but in this case removing AB, AC and BC will result in a model that is not hierarchical. The hierarchy principle indicates that if a model contains a higher-order term, it should contain all the lower-order terms that compose it. Hierarchy promotes a type of internal consistency in a model, and many statistical model builders rigorously follow the principle [23, 24]. The regression equations in terms of actual factors are given below,

**Solvent type: Hexane**

$$Yield\ (\%) = +52.750 - 35.369A + 10.813B - 0.623AB + 9.552A^2 \quad (12)$$

**Solvent type: Ethanol**

$$Yield\ (\%) = +17.619 - 29.396A + 11.77B - 0.623AB + 9.552A^2 \quad (13)$$

**Solvent type: Petroleum ether**

$$Yield\ (\%) = +50.822 - 35.409A + 10.751B - 0.623AB + 9.552A^2 \quad (14)$$

Fig. 3 shows the relation between the actual value of the experiment and value predicted by the model equation developed by the design expert software 7.0.0

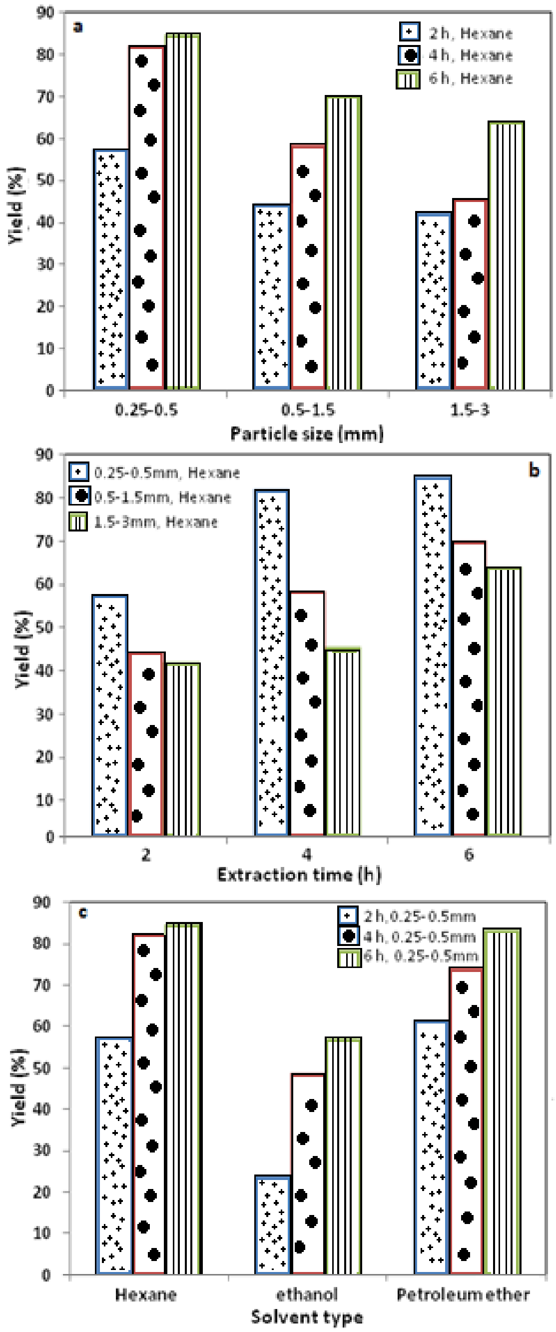


Fig.2. Effect of (a) Particle size, (b) Extraction time, (c) Solvent type on the Mango seed kernel oil yield (%)

Table 4. Analysis of variance (ANOVA)

| Source | Sum of squares | Degree of freedom | Mean square | F value | P value Prob > F |
|---|---|---|---|---|---|
| Model | 8362.2 | 11 | 760.2 | 35.6 | < 0.0001 |
| A | 16022.1 | 1 | 1602.1 | 77.1 | < 0.0001 |
| B | 3072.9 | 1 | 3072.9 | 147.8 | < 0.0001 |
| C | 3185.4 | 2 | 1592.6 | 76.6 | < 0.0001 |
| AB | 16.91 | 1 | 16.91 | 0.81 | 0.38 |
| AC | 130.4 | 2 | 65.19 | 3.14 | 0.0728 |
| BC | 15.68 | 2 | 7.84 | 0.38 | 0.6921 |
| A^2 | 316.9 | 1 | 316.85 | 15.24 | 0.0014 |
| B^2 | 21.9 | 1 | 21.94 | 1.06 | 0.3205 |
| Residual | 311.8 | 15 | 20.94 | | |
| Cor Total | 8673.9 | 26 | | | |

**Parameter optimization**

Using optimization function in design expert software 7.0.0, it was predicted that at the following operating conditions of 0.39 mm particle size, 5.67 h extraction time and hexane as solvent, a maximum oil yield of 85.01% could be obtained, which agreed well with the experimental value 84.81%. A minimum yield of 16.99 % was predicated at particle size of 1.4 mm, 2.22 h and ethanol as solvent. This was also in agreement with the experimental value (Fig. 3).

**Mango seed kernel oil characterization**

Fig.4 shows the production of mango seed kernel oil. Using the process parameters that gave a maximum oil yield, the particle size range 0.25-0.5mm, extraction time of 6h and hexane as solvent, the oil was extracted and characterized. The phenolic content was determined by using all the solvents. The moisture and volatile matter of oil constituted about 2.2%. Specific gravity was found to be 0.905. The kinematic viscosity of oil was $5.4\times10^{-5}m^2/s$. The pH value of oil was found to be 5.9±0.36. pH was in the range of 5.6 to 6.5, which is slightly neutral. In preparation of skin and hair care materials, the preferable pHvalue is in the range of 3.5- 6.5, suggesting its application in the cosmetic industry. Refracto meter was used to determine the refractive index of the kernel oil and AOAC official method 921.08 was implemented. A refractive index of 1.456 at a temperature of 40°C was obtained. Refractive index indicates the purity of oil. The lower the refractive index is the higher the quality of oil. Saponification value of mango seed kernel oil was 184.66 mg KOH/g of oil. High saponification value implies greater a proportion of fatty acids of low molecular weight. The values obtained for saponification value of mango seed kernel oil was favorably comparable with the saponification value of olive oil (185 - 196) which is a well-known vegetable oil in cosmetics industry. High saponification value of the mango kernel oil suggests the use of the oil in the production of liquid soap, shampoos and lather shaving creams. The oil has 3.85% of unsaponifiable matter. The result obtained was in agreement to the reported values: 3.45% and 2.78% respectively [17,25].

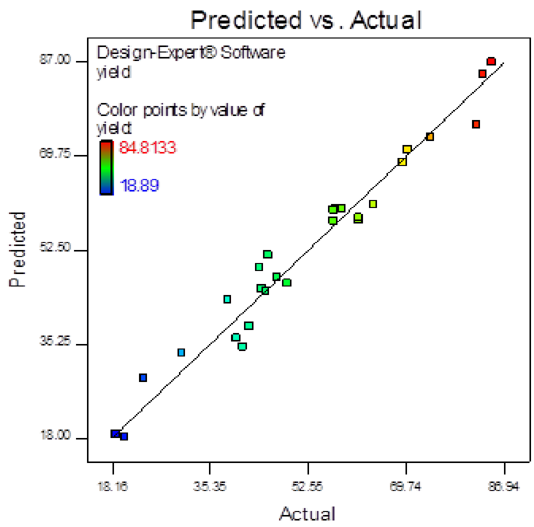


Fig. 3. Actual versus predicted values of Mango seed kernel oil.

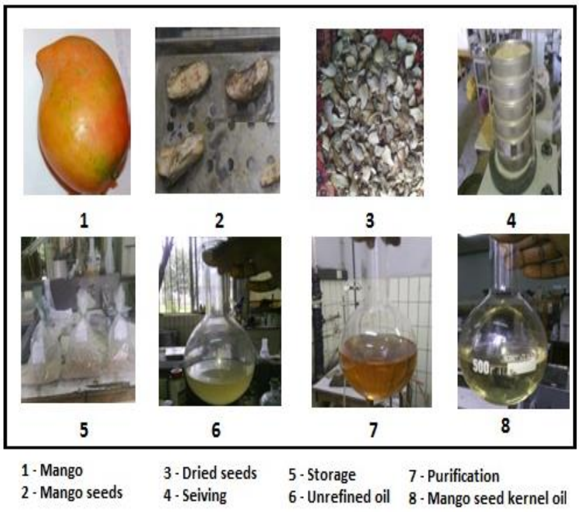


Fig. 4. Production of mango seed kernel oil from mango seeds

Unsaponifiable matters are substances soluble in oil which fails to form soap when blended with sodium hydroxide. The presence of high unsaponifiable matter, 3.85 guarantees the use of mango seed kernel oil in cosmetics industry.

The average acid value of mango seed kernel oil is 2.38±0.33 which is relatively smaller. The low acidity of oil is an indication of oil which is free from hydrolytic rancidity and enables the direct use of such oil without further neutralization [4].

The low free fatty acid content, 1.18 was indicative of low enzymatic hydrolysis. This could be an advantageous that mango seed kernel oil cannot develop flavor during storage. Iodine value of mango seed kernel fat was 40.44g/100g of oil. The result indicated as mango kernel oil, low iodine value so it has high resistance to oxidation and longer shelf life. The oil could be classified as a non-drying oil since its iodine value is lower than 100. Certainly, the oil can also be used extensively as lubricants and hydraulic brake fluids. Peroxide value is one of the most widely used test for oxidative rancidity in oils. It is a measure of the concentration of peroxides and hydroperoxides formed in the initial stages of lipid oxidation. Generally, the peroxide value should be less than 10 mg/g oil in the fresh oils. Peroxide value of mango seed kernel fat was 2.92 meq peroxide oxygen/kg. Oils with high peroxide values are unstable and easily become rancid [26]. Peroxide values were good indices for the stability of the oil. So mango seed oil had a high quality due to the low level of peroxide value. Total phenolic content was found to be 83.2 mg/g, 115.8 mg/g and 79.6 mg/g for hexane, ethanol and petroleum ether extracts respectively. A total phenolic content of 98.7mg/g has been reported earlier [16]. A total phenolic content of 118.1mg/g has been reported earlier [27]. The oil extracted with ethanol resulted in high phenolic content followed by hexane and petroleum ether. The potential use of phenolic compounds for the development of new skin care cosmetics has been emphasized. Phenolic compounds can be used as skin whitening, sunscreen and anti-wrinkle agents [28]. In addition, phenolic compounds are the main component responsible for antioxidant activity [29]. This is mainly due to their redox property which can play an important role in absorbing and neutralizing free radicals. So the presence of high phenolic content in mango seed kernel implies that high free radical scavenging activity. Higher un saponifiable matter gives the Ethiopian mango (Assosa variety) higher opportunity to be used in cosmetics industry.

## CONCLUSIONS

Mango seed kernel oil was extracted from mango seed kernel using soxhlet extractor. A maximum oil yield of 84.81% was obtained for the seed kernel particle size range of 0.25-0.5mm with hexane as solvent for the extraction time of 6 h. A minimum oil yield of 18.87% was obtained for a particle size range of 0.5-1.5mm, with ethanol as solvent for the extraction time of 2 h. Due to the presence of a high percentage of unsaponifiable matter and phenolic content, the oil extracted from mango seed kernel guarantees, its application in the cosmetics industry.

## REFERENCES


[1] Brody, T., "*Nutritional Biochemistry"*, San Diego, CA: Academic Press. 2nd Edn., pp: 761-794, 1994.

[2] Lawis, C., FDA, "*Clearing up cosmetics confusion,Food and drug administration"*, 2011.

[3] Soong, Y.Y., and Barlow,P.J., "*Quantification of gallic acid and ellagic acid from longan (Dimocarpus longan Lour.) seed and mango (Mangifera indica L.) kernel and their effects on antioxidant activity"*, Food Chemistry, 97(3),2006, 524-530.

[4] Arogba, S.S., "*The performance of processed mango (Mangifera indica) kernel flour in a model food system"*, Bioresource Technology, 70, 1999, 277-81.

[5] Fowomala, M.A., "*Some nutrients and antinutrients content of mango (Magnifera indica) seed"*, African journal of food science, 4(8), 2010, 472 – 476.

[6] Kittiphoom, S., "*Utilization of Mango seed"*, International Food Research Journal, 19(4), 2012, 1325-1335.

[7] FAOSTAT., "*Agriculture Statistics"*, Food and Agricultural Organization of the United Nations (FAO), Rome, Italy , 2015.

[8] CSA., "*Agricultural sample survey report on area and production of major crops in 2013/14"*. Statistical Bulletin 532, Addis Ababa, Ethiopia, 2014.

[9] James, S., Rowlands, C., Kamara, J.K., and Haddis, B., "*Analysis of Mango Value Chain from Homosha and Assosa to Addis Ababa"*, September 2008. The Ssemwanga Centre for Agriculture and Food, World Vision Australia, World Vision Ethiopia, 2009.

[10] Aithal, A., and Wangila J., "*Rapid assessment of fruit markets in Ethiopia, based on research in Addis Ababa, Mekele and Awassa: Final report for Improving Productivity and Market Successes (IPMS) for Ethiopian Farmers Project"*, Addis Ababa. World Agroforestry Centre (ICRAF), Nairobi, 2006.

[11] AOAC., "*Association of official analytical chemists. Official method of analysis 960.19. pH value of oil and fat"*, 14th edition, 1995.

[12] AOAC. "*Association of official analytical chemists. Official method 920.160, 920.212, 933.08, Saponification number of oil and fat"*, 17th edition, 2000.

[13] Brand, W.W., Cuvelier, M.E., and Berset, C., "*Use of total phenolic content and a free radical method to evaluate antioxidant activity"*. Food Science and Technology 28, 1995, 25-30.

[14] Anuradha Jabasingh, S., "*Utilization of pretreated coir pith for the optimized bioproduction of cellulase by Aspergillus nidulans"*, International Biodeterioration and Biodegradation, 65 (1), 2011, 1150-1160.

[15] Zivorad, R.L., "*Design of experiments in chemical engineering"*, Wiley- Vch Verlag GmbH and Co. KGaA, 2004.

[16] Kittiphoom, S., and Sutasinee, S., "*Mango seed kernel oil and its physicochemical properties",* International Food Research Journal, 20(3), 2013, 1145-1149.

[17] Saiprabha, M.M., and Goswami-Giri, A.S., "*Composition and Characterization of Refined Oil Compared with Its Crude Oil from Waste Obtained from mango (Mangifera indica)"*, Asian J. Research Chem. 4(9), 2011, 1415-1419.

[18] Ebewele, R.O., Iyayi, A.F., and Hymore, F.K.,"*Considerations of the extraction process and potential technical applications of Nigerian rubber seed oil"*, International Journal of the Physical sciences, 5(6), 2010, 826-831.

[19] Meziane, S., and Hadi, H., "*Kinetics and thermodynamics of oil extraction from olive cake"*, Journal of American Oil Chemist Society, 85, 2008, 391-396.

[20] Wan, P.J., Pakarinen, D.R., Hron, R.J. Sr., Richard, O.L., and Conkerton, E.J., "*Alternative hydrocarbon solvents for cotton seed extraction"*, Journal of American oil chemist society 72, 1995, 653-659.

[21] Hanmoungjai, P., Pyle, L., and Niranjan, K., "*Extraction of rice bran oil using aqueous media"*, Journal of Chemical Technoogy and Biotechnology, 75, 2000, 348-352.

[22] Anuradha Jabasingh, S., and Valli Nachiyar, C., "*Optimization of cellulase production by Aspergillus nidulans: application in the biosoftening of cotton fibers"*, World Journal of Microbiology and Biotechnology, 27(1), 2011a, 85-97.

[23] Montgomery, D.C., "*Design and analysis of experiment"*. John Wiley and Sons, Inc. fifth edition, 2001.

[24] Anuradha Jabasingh, S., and Valli Nachiyar, C., "*Utilization of pretreated bagasse for the sustainable bioproduction of cellulase by Aspergillus nidulans MTCC344 using Response surface methodology"*, Industrial crops and products, 34(3), 2011b, 1564-1571.

[25] Abdalla, E.M., Darwish, S.M., Ayad, E.H.E., and El-Hamahmy, R.M., "*Egyptian mango by-product. Compositional quality of mango seed kernel"*, Food Chemistry, 103, 2007, 1134-1140.

[26] Ojeh, O., "*Effects of refining on the physical and chemical properties of cashew kernel oil"*, Journal of Fats and Oils Technology, 16, 1981, 513-517.

[27] Saranyu, K., and Rakrudee, S., "*Antioxidant and antibacterial activities of selected varieties of thai mango seed extract"*, Pakistan journal of pharmaceutical sciences, 24(1), 2011, 37- 42.

[28] González, S., Fernández-Lorente, M., Gilaberte-Calzada, Y., "*The latest on skin photoprotection"*, Clinics in Dermatology, 26(6), 2008, 614–626.

[29] Dinesh, P., Boghra, V.R., Sharma, R.S., "*Effect of antioxidant principles isolated from mango (Mangifera indica L.) seed kernels on oxidative stability of ghee (butter fat)"*, Journal of Food Science and Technology,37(1), 2000, 6-10.

# HOUSING PROVISIONS AND AFFORDABILITY IN PRIVATE RESIDENTIAL REAL ESTATES IN ADDIS ABABA

Selam Yohannes and Abebe Dinku
School of Civil and Environmental Engineering
Addis Ababa Institute of technology (AAiT), Ethiopia
Corresponding Author's E-mail: seleyoh@gmail.com

## ABSTRACT

*Based on the current rate of growth (3.02%), the population of Ethiopia is expected to double in the next 30 years and cross 210 million by 2060 implying a higher demand in housing needs. It is learnt from the trend of housing development in Addis Ababa that reducing the housing backlogs has been a challenge to the Ethiopian city administration. Following the change of government in 1991, the Addis Ababa City Administration has considered private real estate sector to be one of the actors in housing development.*

*In this article, housing provisions and affordability of private residential real estates in Addis Ababa are evaluated. The study includes: a brief overview of the affordability situation in residential real estates in selected countries, assessing the affordability of the private residential real estates in Addis Ababa and the standards of housing in relation to their costs are analyzed.*

*It is found from the study that the private residential real estates are unaffordable to the average income holders of Addis Ababa residents. In addition, the standards of the selected private residential real estates lack excellence which is not consistent with the prices of the housing units. It is further recommended that a relevant housing policy should be introduced that accommodates low/middle income residents.*

***Keywords**: affordability, housing developments, income and expenditure, real estate*

## INTRODUCTION

According to the recent statistics, Addis Ababa, which is the capital city of Ethiopia, has a population of 4.6 million [1]. The dramatic increase in population implies a higher demand for housing which in turn increases the need for residential real estate and infrastructural development in the City.

Lack of sufficient and affordable housing is one of the major problems in Addis Ababa as well as in other cities and towns across the country. Even though there is an increase in the supply of housing by both the government agencies and private real estate developers, there is still a huge gap between housing needs and supply in Addis Ababa. In 2002, the number of housing units available in Addis Ababa was about 60% of the total requirements and had a backlog of 230,000 housing units [2]. In 2015, the housing needs reached about 2,250,831 units, which equated to a demand of 225,000 new housings per annum [3].

Housing affordability compatible with different income level of the city residents has to be given sufficient attention. Based on the previous experiences, it is recognized that the prices of housing tend to increase as the demand for housing increases. For instance, in 2008, the cheapest private real estate houses for small residential household ranged from 1-3 million birr while 92% of Addis Ababa residents earned a monthly income of less than \$167 a month (3,340 Eth birr) [4]. Subsequently, in 2016, the cheapest price reached a range of 3-6 million birr making it unaffordable for the majority of Addis Ababa residents. This substantial increase in trend is a major concern to many and has created a significant doubt over the affordability of housing for the vast portion of the population.

In this article, the focus is limited to private residential real estate developments regarding housing provisions and affordability situation in Addis Ababa. The affordability of housing is analyzed by using the data obtained from the Central Statistical Agency (CSA) that provides details of income and expenditure of Addis Ababa residents. Among the total of 125 registered real estate developers in Addis Ababa, seven private real estate developers were considered for the study.

## LITERATURE REVIEW

### Housing development in Addis Ababa

During the period between 1975-93, housing provisions in Addis Ababa were mainly restricted to: private real estates, central government effort and kebele low cost houses, co-operatives, individual/ private housing, international NGOs (upgrading and minor redevelopment works), informal/squatter settlers (chereka bet), pavement dwellers and sites and services which are briefly discussed as follows [5].

*Private developers (Real estates):* The private sector involvement had been restricted during the period between 1974 – 1991. This was mainly due to the socialist ideology of the government that was dictated by the 1974 proclamation. A report by the World Bank in 2005 indicated that the private real estate developers cover only 0.6% of the housing stock [6]. Even though, the figure reached to 3.8% between the period 2000-2011, it was still very low when compared with 61% by the government and 35.1% by individuals (cooperative and lease) [7].

*Governmental effort:* Housing provision through condominium is the recent phenomena in Addis Ababa. Condominium is an individual ownership of a unit in an apartment building and the construction technique that is being used is claimed, though debatable, to result in low cost/ affordable housing. The Addis Ababa city government is currently engaged in the construction of condominiums categorized in to different schemes: 10/90, 20/80 and 40/60. During the condominium lottery held in April 2010 by the City administration, a total of 485,000 individuals, over one-tenth of Addis Ababa residents, have applied for condominium units though only 10,700 apartments were made available, which is only 2.2 percent of the demand [8]. This shows that, despite the government continuous effort, there is acute shortage of residential houses in Addis Ababa.

*Co-operatives*: Cooperatives are formed by groups of people who gather as an entity to perform the function of a developer. In the absence of affordable private sector in real estate development, cooperatives are one of the efficient options in filling the gaps. They were also one of the most practiced forms of housing development between 1975 and 1991. Cooperatives were allowed to purchase building materials at subsidized rates and had privileges for preferential loans at an interest rate of 4.5% while the normal interest rate at that time was 10% [3].

*Individual or private efforts to own a house:* Limited proportion of the city dwellers were privileged to own plots of land, upon a payment of facilitation fee only, from the government to build their residential houses. This initiative encouraged many to build a house of their design and promoted private ownerships.

*International NGOs:* Some NGOs have also been engaged in upgrading urban houses and provision of facilities and services. NGOs like Concern, Oxfam and Norwegian Save the Children Fund have been involved in upgrading of slum areas and were working together with communities in poverty mitigation efforts in both rural and urban centers in Ethiopia [3].

*Squatter and informal settlements by the urban poor:* This refers to those rentals or residential housing units built on public owned land without formal legal claims, authorization and permit from the concerned authorities. Extended shelters are the other forms of informal settlements that have been affecting the physical structure of the city.

*Sites and services:* There have been experiences with this kind of housing arrangement in the 1980's. In this scheme, the government provided land and a facility so that the residents can develop their own housing. The success of the scheme was limited because of many implementation weaknesses. This approach was executed in Bole Bulbula area, where it was noticed that the land remained unused for many years resulting wastage of scarce resources.

**Private residential real estates and their affordability**

It is widely recognized that provisions of affordable housing for the increasing population in Addis Ababa has been a challenge for over many years. Given the acute housing shortage, the limited financial capacity of urban dwellers and the scarce governmental resources in fulfilling the public demand posed a challenge to policy makers and professionals in the housing sector. The problem is further aggravated by many factors that include unemployment, increase in living and material costs that require continuous effort by all stakeholders. In addition, it is worth noting that affordability is a relative term which is influenced by the built-up area and site location. Therefore, there is a need for research based innovative approach that identifies the challenges and proposes effective actions.

It is widely understood that housing affordability is affected mainly by two distinct variables; capital and occupation variables. Capital variable is associated with costs in purchasing a house from the market and the ability to finance purchase, whereas occupation variables are associated with costs in maintaining the house. Occupation variable comprises the ability to carry the costs related with land lease and rates, service costs, building maintenance, loan repayment and interest rates [9].

Though, private real estate development is one of the housing sectors engaged in providing housing for the dwellers in Addis Ababa, it was reported that the beneficiaries of the effort are mainly few high-income groups. A study made in 2011, showed that 80% of the city population are categorized under the low-income group. The study further indicated that among 125 registered private residential real estate developers, 83.3%of them targeted high income while only 16.7% respond to the middle-income groups [3].

Demand and supply gap by itself has a high contribution to the affordability situation of housings in Addis Ababa. Based on the 1994 statistical data, the supply of housing units (374,742) was less than the demand (414,262) showing a deficit of 9.5% housing units [10]. The data of government planning and policy commission reported that the deficit has increased to 24.8% within the subsequent ten years (1994-2004), even if the total housing stock delivered has risen to 471,429 with 2.5% average annual increment. The unfulfilled demand for residential housing in 2004 was, therefore, 116,806. Besides, different studies indicated that about 80% of the Addis

Ababa houses (269,814) that are located in the inner part of the city need complete replacement because of dilapidation [11]. In 2010, the housing demand reached to 456,000 housing units.

**An overview of the affordability of housing in selected countries**

Affordability issue is a serious concern for most of the developed and developing countries.

**China**

High housing price is a major issue in a number of big cities in China. Since 2005, there was a critical housing affordability problem for middle and low-income families. In 2004, the housing price increased at an annual rate of 17.8% which is almost twice the income growth rate of 10%. In an attempt to boost the housing supply to middle and low-income families, the Chinese government formulated favorable policies, designed and implemented large housing schemes and introduced the Housing Provident Fund program (HPF). HPF provides a mechanism allowing potential purchasers who have an income to save and eventually purchase a unit dwelling [12].

The HPF in China included a subsidized savings program linked to a retirement account, subsidized mortgage rates and price discounts for housing purchase. For residents who earn an annual income between 30,000 – 70,000 RMB which is for middle to low income household, the public housing program provides housing having 60 – 110 sq. m at an affordable prices which is usually 50-70% lower than the market price [12].

**Germany**

The standard and cost of housing facilities vary greatly among different German cities. The majority of German population earns about 43,596 EUR annually. According to the 2015 statistical data, 16.64% of the population earns more than 92,571 EUR; 42.79% earn more than 62,431 EUR and 78% earn more than 43,596 EUR [13].

Average purchase price for a property in Germany are relatively low. The price ranges from 1,500 - 2,500 EUR per square meter. The average price for a 30-square meter property (a small apartment) is around 60,000 EUR, while 100 square meter apartment averages around 250,000 EUR. Prices are typically up to 50 percent higher in Berlin and Munich than in other cities. Financing is usually provided by banks for about 60-70% of the buying price as mortgage loan [13]. Despite favorable market price and supply, however, only 42% of Germans own their own home when compared to 65 percent in the USA and 69% in the UK [13].

**United Kingdom**

Since April 2013, there is equity loan available for new property buyer’s worth up to 300,000 pounds in the United Kingdom. The equity loan is free of charge for the first five years and can be repaid in 25-years mortgage. Therefore, when an average monthly income is compared with the monthly housing mortgage payment, it shows that it is fairly affordable by many citizens [14].

**South Africa**

In South Africa, two bed room villa houses were sold for only 360,000 Rand in Johannesburg during the period 2008 – 2010. In 2016, the housing price ranges from 478,203 to 1.93 Million Rand [15]. Thus, when the housing cost is compared with the monthly income of 21,007 Rand, the mortgage payment for 30 years is unaffordable by the majority residents of big cities. However, there are alternative schemes for lower income level in South Africa.

## Zambia

Zambia has a housing provision which accounts middle and low-income groups. The housing costs range from 24,382 – 68,363USD where the average monthly income is 2,425USD. Therefore, for a mortgage payment of 30 years, the houses are reasonably affordable.

Table 1 presents the summary of affordability of houses in the selected countries.

Table 1: The affordability of housing in selected countries [12] [13] [14] [15]

| Countries | Monthly average income (middle income groups) | Total housing price including interest payment | Monthly installment | Remarks |
|---|---|---|---|---|
| China | (3,000-5,000)RMB (≈ 450 - 750 USD) | Big cities (20,000-30,000) RMB Other cities (8,000-20,000) RMB | 116.70 RMB for 10 years | Affordable when compared with per capita income |
| German | 3,633 EUR (≈ 4,214 USD) | 65m$^2$ costs 150,000 EUR 30m$^2$ costs 60,000 EUR | 200 and 500 EUR for 30m$^2$ and 65m$^2$ in 25 years resp. | Affordable when compared with per capita income |
| UK | 2,267 Pound (≈ 2,947 USD) | About 300,000 Pounds | 1,000 pounds in 25 years | Fairly affordable when compared with per capita income |
| Zambia | (417 - 2,425 USD) | 68,363 USD there is also low-cost houses (65m$^2$ costs 24,382 USD) | 379.79 USD in 15 years | Affordable when compared with per capita income |
| South Africa | 21,007 Rand (≈ 1,533.51 USD) | 478,203 Rand to 1.93 Million Rand (34,908.8 USD) | 15,940 Rand in 30 years | Not affordable for low income groups when compared with per capita income |

## METHODOLOGY

This study involves both qualitative and quantitative data that were collected from questionnaires, interviews, document analysis and observation. Representative stakeholders, who are involved directly or indirectly in private residential real estate development, were interviewed. The interviewed parties included: seven real estate developers, five banks/financers (one public and four private banks), municipalities/urban development offices and end users. Interviews were made to study the affordability situation and the standard of private residential real estates. The income and expenditure values were taken from the Central Statistical Agency to analyze the affordability situation in Addis Ababa.

Out of the total 125 registered real estate developers in Addis Ababa investment agency, only 13 developers were actively operating in 2016.

From these actively operating real estate developers, seven of them were selected using the lottery method which is among the simple random sampling technique. The main focus of this study was limited to housing provisions and its affordability. The assessment on the affordability of the real estate houses considered their standard in terms of aesthetics, construction materials and delivery date.

## FINDINGS AND DISCUSSION

### Housing provisions and challenges in Addis Ababa real estates

Based on the 2015 Ministry of Urban Development and Housing (MOUDH) data, the formal and informal sector of housing supply accounts for 69.8% and 30.2%, respectively. Within the formal sector; housing supply by the real estate developers was only 0.4% while 49.6% and 19.8% were supplied by the government and individuals (cooperatives and lease), respectively.

Due to the dramatic increase in the population of Addis Ababa in recent years, there were about 900,000 people who are on a waiting list for a government sponsored residential apartments (condominiums). Based on the past performances, it is hardly possible to balance the demand and supply gap with in the near future. Without innovative approach, it is likely to see a wider gap between demand and supply that would result in an increase in the prices of residential houses. On the other hand, real estate developers are observed misusing the land for commercial use than its originally intended purpose (residential development). As a result, the government appears to have lost its inspiration in providing incentives to private developers.

Based on international experiences, real estate developments are usually financed mainly by bank loans, client's advance payment and own equities. However, based on the interviews made in five (one public and four private) banks, it was learned that bank loan for private real estate's accounts for only 1% of the bank's business.

The study further revealed that, the sources of finance for real estate developers are 0-1% from financers, 75% from client installed payments and 24% from their own equity/savings. These data shows almost no loan is given for real estate developers over the last years. It is also argued that, due to lack of collateral, financers/banks do not provide sufficient loan for real estate developers which results in substantial delay and even compromised quality. Therefore, the main sources of finance for the real estate developers remain to be from the buyers advance payments, real estate developer's own source, profit from the developers other business if any and contribution from high income buyers who tend to pay in full amount for the purchase of houses.

Usually, banks tend to finance clients to buy houses by providing loan for only limited percent of the contribution cost after the client pays the down payment for the developers. For this reason, some real estate developers have established partnerships with selected financial institutions.

However, to all disappointments, buyers could not access loan by pledging the real estate house which is under construction since the title deed belongs to the developer until the final handover. This puts young and potential buyers in pressure and thus accessing loans becomes extremely difficult.

Generally, loan from banks is limited to people with high income group having substantial assets and convincing cash flows. Lack of long-term finance is a wide spread constraint facing private businesses in Ethiopia in general and the real estate sector in particular. Without adequate funding, developers find it difficult to start and complete their projects on time, within budget and without compromising quality.

## AFFORDABILITY ANALYSIS OF PRIVATE RESIDENTIAL REAL ESTATES AND PUBLIC HOUSES

### Income/ expenditure of Addis Ababa residents in 2016

In order to judge whether the price set by the private real estate developer are affordable or not, an analysis should be made between the average housing price and the average household income. The average household incomes are determined, based on the household expenditure of potential buyers in Addis Ababa.

Income quintile is a method to measure the household income of residents, ranking from poorest to wealthiest, and then group into 5 income quintiles, (1 being the poorest and 5 being the wealthiest), each quintile containing approximately 20% of the population. Households are often divided into quintiles according to their annual household expenditure. The expenditure for different quintile ranges were gathered from the government source and are summarized in Table 2 [16].

Table 2: Household expenditure at country level (Total 2010/11 National average prices)

| Quintile | % of HHs | Annual country level household expenditure in Birr | | |
|---|---|---|---|---|
| | | Lower Limit | Upper Limit | Mean |
| I | 20 | 1,471.48 | 11,369.98 | 6,420.73 |
| II | 20 | 11,369.99 | 15,765.28 | 13,567.64 |
| III | 20 | 15,765.29 | 20,657.00 | 18,211.15 |
| IV | 20 | 20,657.01 | 28,346.50 | 24,501.76 |
| V | 20 | 28,346.51 | 53,572.83 | 40,959.67 |

For the analysis, the GDP annual growth rate was used to forecast the total income per capita for 2015/16. The GDP annual growth rate for Addis Ababa is calculated by dividing the total income by its total population and it is summarized as shown in Table 3 below.

Table 3: GDP annual growth rate [16]

| | 2009/10 | 2010/11 | 2011/12 | 2012/13 | 2013/14 | 2014/15 | 2015/16 |
|---|---|---|---|---|---|---|---|
| GDP annual growth rate | 10.4 | 11.4 | 8.8 | 9.7 | 10.5 | 8.5 | 8.7 |

The growth rate at the final year can be determined by multiplying the GDP annual growth rates within five years starting from 2011/12 as shown below.

GDP annual growth rate
=(1 + the nth GDP growth at current price) x 100/100 [Eq. 1]
= (1.088 x 1.097 x 1.105 x 1.085 x 1.087) x 100/100 = (1.56) x 100/100 = 156 %.

This means, the total income per capita of Addis Ababa residents have grown by 156% for the year 2015/16.

The expenditure of the household can then be determined by multiplying each value on Table 3 of the expenditure quintile measurement with 3.9 (the average household size of Addis Ababa's population).

As a result, the household expenditure quintiles for 2015/16 can be obtained by multiplying average expenditure quintile of 2010/11 fiscal year by the growth factor (156%). The multiplied figures are tabulated as shown on Table 4.

For a healthy economy, there should be a fair balance between income and expenditure. For this analysis purpose, 10% of the total income is considered to be saved by the Addis Ababa residents.

For instance, the total income for low income groups becomes;

Total income – Expenditure = Saving [Eq.2]

Total income – 39,096.49 = 0.1*Total income = 43,440.54 birr

Performing the same calculation for all the quintile (1-5), the total household income of Addis Ababa residents is tabulated as shown on Table 4 below.

Table 4: Household expenditure and income of household (2015/16)

| Expenditure Groups | Expenditure Quintiles | | | | |
|---|---|---|---|---|---|
| | I | II | III | IV | V |
| Annual expenditure in birr on 2010/11 | 25,061.85 | 52,913.78 | 71,023.47 | 95,556.83 | 159,742.70 |
| Annual expenditure in birr on 2015/16 (Multiplied by 1.56) | 39,096.49 | 82,545.50 | 110,796.61 | 149,068.66 | 249,198.61 |
| Household income of Addis Ababa residents (2015/16) | 43,440.54 | 91,717.22 | 123,107.34 | 165,631.84 | 276,887.34 |

Table 4 shows the household income for those in the mean highest, median and lowest quintile being 276,887.34; 123,107.34 and 43,440.54 birr respectively. This shows that there is a large gap in income level of Addis Ababa residents. Thus, the monthly income of Addis Ababa residents is determined by dividing the annual household income by the number of months in a year (12 months). As a result, 23,073.95; 10,258.95 and 3,620.05 birr are the average monthly gross income values for high, middle and low income groups respectively.

**Private residential real estate housing prices and their payment schedules**

Table 5 shows the prices of selected real estate apartments, in birr per square meter and the payment schedule in percent to be paid during different phases of the construction for the sampled real estates in Addis Ababa.

Table 5: Prices of selected real estate houses and annotated payment schedule

| No. | Real estate developers | Total cost (Birr) | Birr per square meter | Payments schedule in percent (%) during different phases of construction |
|---|---|---|---|---|
| 1 | Real estate 1 (94.48 sq. m) 2 bed room apartment | 2,144,025.0* | 22,692.9 | 25, 75 |
| 2 | Real estate 2 (157 sq. m) 3 bed room apartment | 3,580,100.0* | 22,803.2 | 30, 10, 20, 20, 12, 8 |
| 3 | Real estate 4 (174 sq. m) 3 bed room apartment | 5,735,500.0* | 32,962.6 | 30, 20, 15, 15, 10, 5, 5 |
| 4 | Real estate 5 (114 sq. m) 2 bed room apartment | 2,775,849.0* | 24,349.6 | 50, 50 |
| 5 | Real estate 6 (94.70 sq. m) 2 bed room apartment | 1,583,351.3* | 16,719.7 | 20,25,25,25,5 |
| 6 | Real estate 7 (87.9 sq. m) 2 bed room apartment | 2,637,000.0* | 30,000.0 | 30, 25, 30, 15 |

* Average prices that have considered different parameters including location variable

The payment for the real estate houses are arranged in installment payable at different phases of construction. For instance, in “Real estate 1” shown on Table 5, the arrangement is (25%, 75%). This means the down payment is 25% of the total cost of housing while the remaining 75% will be paid in four-month intervals until the money is fully paid. The installments are variable and depend on the will of individual developers.

## Affordability analysis and eligibility of a buyer to acquire loan from banks

The potential of getting loan from a bank is analyzed considering the high monthly income value of Addis Ababa residents, which is 23,073.95 birr.

Currently, one of the private banks has a link with most of the real estate developers and created fair arrangement for clients to borrow money by providing fixed assets as collateral. Loans from the bank are usually required to be paid back by the borrowers in a trend set by the bank. As stated on the labor law, it is one third of the borrower’s gross income that is paid every month. Based on an average income of 23,073.95 birr the monthly installment will be one third of it, resulting a payment of 7,691.32 birr per month.

As a routine procedure, banks tend to provide 30% of loan for “real estate 2” from the remaining 70% payment. Therefore, for “real estate 2”, the remaining 70% becomes 2,506,070 birr (see Table 5). Hence, 30% of loan from 2,506,070 birr equates to 751,820 birr.

The payment to the bank at the end of every month is calculated by using Excel PMT function (Eq. 3) or the formula (Eq. 4) as shown below:

Monthly payment to the bank
= PMT (rate, Nper, pv, [fv], [type]) [Eq. 3]

where: -
PMT : Payment function
Rate : Interest rate for the loan
Nper : Total number of payments for the loan
Pv : Present value or the total amount worth now
Fv : Future value
Type: is a logical value: - Payment at the beginning of the period = 1, Payment at the end of the period = 0

OR by using the following formula:

$$A = P\left\{\frac{i(1+i)^n}{(1+i)^n - 1}\right\} \qquad \text{[Eq. 4]}$$

Note that for all loan repayment calculations ‘Real estate 2” is considered so that the comparison of the analysis can be observed. On all calculations, however, grace period is not considered.

### Sample calculation for five years loan repayment:

According to the survey done on the loan period of banks in Addis Ababa, only short term loans are made available which is usually a maximum of five years. For “Real estate 2”, at an interest rate of 16% and total number of 60 installment, Nper (which is at the end of each month for 5 years) becomes,

Monthly payment for loan to the bank
= PMT (16%/12, 60, 751820) = <u>18,282.83 birr</u>

As pointed out earlier, the monthly installment to the bank shouldn’t exceed one third of the household income or 7,691.32 birr per month. In this case, 18,282.83 birr is much higher than 7,691.32 birr. Therefore, a person cannot get loan from the bank and can’t also afford to buy the real estate apartment.

Similarly, in “Real estate 6”, two bed room apartment costs 1,583,351.29 birr. One of the banks has an arrangement with “Real estate 6” to give 50% loan from the total property price which is 791,675.65 birr. Note that, 50% loan will be released from the bank after the borrower/buyer pays the first 50% of the total cost to the developer.

Then, the monthly payment to the bank for the return of the loan is calculated using PMT, which amounts to 19,252.01 birr. In this case, the monthly payment to the bank is greater than one third of the high income holder. Thus, the bank cannot lend money and clients can't afford to buy the real estate apartment.

**Sample calculation for fifteen years loan repayment:**

For "Real estate 2"; at an interest rate of 16%, and a total number of payment (Nper) installment of 180 (which is at the end of each month for 15 years),

Monthly payment for loan to the bank
= PMT (16%/12, 180, 751820) = <u>11,041.99 birr</u>

In this case, 11,041.99 birr is still greater than 7,691.32 (one third of income) birr. Therefore, a person with an average high income cannot get loan from the bank and can't also afford to buy the real estate apartment.

**Sample calculation for thirty years loan repayment:**

For "Real estate 2", at an interest rate of 16% and a total number of payment (Nper) installment of 360 (which is at the end of each month for 30 years),

Monthly payment for loan to the bank
= PMT (16%/12, 360, 751820) = <u>10,110.15 birr</u>

In this case, 10,110.15 birr is greater than 7,691.32 (one third of income) birr. Therefore, a person cannot get loan from the bank and can't also afford to buy the house.

**For thirty year loan with 11% interest;**

For "Real estate 2", at an interest rate of 11% and a total number of payment (Nper) installment of 360 (which is at the end of each month for 30 years).

Monthly payment for loan to the bank
= PMT (11%/12, 360, 751820) = <u>7,159.76 birr</u>

In this case, 7,159.76 birr is less than 7,691.32 (one third of income) birr. Therefore, a person can get loan from the bank and can also afford to buy the house.
This study verified that the private residential real estates are not affordable for almost all income groups in Addis Ababa unless the interest rate is decreased, payment period is relaxed and household income is increased.

It was the GDP growth rate that was used to account for the household income. But GDP has some short coming where it fails to count the economic activity that do not necessarily increase the household income.

Human development index (HDI) is relatively a better tool in explaining the income distribution. Had the analysis be based on this index, the result on the household income level would have been reduced which in turn could have aggravated affordability situation.

**Affordability of public housings in relation to income of Addis Ababa residents**

The government has introduced public housing schemes with initial down-payment options of 10, 20 or 40 percent of the house value that can be saved over a period of time at the government-owned Commercial Bank of Ethiopia (CBE), which is also the mortgage provider for the remaining 90, 80 and 60 percent respectively.

The construction costs of the public condominiums under the scheme are, however, adjustable based on the market price of construction materials and labor. The total cost and expected monthly payments for the three types of housing schemes are summarized on Table 6.

Table 6: Public housing schemes (10/90, 20/80 and 40/60) [17]

| No. | Housing schemes | Size of the apartment | Total cost (Birr) | Cost per sq. m. | Monthly payment to the bank |
|---|---|---|---|---|---|
| 1 | 10/90 (10% saved for three years and 90% loan provided by the CBE) | Studio flat (31 $m^2$) | 67,320.0 | 2,171.60 | 187.00 |
| 2 | 20/80 (20% saved for seven years and 80% loan provided by the CBE) | One bed room (50 $m^2$) | 127,000.0 | 2,540.00 | 302.40 |
| | | Two bed room (70 $m^2$) | 224,000.0 | 3,200.00 | 533.30 |
| | | Three bed room (85 $m^2$) | 304,000.0 | 3,576.47 | 723.80 |
| 3 | 40/60 (40% saved for five years and 60% loan provided by the CBE) | Two bed room (50 $m^2$) | 701,270.0 | 4918.00 | 4,675.10 |
| | | Three bed room (70 $m^2$) | 847,650.0 | 4918.00 | 5651.00 |
| | | Four bed room (85 $m^2$) | 950,000.0 | 4918.00 | 6333.3 |

The 40/60 scheme welcomes diaspora Ethiopians and encourages those who can deposit to pay upfront. For the 40/60 group savings will earn a 5.5% interest over the 5 years and the loans will have 7.5% interest instead of 9.5% market rate to be paid in 17 years. According to the latest data, the original price of 40/60 was increased by the Commercial Bank of Ethiopia (CBE) from the previous 3,200 birr per square meter to 4,918 birr per square meter on the delivery date. In total, there is an increment of 124,000 birr by the CBE during the delivery of houses. This is claimed to be from the increasing interest payments. Therefore, it is difficult to conclude on the affordability of condominium houses while there is such type of unexpected price increment on the buyers.

Using the expenditure and GDP data for Addis Ababa presented on the previous sections, the monthly gross income ranges for low, middle and high ranges are (828.90– 6,405.10), (8,881.10– 11,636.80) and (15,968.50– 30,179.40), respectively. This means, if the prices of the public houses remain constant, it will be affordable for middle income groups.

However, if there are price adjustments due to price escalation of construction materials, the housing scheme might end up being unaffordable to the average Addis Ababa residents which have not yet received their houses.

**Cost comparison of the public and private real estate housing with the market**

The cost per square meter for public and private real estate houses are shown on Table 7. The market price was also checked to evaluate the cost differences that exist between the public as well as the private real estate houses. The comparison shows that, the cost per square meter of the public houses are on average 70.5% lower than the market price. This means, the official cost of public houses is only 29.5% of the average market price indicating that it will be difficult to expect quality apartments. This analysis, however, does not account for the price escalation that may arise due to inflation and other cost factors. On the other hand, the costs per square meter of private real estates are on average 132% higher than the market price.

Table 7: Cost comparison of the public and real estate housing with the market

| Market price(Cost per m$^2$) | Public houses (Cost per m$^2$) | Public houses avg. cost difference (%) | Real estate houses (Cost per m$^2$) | Real estate houses avg. cost difference (%) |
|---|---|---|---|---|
| 6,000-18,000 | 2,171.6 – 4,918 | -70.5% | 22,692.9 - 32,962.6 | +132% |

**Overview of the standard of private residential real estate houses**

In this study, the standards of real estate houses were observed from three perspectives: (i) Construction supervision, design and material on site, (ii) Completion time and delivery of houses according to the contract and (iii) The quality of real estate houses in relation to provision of infrastructure and services. These three items were considered in the study since affordability assessment relates with the standards of the delivered housing [18].

**Construction supervision, design and material on site:**

Each real estate has its own way of price fixing. Construction supervision and construction materials used during construction can be taken as methods in determining the standard of housing. Table 8 shows the outline summary of the real estate's construction material and supervision during the construction.

As "Real estate 2" is simultaneously a consultant and an owner of the project, the existence of conflict of interest is inevitable. This may lead to compromised quality of the houses. Despite the low-cost materials used by "Real estate 2", "3"and "4", the price set for purchasing the houses are very high which shows potentially unreasonable profit margin. Since "Real estate 5" is an international developer, all designs and documents are done using foreign language. Therefore, it is difficult to comment on it.

Before setting the prices of the houses, due care and careful assessment should be made on different factors that affect the housing prices. Since customers consider different alternatives before concluding contract, it is unfair to make a substantial price adjustment afterwards unless otherwise there are unforeseen conditions. However, "Real estate 6" adjusted the housing price that created inconvenience to the customers. "Real estate 7" adopts design-build-transfer project delivery method where the contractor has a share with the real estate company and contractors are thus selected to do the project without competitive bidding. In all sampled real estates, there were no new major technologies used during the execution of the project to speed up the construction work.

Table 8: Construction material, design and supervision

| No. | Private residential real estate developer | Data gathered regarding construction material and supervision | Description | Birr/ $m^2$ |
|---|---|---|---|---|
| 1 | Real estate 2 | Three classification based on wall and slab material | Low cost – ribbed slab and prefabricated beam<br>High quality – solid slab and HCB wall material<br>Top quality – solid slab and brick wall material | 22,803.20 |
| | | Have the same consultant and owner | This arrangement will create conflict during supervision and quality control | |
| 2 | Real estate 3 | Use low cost wall making material | Hydra foam wall material which does not require external finishing works | 7,000.00 |
| 3 | Real estate 4 | Low cost material used | Agro stone partition wall and ribbed slab system | 32,962.60 |
| 4 | Real estate 5 | Chinese construction company | Use their own language (Chinese) on the design which makes it difficult to comment on the designs and documents. | 24,349.60 |
| | | One company designs and constructs the apartments | The apartments were constructed by totally adopting Chinese code/ standards | |
| 5 | Real estate 6 | Price increment due to design change | Unexpected cost due to price escalation | 16,719.70 |
| 6 | Real estate 7 | Increase working hours in an attempt to deliver on time | Use ready mix concrete or night construction permit (work 18hrs per day). | 30,000.00 |

**Completion time and delivery of houses**

Delay in completion time and delivery of houses is one of the common problems identified in all the sampled private real estates. According to the interview data, delay in the delivery of finishing materials, price escalation, lack of foreign currency, inaccessibility to loan, unavailability of municipality supervising inspector at different stages of the project implementation, delay in client approval, design change either from the client or the design team and unpredicted conditions on the site are some of the challenges that causes delay in completion time and housing delivery. In order to reduce the late delivery of houses, the government has set a penalty on real estate developers.

Even if some of the root causes that push late delivery are beyond the control of real estate developers, the penalty alone could not alleviate the problem. Due to internal and external factors, unfortunately, developers are unable to meet the deadlines. This creates unnecessary disputes between the developers and the clients.

**Infrastructure and services in a real estate sector**

The commercial amenities around the developed real estates like shopping malls, supermarket and gymnasium differ depending on the location of the development. It is observed during site visits that 71.4% of the sampled real estates do not have any commercial buildings within the real estate housing compound. Only “Real estate 5” and “Real estate 6” have made some effort to implement those facilities.

Regarding greenery and parking area, there is a standard set by the Municipality of Addis Ababa where most of the villa houses satisfy parking and greenery requirements. However, apartments in “Real estate 4” and “Real estate 7” are either confined or do not have any space for greenery area and the parking space is underground where only one parking space is provided for one household especially the ones located around Bole area. Even though there are rules and regulations set by the municipality, the monitoring and control is minimal and the office lacks proper professional handling in the permit approval processes.

## CONCLUSIONS

The major conclusions are listed as follows:

1. Given the average household income of the Addis Ababa city residents, the housing price by private real estate developers are not affordable by all income levels.

2. Due to the internal factors (such as, delay in the delivery of finishing materials and design change) and external factors (such as, lack of foreign currency and price escalation), the contribution of real estate sector in reducing housing demand for the majority appears to be nonexistent.

3. The selection of quality materials and application of innovative methods have not been given sufficient attention by the private residential developers.

4. Minimal efforts have been exerted to adopt the world’s best practices incorporating low interest rate management and extended loan repayment scheme.

5. Almost no loan is given to private real estate developers from public as well as private banks and the real estate’s income depends mainly on advance payments and their own resources.

## RECOMMENDATIONS

The following recommendations are forwarded:

1. In order to make private real estates affordable to the average income residents, all concerned stakeholders should jointly work in reducing the impacts of the internal and external factors.

2. Municipalities and relevant offices should enhance close follow up and supervision on land utilization rather than blocking new land allocations.

3. The government should reconsider the introduction of special interest rates for mortgage loans and set a policy on price allocation of real estate developers based on quality, location and housing delivery time.

4. Real estate developers and financial institutions should work together in finding ways to facilitate long term payment arrangement lasting 25-30 years.

5. International real estate developers need to be encouraged to invest on housing development in Addis Ababa to facilitate technology transfer and stabilize building cost.

## REFERENCES

[1] United Nations, Department of Economic and Social Affairs, Population Division (2016), World Population Prospects: The 2016 Revision, Key Findings and Advance Tables.

[2] Taffese W.Z., Low cost Eco-friendly building material: A case study in Ethiopia, Ethiopian Institute of Architecture, EiABC, Addis Ababa, 2012.

[3] Paulos Birhanu, Study on private residential real estate development in Addis Ababa, (M.Sc. Thesis), AAiT, School of Civil and Environmental Engineering, Addis Ababa, 2011.

[4] Elias Yitbarek Alemayehu, Revisiting «Slums», Revealing Responses: Urban upgrading in tenant-dominated inner-city settlements, in Addis Ababa, Ethiopia. (PhD Thesis) Trondheim: Norwegian University of Science and Technology, 2008.

[5] Wubshet Berhanu, Real estate developments and the housing supply issue in Ethiopia the case study in Addis Ababa, (Journal of EEA, Vol 21) Department of Architecture and planning, 2004.

[6] Bisrat Kifle, Public housing: the condominium approaches the case of Addis Ababa, (M.Sc. Thesis) EiABC, Addis Ababa, 2008.

[7] Abnet Berhe, An overview of housing in Ethiopia, EiABC, Addis Ababa, Ethiopia, 2017.

[8] Habitat, The challenge of slums: Global report on human settlements (2003), Development context and the millennium agenda: Revised and updated version, 2010.

[9] Kiros Aqubamichail, Factors affecting the real estate market: the case of Addis Ababa city, (M.Sc. Thesis), Addis Ababa University, Addis Ababa, 2009.

[10] Central Statistical Agency, CSA data, The 1994 Population and Housing Census of Ethiopia: Results for Addis Ababa, Volume II Analytical Report, Addis Ababa, Ethiopia, 1999.

[11] Azeb Kelemework, Housing for the poor in Addis Ababa, Addis Ababa city administration housing agency, Addis Ababa, Ethiopia, 2011.

[12] Jianbo, L. and Palomar J., Housing Policy in the People's Republic of China: Success and Disappointments, Peking University (Beijing University), Center for Real Estate Law, China, 2015.

[13] Flippo H. & son publishing Co. LLC, Average salary survey: http://www.averagesalarysurvey.com/ germany,German Housing/House and Home-Apartments, condos, houses The German Way & More.htm, updated on 2015.

[14] Office for National Statistics: New port, House price simple averages, Updated on 2018.

[15] Income and expenditure survey: South Africa statistical release, 2012, /www.statsssa.gov.za/

[16] Ministry of Finance and Economic Cooperation (MoFEC), Annual statistics, Updated on 2016, /www.africaneconomicoutlook.org/

[17] Tesfaye Getnet, Capital Ethiopia newspaper, updated on 2017, /www.capitalehiopia.com/.

[18] Selam Yohannes, Experiences and prospects of private residential real estate development in Addis Ababa, (M.Sc. Thesis), AAiT, School of Civil and Environmental Engineering, Addis Ababa, 2016.

# CALIBRATION OF THE PRIESTLEY-TAYLOR EVAPORATION MODEL FOR ETHIOPIA

Yilma Seleshi

School of Civil and Environmental Engineering, Addis Ababa Institute of Technology, Addis Ababa University, Ethiopia
Email - yilma.seleshi@gmail.com,

**ABSTRACT**

*In practice reservoir planning and operations, irrigation design and water balance studies require estimates of reliable evaporation. The universal standard models of the Penman $E_0$ and the Penman-Monteith $ET_0$ are used to estimate open water evaporation and evapotranspiration respectively. The models rely on accurate measurements of climatic elements such as temperature, humidity, wind speed, and solar energy with good spatial and temporal coverage. However, practicing hydrologists, irrigation engineers and planners face challenge of reliable estimate of evaporation when only temperature data are available as the case in many study areas of Ethiopia and elsewhere. To overcome this challenge, a number of simplified temperature-based evaporation models notably the Priestley-Taylor, Blaney-Criddle and Hargreaves have been developed. Their applicability is, nevertheless, subject to rigorous local calibrations and without calibration they have limited validity to tropical areas.*

*There is a need, thus, to precise estimate of $E_0$ and $ET_0$ based on only temperature data for Ethiopia. This paper presents locally calibrated coefficients α for the Priestley-Taylor model applicable for Ethiopia to estimate open water evaporation $E_o$ and Reference Evapotranspiration $ET_0$ based on maximum and minimum temperature as well as readily derivable elevation and radiation data. In order to calibrate α, regression is done between the Priestley-Taylor model estimate (independent variable) and $E_o$ Penman model estimate as dependent variable for each month of the 167 Class I stations. Similarly, regression is done between the Priestley-Taylor estimate (independent variable) and $ET_o$ Penman-Monteith model estimate (dependent variable). It is found that the Priestley-Taylor coefficients α applicable over Ethiopia to estimate monthly $E_0$ is 1.11 and to estimate $ET_0$ is 0.96.*

**Keywords:** *Ethiopia, Irrigation-water -requirement, Open water Evaporation, Priestley-Taylor, Penman-Monteith Reference-Evapotranspiration, Reservoir,*

## INTRODUCTION

In practice reservoir planning, operation, irrigation scheduling design and catchment water balance studies require estimates of reliable evaporation which is dependent on accurate measurements of climatic elements such as temperature, humidity, wind speed, and solar energy with good spatial and temporal coverage. However, practicing hydrologists, irrigation engineers and planners face challenge of reliable estimate of evaporation when only temperature data are available as the case in many study areas of Ethiopia and elsewhere. The objective of this paper is to develop a locally calibrated open water evaporation and evapotranspiration estimates based on Priestley-Taylor [1] model dependent on only temperature, solar radiation (sunshine hours) and elevation data.

In this paper two idealized standard evaporation rates are defined following Shuttleworth [2] & McMahon [3]. The first is Potential Evaporation $E_o$ which is defined as the quantity of water evaporated per unit area, per unit time from an idealized, extensive free water surface under ambient atmospheric condition. The second is *Reference Evapotranspiration* $ET_o$ the rate of evaporation and transpiration from idealized actively growing, green grass crop, completely shading the ground, with a fixed crop height of 0.12m, an albedo of 0.23, and a surface resistance of 69 s/m and not short of water.

When reliable climatic data including maximum and minimum temperatures, relative humidity, wind speed and radiation are available at / near the project site, an improved estimate of $E_0$ and $ET_0$ can be made using well-established global standard Penman and Penman-Monteith models respectively in case where there are only temperature data, selecting reliable evaporation estimation models is still a challenge in Ethiopia.

To overcome this challenge, elsewhere, a number of temperature-based evaporation models notably the Priestley-Taylor, Blaney-Criddle and Hargreaves have been developed for non-tropical areas. Based on non-water-limited field data, Priestley-Taylor adopted $\alpha = 1.26$ for “advection-free” saturated surfaces [4]. Likewise based on field data in northern Spain, Castellvi et al. [5] found that $\alpha$ exhibited large variations seasonal (up to 27 %) and spatial from 1.35 to 1.67.

Shakir [6] evaluated performances of four evaporation estimate methods, namely; Bowen ratio energy balance, mass transfer, Priestley–Taylor and pan evaporation, based on 4 years experimental data over the semi-arid region of India and found that Priestley-Taylor model with $\alpha = 1.31$ has acceptable performance considering its limited data requirement.

Adem et. al. [7] found that Penman Monteith, Enku and Thornthwaite's method fitted well the observed Pan data of the Bahir Dar station. They further indicated that Blaney-Criddle, Priestley & Taylor, and Hargreaves methods should be recalibrated for local condition before use over the Ethiopian highlands.

As discussed above, the applicability of Priestley-Taylor model often subject to rigorous local calibrations. Shuttle worth [3] recommended that in the absence of wind, relative humidity and solar radiation measurements, $E_0$ & $ET_0$ estimate can be made using Priestley-Taylor model provided the Priestley–Taylor model is calibrated with local condition based on the Penman and Penman-Monteith methods.

The objective of this paper is thus to develop regional evaporation estimation method under inadequate data using the well-known Priestley-Taylor model for Ethiopia covering various climatic zones.

## DATA

Ethiopia has a total area of 1.13 million $km^2$ of which 1.12 million $km^2$ is land area and the remaining 7,444 $km^2$ is lakes and ponds. Ethiopia climate is diverse, 10% is hot-arid *(Berha)* with elevation < 500 mals; 52% of the area is warm semi-arid (Kola) with elevation between 500-1500 masl; 27% is cool *sub-humid* (Weynadega) with elevation between 1500-2300 masl; 10% is cool to humid (Dega) with elevation between 2300-3200 masl and 1% Cold to moist (Wurch) with elevation > 3,200 masl. High spatial variability of temperature is observed in Ethiopia following altitude [8].

Meteorological measurements and data management and dissemination over diverse Ethiopia climate is a responsibility Ethiopian Meteorological Agency. The Agency in 2016 operates 909 meteorological stations including: (a) 167 Principal (Class I) stations with key observations on rainfall amount, maximum and minimum temperature, relative humidity, wind speed at 2 m and at 10 m, sunshine duration and pan evaporation; (b) 359 ordinary stations (Class III station) which only three meteorological elements are observed, i.e. maximum and minimum air temperatures of the day, and total rainfall amount in 24 hours; and (c) 383 (Class IV) daily rainfall amount manual observation stations.

For this study the National Meteorological Agency kindly provided 167 stations monthly maximum and minimum temperatures, relative humidity, wind speed and radiation (sunshine hour) data for the period 2011-2015 inclusive representing Ethiopia diverse climate. Figure 1 shows the locations of these stations.

Elevation wise, 11 stations are located below 600 masl, 19 stations are located between 600-1200 masl, 45 stations are located between 1200-1800 masl, 58 stations are located between 1800-2400 masl and 34 stations are located above 2400 masl.

The average percent of monthly missing data over 2011-2015 period for 167 stations for temperature is 6%, sunshine hours is 8%, relative humidity is 12% and wind speed is 15%. Part of the missed data for each station is filled using average climatic data produced in the Ethiopian river basin master plan studies by the Ministry of Water, Irrigation and Electricity of Ethiopia with the assumption that observation value of the five elements remains stationary in the last 30 years.

The remaining stations average data is estimated based on nearby (with 40 km radius and similar elevation) stations observed data. Outlier data have been observed in particular wind speed data (monthly average wind speed greater than 4 m/s) and such data has been excluded by comparing with neighboring stations data and its own monthly data of other year.

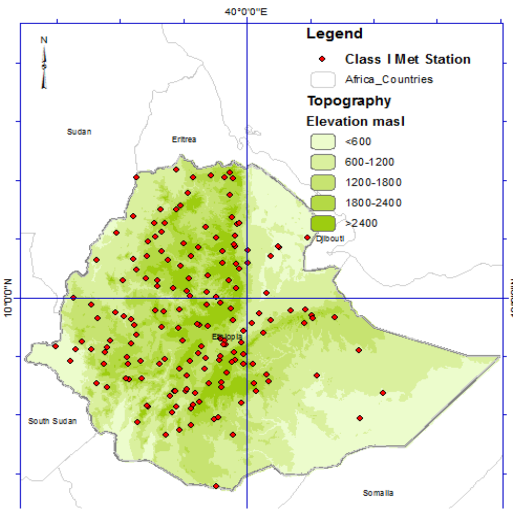


Figure1: Location of Class I meteorological stations used in this study overlaid on elevation raster

**METHOD**

There is a need to reliable estimate of $E_0$ and $ET_0$ based on readily available local data such as temperature, solar radiation and elevation. The Priestley-Taylor model accounts the local available data but the coefficients α should be locally calibrated to account the aerodynamic effect.

The method employed in this paper is to calibrate Priestley-Taylor coefficients α applicable for Ethiopia to estimate $E_o$ and $ET_0$ using regression equations between the Priestley-Taylor model estimate (independent variable) and $E_o$ Penman model estimate as dependent variable using monthly data. Similarly, regression is done between the Priestley-Taylor estimate (independent variable) and $ET_0$ Penman-Monteith model estimate (dependent variable). Detailed description of $E_0$ and $ET_0$ models are given below.

It is well known that the two main factors influencing evaporation from an open water surface (lakes, reservoirs) are the supply of energy at the evaporative surface and the ability to transport vapor away from the evaporative surface which depends on the wind velocity over the surface and the specific humidity gradient in the air above it. Model used for estimating $E_0$ and $ET_0$ are discussed below.

In practice Potential Evaporation $E_0$ (mm/day) is estimated using internationally accepted Penman Model (Equation 1) provided all climatic data required by the model are available [4].

$$E_o = \frac{\Delta}{\Delta+\gamma} E_r + \frac{\gamma}{\Delta+\gamma} E_a \qquad (1)$$

with

$$E_r = 8.64 * 10^7 \frac{1}{l_v \rho_w} (R_n - H_s - G) \qquad (2)$$

*Where* $E_r$ *and* $E_a$ are evaporation estimate (mm/day) based on energy balance method and aerodynamic method respectively; $R_n$ is net radiation (W/m$^2$); $H_s$ is sensible heat flux diffused to surroundings atmosphere to raise the temperature (W/m$^2$); G is ground heat flux (W/m$^2$); $l_v$ is latent heat of vaporization (J/kg) = 2.501*$10^6$ - 2361T and T is average air temperature ($^oC$); and $\rho_w$ is water density ($kg/m^3$). If Hs and G is approximated as 0, Model 1 is the Penman model. The gradient of the saturated vapor is pressure curve $\Delta = de_s/dT$ ($Pa/^oC$) at air temperature is calculated using Equation 3.

$$\Delta = \frac{4098\, e_s}{(237.3 + T\,)^2} \tag{3}$$

$$e_s = 611\left( \begin{array}{l} \exp\left( 17.27 \dfrac{T_{\max}}{237.3 + T_{\max}} \right) + \\ \exp\left( 17.27 \dfrac{T_{\min}}{237.3 + T_{\min}} \right) \end{array} \right) / 2 \tag{4}$$

$$R_h = \frac{e}{e_s} \tag{5}$$

*Where* $e_s$ is air saturation vapor pressure at the ambient temperature in Pascal (Pa = $N/m^2$), $T_{max}$ and $T_{min}$ are maximum and minimum air temperature in $^oC$, $e_a$ is actual vapor pressure ($N/m^2$), and $R_h$ is relative humidity (%).

The psychrometric constant, $\gamma$, (kPa $°C^{-1}$) is given by:

$$\gamma = \left( \frac{C_p\, p}{\varepsilon \lambda} \right) \tag{6}$$

Where $p$ is atmospheric pressure (kPa), $\lambda$ is Latent heat of vaporization (MJ $kg^{-1}$), $C_p$ is specific heat at constant pressure, 1.013 $10^{-3}$ (MJ $kg^{-1}$ $°C^{-1}$), and $\varepsilon$ is ratio molecular weight of water vapor / dry air = 0.622. Atmospheric pressure at a given altitude is estimated from Equation (7):

$$p = 101.3 \left( \frac{293 - 0.0065\, Z}{293} \right)^{5.26} \tag{7}$$

*Where p is a*tmospheric pressure (kPa) and *Z* is site elevation above sea level (m).

Besides the supply of heat energy, the second factor partly controlling the evaporation rate from an open water surface is the ability to transport water vapor away from the evaporative surface. The transport rate is governed by the humidity gradient in the air near the surface and the wind speed across the surface. The second term of evaporation equation Ea is estimated using

Aerodynamic method (m/s) (multiply by [1000 mm/m *86400 s /day] to get in mm/day), $e_s$ is saturation vapor pressure at the ambient temperature T (Pa), $e_a = e_d$ = actual vapor pressure estimated using dew

$$E_a = B(\, e_s - e_a\,) \tag{8}$$

$$B = \frac{0.622\, k^2 \rho_a u_2}{p\, \rho_w [\ln(\, z_2 / z_0\,)\,]^2} \tag{9}$$

point temperature $T_d$ or by multiplying $e_s$ by the relative humidity $R_h$ (Pa), $B$ is the vapor transfer coefficient (m $Pa^{-1}s^{-1}$), $k$ is the Von Karman constant is 0.4, $u_2$ is the wind velocity (m/s) measured at height $z_2$ (200 cm) and $z_0$ roughness height taken as 0.08 cm for open water body, $p$ is atmospheric pressure in Pa, $\rho_a$ is density of moist air ($kg/m^3$) and $\rho_w$ is density of water ($kg/m^3$).

Density of water and air at given location as function of temperature T ($^oC$) and pressure $p$ (Pa) are estimated using Equation 10 and 11, respectively.

$$\rho_a = \frac{p}{287(1+0.608\frac{0.622e_a}{p})T(K)} \quad (10)$$

$$\rho_w = -0.0002T^3 + 0.0119T^2 - 0.3968T + 1003 \quad (11)$$

The net radiation, the difference between net radiation absorbed and emitted is estimated using Equation 12 as given in FAO #56 paper:

$$R_n = (1-\alpha)(0.25+0.50\frac{n}{N})S_o - \left(1.35\left(\frac{(0.25+0.5n/N}{0.75+2Z/100{,}000}\right)-0.35\right)\sigma T^4 \quad (12)$$
$$(0.34-0.14\sqrt{e_a})$$

Where $R_n$ is Net radiation (MJ $m^2$ $day^{-1}$); $\alpha$ *is* albedo and is 0.08 for open water; *n/N is* ratio of actual (n) to maximum possible hours of sunshine (N); $S_0$ is mean solar radiation from cloudless sky from (MJ $m^2$ $day^{-1}$); $e_a$ *is a*ctual vapor pressure (kPa); $\sigma$ is the Stefan Boltzmann constant = $4.903x10^{-9}$ M J $m^{-2}$ $day^{--1}$ $K^{-4}$; *T is* the absolute average air temperature of the evaporating surface in degrees Kelvin (°C + 273); Z site elevation masl; and N is $(24/\pi)^*\ \omega_s$.

The extraterrestrial radiation, $S_o$, $MJ/m^2/day$ for each day of the year and for different latitudes can be estimated from the solar constant, the solar declination and the time of the year by

$$S_o = \frac{24*60}{\pi} Gsc\, d_r$$
$$(\omega_s \sin\phi \sin\delta + \cos\phi \cos\delta \sin\omega_s) \quad (13)$$

Where $G_{sc}$ is solar constant = 0.0820 $MJ/m^2/min$; $d_r$ the inverse of the square of the relative distance Earth-Sun is estimated by $d_r = (1+ 0.033 \cos(2\pi J/365)$; J is the Julian day number (with J=1 for Jan 1 and J= 365 for 31 Dec); φ is the altitude in radian; sunset hour angle in radian $\omega_s$= arccos(-tan φ tan δ); and the solar declination (in radian) δ= 0.4093sin(2πJ/365 – 1.39). For monthly calculations, J at the middle of the month is used in calculating $S_0$ as recommended in FAO # 56 Paper.

*Monthly* $S_o$ value of with smaller interval applicable for $2^0$ -15 $^0$ North which cover Ethiopia is calculated and average sunshine hour to be used on Priestley-Taylor model in the absence of local data nearby the project site are given in Table 1.

FAO-Allan et al [9] adopted the Penman-Monteith combination method as a new standard for estimating Reference Evapotranspiration $ET_o$ in both arid and humid climates and is given by:

$$ET_O = \frac{0.408\Delta(R_n - G) + \gamma\frac{900}{T+273}U_2(e_s - e_a)}{\Delta + \gamma(1+0.34U_2)} \quad (14)$$

Where $ET_o$ *is* Reference Evapotranspiration (mm/day); $R_n$ is net radiation at crop surface ($MJ/m^2/d$); *G* is soil heat flux ($MJ/m^2/d$) and estimated from *G* = 0.4 (T $_{\text{month n mean temperature}}$ $^O$C - T $_{\text{month n-1 mean temperature}}$ $^o$C); 900 is conversion factor; *T* is average air temperature at 2 m ($^o$C); $U_2$ is wind speed measured at 2 m height (m/s); $(e_s - e_a)$ *is* vapor pressure deficit (kPa); Δ is slope of vapor pressure curve (kPa/$^o$C); and γ is hygrometric constant (kPa/$^o$C).

The crop evapotranspiration ETc of another crop growing under the same conditions as the *reference crop* is calculated by multiplying ETo by *crop coefficient* $k_c$ the value of which changes with the stage of growth of the crop. It is to be noted that the $k_c$ predicts ETc under standard conditions. This represents the upper envelope of crop evapotranspiration and represents conditions where no limitations are placed on crop growth or evapotranspiration due to water shortage, crop density, or disease, weed, insect or salinity pressures [9].

Table 1: Estimated extraterrestrial radiation, $S_o$, MJ/m$^2$/day from 2.0-15. 0 North and average sunshine hour.

| N(deg) | Jan | Feb | Mar | Apr | May | Jun |
|---|---|---|---|---|---|---|
| 2.0 | 35.38 | 36.90 | 37.80 | 37.05 | 35.28 | 34.17 |
| 2.5 | 35.17 | 36.76 | 37.77 | 37.12 | 35.43 | 34.36 |
| 3.0 | 34.97 | 36.62 | 37.73 | 37.20 | 35.59 | 34.54 |
| 3.5 | 34.76 | 36.48 | 37.70 | 37.27 | 35.74 | 34.73 |
| 4.0 | 34.55 | 36.34 | 37.66 | 37.33 | 35.89 | 34.91 |
| 4.5 | 34.34 | 36.19 | 37.62 | 37.40 | 36.03 | 35.09 |
| 5.0 | 34.12 | 36.04 | 37.57 | 37.46 | 36.18 | 35.27 |
| 5.5 | 33.91 | 35.89 | 37.52 | 37.52 | 36.32 | 35.44 |
| 6.0 | 33.69 | 35.74 | 37.47 | 37.57 | 36.46 | 35.62 |
| 6.5 | 33.47 | 35.58 | 37.42 | 37.63 | 36.60 | 35.79 |
| 7.0 | 33.25 | 35.42 | 37.37 | 37.68 | 36.73 | 35.96 |
| 7.5 | 33.02 | 35.26 | 37.31 | 37.73 | 36.86 | 36.12 |
| 8.0 | 32.79 | 35.10 | 37.24 | 37.77 | 36.99 | 36.29 |
| 8.5 | 32.57 | 34.93 | 37.18 | 37.81 | 37.12 | 36.45 |
| 9.0 | 32.33 | 34.76 | 37.11 | 37.85 | 37.24 | 36.61 |
| 9.5 | 32.10 | 34.59 | 37.04 | 37.89 | 37.36 | 36.76 |
| 10.0 | 31.87 | 34.42 | 36.97 | 37.92 | 37.48 | 36.92 |
| 10.5 | 31.63 | 34.24 | 36.89 | 37.95 | 37.60 | 37.07 |
| 11.0 | 31.39 | 34.06 | 36.81 | 37.98 | 37.71 | 37.22 |
| 11.5 | 31.15 | 33.88 | 36.73 | 38.01 | 37.83 | 37.37 |
| 12.0 | 30.91 | 33.70 | 36.65 | 38.03 | 37.94 | 37.52 |
| 12.5 | 30.66 | 33.51 | 36.56 | 38.05 | 38.04 | 37.66 |
| 13.0 | 30.42 | 33.33 | 36.47 | 38.07 | 38.15 | 37.80 |
| 13.5 | 30.17 | 33.14 | 36.38 | 38.08 | 38.25 | 37.94 |
| 14.0 | 29.92 | 32.94 | 36.28 | 38.09 | 38.35 | 38.07 |
| 14.5 | 29.66 | 32.75 | 36.19 | 38.10 | 38.44 | 38.21 |
| 15.0 | 29.41 | 32.55 | 36.09 | 38.11 | 38.54 | 38.34 |

| N(deg) | Jul | Aug | Sep | Oct | Nov | Dec |
|---|---|---|---|---|---|---|
| 2.0 | 34.59 | 36.15 | 37.28 | 36.94 | 35.61 | 34.75 |
| 2.5 | 34.76 | 36.25 | 37.28 | 36.84 | 35.43 | 34.53 |
| 3.0 | 34.93 | 36.36 | 37.29 | 36.73 | 35.24 | 34.31 |
| 3.5 | 35.10 | 36.46 | 37.29 | 36.63 | 35.05 | 34.09 |
| 4.0 | 35.26 | 36.55 | 37.29 | 36.51 | 34.86 | 33.86 |
| 4.5 | 35.43 | 36.65 | 37.28 | 36.40 | 34.67 | 33.63 |
| 5.0 | 35.59 | 36.74 | 37.27 | 36.28 | 34.47 | 33.40 |
| 5.5 | 35.74 | 36.83 | 37.26 | 36.16 | 34.27 | 33.17 |
| 6.0 | 35.90 | 36.91 | 37.25 | 36.04 | 34.07 | 32.93 |
| 6.5 | 36.05 | 37.00 | 37.23 | 35.92 | 33.87 | 32.69 |
| 7.0 | 36.20 | 37.08 | 37.21 | 35.79 | 33.66 | 32.46 |
| 7.5 | 36.35 | 37.16 | 37.19 | 35.66 | 33.46 | 32.22 |
| 8.0 | 36.50 | 37.23 | 37.16 | 35.53 | 33.25 | 31.97 |
| 8.5 | 36.64 | 37.30 | 37.14 | 35.39 | 33.04 | 31.73 |
| 9.0 | 36.78 | 37.38 | 37.11 | 35.26 | 32.82 | 31.48 |
| 9.5 | 36.92 | 37.44 | 37.07 | 35.12 | 32.61 | 31.23 |
| 10.0 | 37.06 | 37.51 | 37.04 | 34.97 | 32.39 | 30.98 |
| 10.5 | 37.19 | 37.57 | 37.00 | 34.83 | 32.17 | 30.73 |
| 11.0 | 37.32 | 37.63 | 36.95 | 34.68 | 31.95 | 30.48 |
| 11.5 | 37.45 | 37.69 | 36.91 | 34.53 | 31.72 | 30.22 |
| 12.0 | 37.58 | 37.74 | 36.86 | 34.38 | 31.49 | 29.96 |
| 12.5 | 37.70 | 37.79 | 36.81 | 34.22 | 31.27 | 29.70 |
| 13.0 | 37.82 | 37.84 | 36.76 | 34.06 | 31.04 | 29.44 |
| 13.5 | 37.94 | 37.89 | 36.70 | 33.90 | 30.80 | 29.18 |
| 14.0 | 38.06 | 37.93 | 36.64 | 33.74 | 30.57 | 28.92 |
| 14.5 | 38.17 | 37.97 | 36.58 | 33.57 | 30.33 | 28.65 |
| 15.0 | 38.28 | 38.01 | 36.52 | 33.40 | 30.09 | 28.38 |

Average sunshine hour to be used on Priestley-Taylor model in the absence of data

| Jan | Feb | Mar | Apr | May | Jun |
|---|---|---|---|---|---|
| 8.30 | 8.17 | 7.56 | 7.53 | 7.03 | 6.41 |
| Jul | Aug | Sep | Oct | Nov | Dec |
| 4.88 | 4.87 | 6.13 | 7.47 | 8.30 | 8.33 |

**Priestley-Taylor method**

The Priestley–Taylor model (mm/day) allows potential evaporation $E_o$ (mm/day) to be computed in terms of energy fluxes without an aerodynamic component is given by:

$$E_o \text{ or } ET_o = \alpha \frac{\Delta}{\Delta + \gamma} E_r \quad (15)$$

Where α is Priestley-Taylor regional coefficient to be calibrated; Δ is slope of vapor pressure curve (kPa/$^o$C); γ is hygrometric constant (kPa/$^o$C); and $E_{PT}$ *is* evaporation estimate (m/s) based Priestley-Taylor method. $E_{PT}$ is in mm/day if Equation 15 is multiplied by 8.64x$10^7$.

In order to calibrate α, for Ethiopia condition, monthly regression is done between the Priestley-Taylor model estimate as independent variable and universal standard Penman model estimate $E_o$ as dependent variable (benchmark data generation). Similarly, regression is done between the Priestley-Taylor estimate (independent variable) and Reference Evapotranspiration Penman-Monteith model $ET_o$ estimate as dependent variable (benchmark data generation). Regressions validity are checked using $R^2$ criteria along with parameter significance. Models residuals are also checked for randomness. Such calibration approach has been employed elsewhere [10, 11].

Finally, for comparison of the performance of the calibrated Priestley-Taylor method is done with known temperature-based models of Blaney-Criddle and Enku's Simple Temperature Method [12] which are described below.

The Blaney-Criddle equation is expressed as

$$ET_O = p(0.46T_{mean} + 8) \qquad (16)$$

Where:

$ET_0$ = estimate of Reference Evapotranspiration (mm/day) averaged over the month

$T_{mean}$ = mean daily temperature (˚C), and p is mean monthly percentage of annual daytime hours and varies between 0.26 and 0.29.

The new simple empirical temperature method developed by Enku [12] is given by

$$ET_O = \frac{(T\max)^n}{k} \qquad (17)$$

Where $ET_0$ is the Reference Evapotranspiration (mm day−1);

n = 2.5

k = 48∗$T_{mm}$ – 330 for combined wet and dry conditions

k = 73∗$T_{mm}$ – 1015 for dry phase

k = 38∗$T_{mm}$ – 63 for the rain phase

$T_{mm}$ ($^oC$) is the long term daily mean maximum temperature for the seasons under consideration.

## RESULTS AND DISCUSSION

Climatic variables such as maximum and minimum temperature, relative humidity, sunshine hours and wind speed relationships with altitudes are checked. If significant, it has a potential for regionalization and to be used in absence of data. It is found that based on 167 stations data, annual minimum and maximum temperatures have significant linear correlations with altitude over Ethiopia (Figure 2) and are given by:

*$T_{min\ daily\ annual\ average}$ ($^oC$) = - 0.0061*Z (m) + 24.4 with $R^2$ = 0.81;* *(18)*

*$T_{min\ daily\ annual\ average}$ ($^oC$) = - 0.0065*Z (m) + 38.9 with $R^2$ = 0.86* *(19)*

In the absence of temperature data at a given location, estimate of the monthly distribution of temperatures as percentage of the mean annual average daily temperature estimated by Equations 18 and 19 are given in Table 2.

Table 2: Ratio of monthly distribution of temperatures.

| Monthly Temperature /Annual average | Ratio for Min. Temp | Ratio for Max. Temperature |
|---|---|---|
| Jan | 0.86 | 1.02 |
| Feb | 0.95 | 1.05 |
| Mar | 1.04 | 1.07 |
| Apr | 1.09 | 1.06 |
| May | 1.10 | 1.04 |
| Jun | 1.08 | 1.00 |
| Jul | 1.07 | 0.92 |
| Aug | 1.06 | 0.91 |
| Sep | 1.05 | 0.96 |
| Oct | 0.98 | 0.98 |
| Nov | 0.89 | 0.99 |
| Dec | 0.83 | 1.00 |

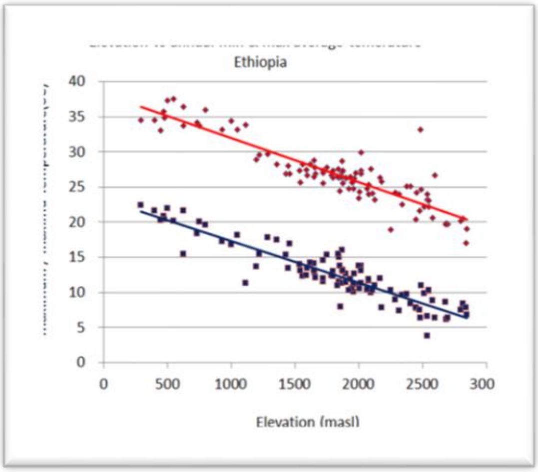


Figure 2: Correlations between annual mean maximum and minimum temperatures with station elevations based on 167 stations data.

On the other hand, as expected no significant correlations are found between relative humidity and altitude although there is a tendency to increase with altitude. It is also noted that Sunshine hours with altitude and wind speed with altitude do not have significant correlations although they have a tendency to decrease with altitude.

Priestley-Taylor coefficient α valid for Ethiopia has been developed based on 167 stations full climatic data representing all climatic zones and seasons. It is found that the Priestley-Taylor coefficient α for use in the estimate of open water evaporation $E_0$ is 1.11. The goodness of fit of the derived model is acceptable with $R^2$ is 0.91 and the residual is found to be random (Figure 3).

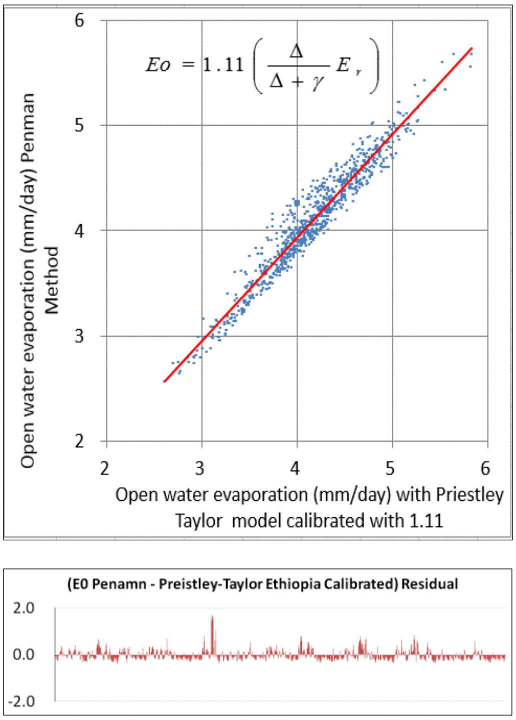


Figure 3: Regression between the Priestley-Taylor model estimate (independent variable) and Eo Penman model estimate (Open water evaporation) using full climatic data as dependent variable for each month of the 167 Class I stations in Ethiopia. Priestley-Taylor coefficient α is found to be 1.11 with $R^2$ = 0.91. The residual is random.

The calculated model standard error is found to be 0.26 (mm/day) and the 95% confidence interval of calibrated Priestley-Taylor α = 1.11 used for estimating $E_0$ is from 1.08 to 1.12.

To extend the Priestley-Taylor model applicability for irrigation water demand assessment, similar regression is made on Reference Evapotranspiration ETo estimated based on Penman-Monteith benchmark model as recommend in FAO 65 paper (Figure 4).

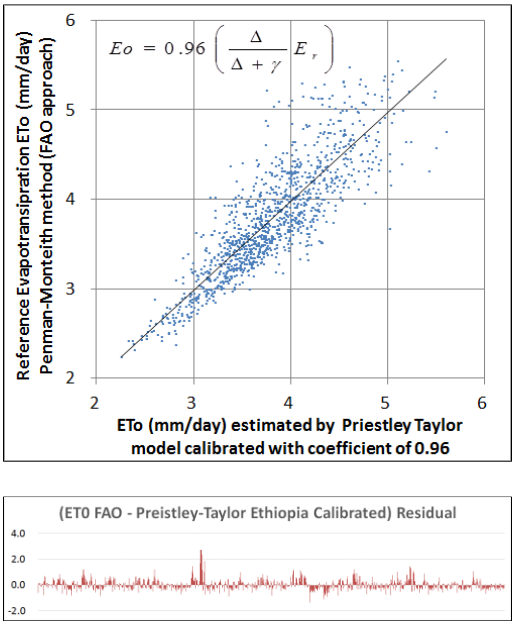


Figure 4: Regression between the Priestley-Taylor model estimate (independent variable) and $ET_o$

Penman-Monteith model estimate using full climatic data as dependent variable for each month of the 167 Class I stations in Ethiopia. Priestley-Taylor coefficient α is found to be 0.96 with $R^2$ = 0.91. The residual is random.

It is found that Priestley-Taylor coefficient α is 0.96. Estimated standard error is 0.39 (mm/day) and the 95% confidence interval of calibrated α = 0.96 for estimate for $ET_0$ is from 0.93 to 0.97.

Furthermore, seasonal variation of α is checked by using month to month regression. It is found that α used for open water evaporation value across the months is practically constant with maximum percentage of change from the average 1.11 is 3.6% in rainy months (Table 3), thus α = 1.11 is adopted for estimating monthly open water evaporation using Priestley Taylor model in Ethiopia.

Table 3: Calibrated monthly Priestley-Taylor coefficient α for estimating open water evaporation

| | α | *Stand Error of α* | *Lower 95% of α* | *Upper 95% of α* | *Model Stand error (mm/day)* | $R^2$ |
|---|---|---|---|---|---|---|
| Jan | 1.13 | 0.006 | 1.119 | 1.144 | 0.233 | 0.997 |
| Feb | 1.13 | 0.006 | 1.121 | 1.146 | 0.256 | 0.997 |
| Mar | 1.13 | 0.006 | 1.118 | 1.141 | 0.247 | 0.998 |
| Apr | 1.11 | 0.006 | 1.098 | 1.120 | 0.252 | 0.998 |
| May | 1.11 | 0.006 | 1.096 | 1.120 | 0.258 | 0.987 |
| Jun | 1.11 | 0.007 | 1.099 | 1.127 | 0.283 | 0.985 |
| Jul | 1.09 | 0.007 | 1.078 | 1.104 | 0.235 | 0.986 |
| Aug | 1.08 | 0.006 | 1.065 | 1.088 | 0.206 | 0.987 |
| Sep | 1.07 | 0.004 | 1.064 | 1.081 | 0.164 | 0.988 |
| Oct | 1.09 | 0.004 | 1.080 | 1.098 | 0.179 | 0.988 |
| Nov | 1.10 | 0.005 | 1.094 | 1.114 | 0.190 | 0.987 |
| Dec | 1.12 | 0.005 | 1.109 | 1.131 | 0.192 | 0.987 |

Seasonal variation of the Priestley-Taylor coefficient α for estimating Reference Evapotranspiration $ET_0$ has a maximum percentage change of 6.5% from base α = 0.96. Lower values of α occurred in rainy months of August, September and October (Table 4). thus α = 0.96 is adopted for estimating monthly the reference evapotranspiration using the Priestley-Taylor model in Ethiopia.

Table 4: Calibrated monthly Priestley-Taylor coefficient α for estimating Reference Evapotranspiration

| | α | *Stand Error of α* | *Lower 95% of α* | *Upper 95% of α* | *Model Stand error (mm/day)* | $R^2$ |
|---|---|---|---|---|---|---|
| Jan | 1.01 | 0.010 | 0.993 | 1.033 | 0.375 | 0.980 |
| Feb | 1.02 | 0.010 | 1.003 | 1.043 | 0.408 | 0.980 |
| Mar | 0.99 | 0.009 | 0.976 | 1.013 | 0.404 | 0.982 |
| Apr | 0.97 | 0.009 | 0.949 | 0.984 | 0.409 | 0.981 |
| May | 0.97 | 0.009 | 0.947 | 0.984 | 0.399 | 0.981 |
| Jun | 0.98 | 0.010 | 0.955 | 0.996 | 0.417 | 0.979 |
| Jul | 0.95 | 0.009 | 0.929 | 0.966 | 0.338 | 0.980 |
| Aug | 0.92 | 0.008 | 0.902 | 0.932 | 0.281 | 0.983 |
| Sep | 0.91 | 0.006 | 0.895 | 0.917 | 0.227 | 0.986 |
| Oct | 0.94 | 0.006 | 0.922 | 0.948 | 0.263 | 0.985 |
| Nov | 0.96 | 0.008 | 0.948 | 0.980 | 0.456 | 0.978 |
| Dec | 0.99 | 0.008 | 0.974 | 1.007 | 0.302 | 0.983 |

The present study clearly confirmed that the Priestley-Taylor evaporation model is required to be calibrated for local condition as there is more than 20% difference between the current estimates of α = 1.11 for open water evaporation estimate in Ethiopia and elsewhere. To illustrate, Priestley-Taylor coefficient adopted a general α = 1.26 Chow [3]. Castellvi et al [4] for the northern Spain recommended α between1.35 to 1.67. Shakir (2008) recommends for semi-arid region of India α = 1.31.

It is to be noted that recent development in USBR [13] study found that for accurate estimate of reservoir evaporation, measurement of weather variables should be done directly over the water surface (buoy weather station).

It is also known that in both arid and semi-arid areas air temperature is lower, relative humidity is higher, and wind speed is elevated when collected over water verses land. As there is no buoy based climatic weather station available in Ethiopia, all calibration of Priestley-Taylor model for Open water evaporation estimate was done based on weather data collected at land base 2 m height. It is recommended to conduct further research to refine the present finding of Priestley-Taylor α = 1.11 for Open water evaporation estimate by correlating buoy based and ground-based temperature measurements.

Finally, the performance of the calibrated Priestley-Taylor model for Reference Evapotranspiration is compared to Blaney-Criddle model and Enku's simple temperature model using bench mark $ET_o$ Penman-Monteith model. Blaney-Criddle method consistently over estimate $ET_0$ across Ethiopia by more than 26% when compared to bench mark $ET_0$ Penman-Monteith model estimate. Enku's model, which was developed based on Ethiopia data, is able to estimate $ET_0$ Penman-Monteith model using only mean daily maximum temperature with only 2.6% variation with bench mark $ET_0$ Penman-Monteith model estimate.

The present calibrated Priestley-Taylor model has less than 1% deviation and thus has a better performs due to its inclusion of local radiation and elevation data in the model. The local net radiation can be estimated using sunshine hours regional values and coordinate of project site using Eq.12 and Table 1.

## CONCLUSIONS

Estimating reliable reservoir evaporation and crop water requirements under inadequate data continue to be a challenge for practicing hydrologist and irrigation engineers and planners. This paper has developed reliable method for tropical Ethiopia under inadequate data condition for estimating evaporation by calibrating the Priestley-Taylor model which uses maximum and minimum temperature data and local data such as solar radiation and elevation. The Priestley-Taylor model applicable over Ethiopia for estimating open water evaporation $E_0$ and Reference Evapotranspiration $ET_0$ are given by $E_o \cong 1.11 \frac{\Delta}{\Delta + \gamma} E_r$ *and* $ET_o \cong 0.96 \frac{\Delta}{\Delta + \gamma} E_r$ respectively.

## ACKNOWLEDGEMENTS

The author is thankful for the National Meteorological Agency of Ethiopia for kindly providing the recent Class 1 stations climatic data. The author is also thankful for the anonymous reviewers' comments which contributed to the improvement of the work.

## REFERENCES

[1] Priestley, C.H.B. and Taylor, R.J. (1972). *"On the assessment of surface heat flux and evaporation using large-scale parameters."* Monthly Weather Review, 100: PP. 81–92.

[2] Shuttleworth, W.J. (1992). *"Evaporation."* In: Handbook of Hydrology, 551 pp., D.R. Maidment (Ed.). McGraw-Hill, New York.

[3] McMahon, T.A., Peel, L.M., Lowe, R,S, and McVicar, T.R, *"Estimating actual, potential, reference crop and pan evaporation using standard meteorological data: a pragmatic synthesis",* Hydrological Earth System Science 17:1331–1363, 2013.

[4] Chow, V.T., Maidment, D.R. and May, L.W, *"Applied Hydrology"*, McGraw-Hill: New York, 1988.

[5] Castellvi, F., Stockle, C.O., Perez, P. J. and Ibanez, M, *"Comparison of methods for applying the Priestley-Taylor model at a regional scale",* Hydrological Process 15: PP.1609–1620, 2001.

[6] Shakir, A., Narayan, C.G. and Ranvir, S. (2008). *"Evaluating best evaporation estimate model for water surface evaporation in semi-arid region, India."* Hydrological Process: Vol. 22, Issue 8, Pages 1093–1106

[7] Adem, A.A., Aynalem, D.W., Tilahun, S.A. and Steenhuis, T.S, "*Predicting Reference Evaporation for the Ethiopian Highlands"*, Journal of Water Resources and Protection. Journal of Water Resource and Protection, 9,1244-1269. https://doi.org/10.4236/jwarp.2017.911081, 2017.

[8] Berhanu B., Melesse, A.M. and Seleshi, Y. *"GIS-based hydrological zones and soil geo-database of Ethiopia",* Elsevier - Catena Vol 104: 21–31, 2013.

[9] Allen, R.G., Pereira, L.S., Raes, D., Smith, M, *"Crop evapotranspiration, guideline for computing crop water requirements",* FAO Irrigation and Drainage Paper # 56, 1998.

[10] Fisher, D.K. and Pringle Iii, H, "*Evaluation of Alternative Methods for Estimating Reference Evapotranspiration",* Agricultural Sciences, 4, 51. https://doi.org/10.4236/as.2013.48A008, 2013.

[11] Gotardo, J.T., Rodrigues, L.N. and Gomes, B.M, *"Comparison of Methods for Estimating Reference Evapotranspiration: An Approach to the Management of Water Resources within an Experimental Basin in the Brazilian Cerrado. Engenharia Agricola"*, 36, 1016-1026. https://doi.org/10.1590/1809-4430-eng.agric. v36n6p1016-1026/2016, 2016.

[12] Enku, T. and Melesse, A.M. "*A Simple Temperature Method for the Estimation of Evapotranspiration",* Hydrological Processes, 28, 2945-2960. http://onlinelibrary.wiley.com/doi/10.1002/hyp.9844, 2014.

[13] USBR, *"Improving Reservoir Evaporation Estimates."* Research and Development Office Science and Technology Program, Final Report ST-2012-7662-1, 2016.

# DESIGN AND IMPLEMENTATION OF VIRTUAL STUDIO TECHNOLOGY INSTRUMENT PLUG-IN FOR KIRAR

Exodus Getahun, Abykab Behailu and Menore Tekeba
zetsgtmu@gmail.com, abykabbehailu11@gmail.com, menore.tekeba@aait.edu.et
School of Electrical and Computer Engineering, Addis Ababa Institute of Technology, AAU

## ABSTRACT

*With the rapid increase of computing resources within the last decade, several real-time applications such as sound editing and processing are becoming more popular. Virtual Studio Technology (VST) was introduced by Steinberg Media Technologies GmbH in 1996 which provided a platform for sound effect developers to implement their own effect plugins. In 1999 a standard framework for software sequencers, so called VST instruments (VSTi), was introduced in which music instruments are simulated in the virtual studio. To design an instrument as part of the virtual studio, a series of steps from audio sample collection and recording to integrating the samples using a plug-in to the VST is required. To the best of our knowledge, there is no VSTi plugins developed for Ethiopic music instruments so far. Therefore, we have effectively used the structure of the VSTi API and its Software Development Kit (SDK) tools to design and implement a plugin for Kirar (Ethiopian music instrument) and effectively integrated and tested. Our plugin was successfully recognized and operated in the Cubase5 and FL studio Digital Audio Workstations (DAWs) as a VSTi instrument which initiates its own graphical user interface (GUI) with full mouse and keyboard controls having 3 level Musical Instruments Digital Interface (MIDI) mapping.*

**Key Words**: DSP, Kirar, MIDI, VSTi,

## INTRODUCTION

Virtual Studio Technology is an interface for integrating audio synthesis and effects plugins with DAW. In simple terms it is a way to get all those hardware instruments effects like racks, key boards and drum machines into music software such as Cubase, FL Studio or Logic Pro and others [1]. According to statement given in [2], VST allows the integration of virtual effect processors and instruments into your digital audio environment. It also includes software recreations of hardware effect units and instruments or new creative effect components into the VST systems [2].

With VST, Steinberg founded the world’s leading and most widely supported standard for plug-ins and virtual instruments in 1996 for the first time in Germany [2]. A few years later, in 1999, Steinberg updated their VST specification which also allows VST plug-ins to receive MIDI data [3]. The current VST version is VST 3.x and marks an important milestone in audio technology with a code base providing many new features with the most stable and reliable VST platform ever. These VST modules have the sound quality of the best hardware units, yet are far more flexible [2]. Prior to 1996 DAW had been used to control keyboards and samplers via

MIDI and then routing all their external hardware through a traditional mixing desk to produce digital music [3].

Since the VST3 SDK is available as a free technology, open in use for any developer, we have used this SDK for our plug-in development and testing [2]. The VST technology is now a days serving as one focal point in machine human interaction to track finger movements in order to take inputs from human fingers movements an instruction to a VST system [4].
In the musical world, there are so many issues which need to be addressed in order to fulfill as possible as desires of music producers and composers. As a composer or musical producer, one needs to have full pack of the required software and hardware gear.
From the many software gears needed, one of the most powerful and modern tool of the time is having adequate VSTi instrument plugins at hand. This raises a question of do we really have enough plugins in the market?

The answer is no, and that's because hundreds of plugins are made and improved every year since the technology has been created in 1996.
One other big factor for creating more VSTi plugins in the industry is that, the more civilized countries become and try to build their musical industry, the more they become digitalized.

This leads to creating a virtual studio technology instrument plugin for their cultural instruments. This approach has been a trend in the musical industry as many of the major musical instrument developer companies have a world and ethnic category on their sound banks.

This brings us to the conclusion that there has to be a VST plugin which represents Ethiopian unique traditional instruments in the industry.
Therefore in this paper, we are going to show the development of VSTi plug-in for Ethiopian traditional music instrument known in Amharic language as Kirar. Important steps of audio sample recording, different digital signal processing methods, development of important modules of the plug-in and its GUI, integration with VST systems and testing are shown in the paper.

## LITERATURE REVIEW

The research article given in [5] presents the review of the impact of VST systems and realization of different hardware instruments into the VST systems in the form of the plug-ins. It discusses the impact of the existence of all those massive instruments in music production industry. It also presents wide spread use of VST and the plug-ins. It concludes that the VST technology has totally revolutionized the music production world and the VST instrument plug-ins are very important components in the VST systems.

The research work given in [6] shows the automatic generation of VST audio plug-ins from MATLAB code using the Audio System Toolbox from Math Works. It provides MATLAB code for three complete examples of plug-ins, discusses problems that may be encountered in generating the plug-ins automatically, and describe a workflow to generate VST plug-ins as quickly and easily as possible.

The dissertation given in [7] discusses the impact of using digital production technologies especially for music production and has made three approaches of the investigation on the impact from multiple perspectives. It also concludes that the digital music technology has made a huge impact on the pedagogical and professional industry because it creates new directions for effectiveness and efficiency of technology implemented for music composition and pedagogy.

A similar work of ours has been done in Plectra series 4 for Turkish traditional music instrument known as Oud as it is given in [10] by Dimitris Plagiannis. As it is shown in Figure 1, they have developed a plug-in of Turkish Oud for commercial purpose and the web article lists the features of the plug-in developed.


Figure 1: GUI of the Turkish Oud VSTi [10]

The importance of VST technology and the plug-ins of hardware instruments to be used in VST systems is well-known and all the literatures supports this statement. Therefore, for Ethiopic style music to play important role in the global music market, the indigenous and traditional music instruments shall have their own plug-ins in the VST systems and this research project has designed, implemented a VSTi plug-in for Kirar and the developed plug-in has been successfully integrated and tested in CUBASE and FL Studio DAWs.

### VST PLUG-IN

Even in its earliest incarnation, the VST system allowed third-party developers to produce real-time effect modules that could “plug in” to the host application (initially Cubase). But later, Steinberg introduced the second version of the VST plug-in standard, which enables to send MIDI data to and from such effects.

This opened an opportunity to developers to add more features such as MIDI control of effect parameters and locking of effect settings to tempo and integrate new instruments into the VST systems for more diverse effects and controls on the soft music productions.

Such advancements in protocol latter enabled MIDI information to be used to run synthesis engines, rather than just simple effects processors [3].

According to the web article on [8], a plug-in is a software unit, which does not usually function by itself, which comes to be grafted as part of a more complex program and enhances the functions of this program. Initially plug-ins appeared on graphic creation software like Photoshop in the form of filters, XPress with Xtensions, the concept of the plug-in was then transposed in to the digital audio domain.

With the audio effects plug-ins which can add audio effects like reverb to the MIDI/Audio sequencers and to the digital audio software and more recently in the form of instruments plug-ins which can add a synthesizer or a virtual sampler to the Midi/Audio program.

For the users these plug-ins have so many advantages such as creation of a modular software configuration, according to the needs, consequently reducing the cost of configuration
[8]. Figure 2 shows example of the instrument plug-ins for NI Guitar Rig 5 which works with VST as multi-effect processor


Figure 2: NI Guitar Rig 5 VST – Guitar multi-effects processor [9]

## Design and Implementation of VSTi plug-in for Kirar

In the process of making VSTi for Kirar, we choose to implement it through four phases. In the first phase, we have collected samples and made pre-processing on the samples of Kirar audio data. In the second phase, we have chosen the DSP methods and algorithms to add effects on the samples collected. Then in the third phase, the software of the plug-in was developed using C++ following MIDI API standards. In the last phase, the plug-in developed has been integrated with the major DAW Platforms (CUBASE and FL Studio in this case) and we have tested the plug-in with these two DAW systems. The phases of the development are described from Sections 4.1 to 4.4 as follows:

### Sampling and Audio Collection of Kirar Music Instrument

Since Kirar has got the standard discrete sounds of music, we sampled 12 WAV files, each representing the 12 default root key/note scale values of a standard MIDI keyboard for 3rd octave. We used standard key frequencies for the third octave only as given in Table 1 below [11] and we have collected the samples for the octave as Kirar is functional for one octave only. We used a standard condenser microphone (Beringer-B1), USB sound card (AVID) and professional audio recorder DAW software (Cubase 5). Then we used audio tuner software (Audio Tuner v1.0) to tune the Kirar in the required frequency. We have made an emphasis on the tuning accuracy of the recorded samples by refining the pitch values so that they go with standard frequency values.

After sampling the KIRAR with standard sampling frequency of 44.1 KHz and root key value, our result was 12 independent 32 bit .WAV sample files, meaning one for each of the 12 notes. As shown in Figure 3, sampling and pitch correction GUI in the VST helps us to see the effect of our sampling.

In addition we have sampled more layers of samples to achieve the 3-level MIDI mapping. The challenges are in getting the samples and accurately deciding on the parameters of the envelope function used.

Table 1: Standard key frequency in hertz (Hz) for the three octaves [11]

| Octave<br>Note | 1 | 2 | 3 |
|---|---|---|---|
| **C** | 32.703 | 65.406 | 130.81 |
| **C♯/D♭** | 34.648 | 69.296 | 138.59 |
| **E♭/D♯** | 36.708 | 73.416 | 146.83 |
| **E** | 41.203 | 82.407 | 164.81 |
| **F** | 43.654 | 87.307 | 174.61 |
| **F♯/G♭** | 46.249 | 92.499 | 185.00 |
| **G** | 48.999 | 97.999 | 196.00 |
| **A♭/G♯** | 51.913 | 103.83 | 207.65 |
| **A** | 55.000 | 110.00 | 220.00 |
| **B♭/A♯** | 58.270 | 116.54 | 233.08 |
| **B** | 61.735 | 123.47 | 246.94 |

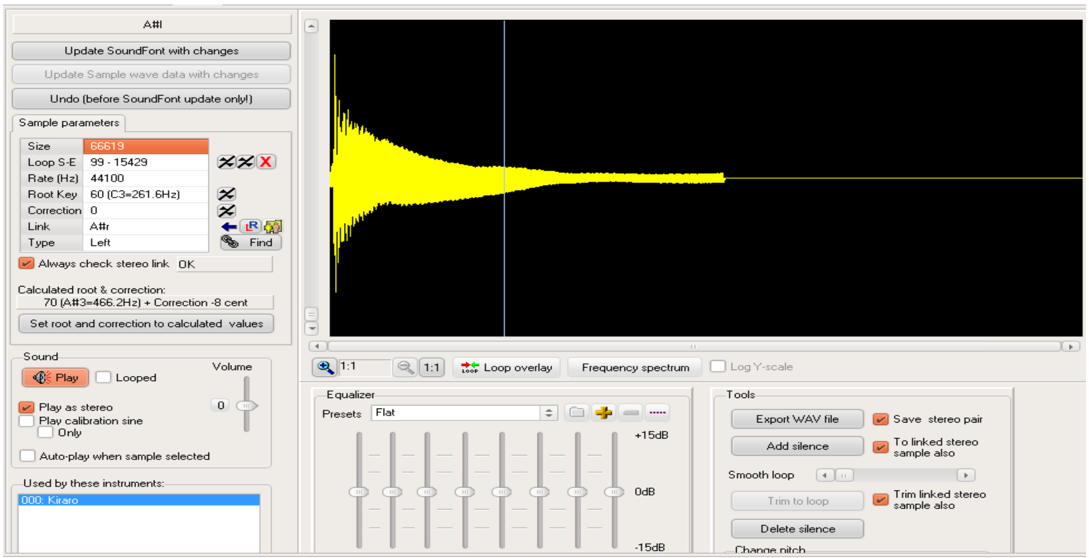

Figure 3: Sampling and pitch correction

## DSP Methods used to Process Samples

After the samples are recorded and collected, different types of processing modules are implemented. Some of the methods used are:

**Midi Filter:** The MiDi Filter receives the input signal and filters it by root key/note and velocity then sends to next module. It allows controlling each MiDi input to give a MiDi output (no generators, no synthesis). We have used the VSTi SDK's built-in MiDiFilter module.

**MidiToCv:** After receiving a filtered input from, MidiFilter, MidiToCv controls the voltage and multiplexes the gate to the Oscillator and Attack, Decay, Sustain and Release (ADSR) module. In addition, it sends the pitch and velocity of the input to the Oscillator.

**KirarOscillator:** An oscillator is a repeating waveform with a fundamental frequency and peak amplitude which forms the basis of most popular music synthesis techniques these days. In addition to the frequency or pitch of the oscillator and its amplitude, one of the most important features is the shape of its waveform. Different types of oscillators, based on their shape, are sinusoidal oscillator, square wave oscillator, saw tooth oscillator, triangular oscillators and others [12]. We have used the built-in VST oscillator with low frequency for our plug-in development.

**ADSR:** An envelope generator (sometimes, called a transient generator) makes an audio signal that smoothly rises and falls as if to control the loudness of a musical note automatically. Amplitude control by multiplication is the most direct, ordinary way to use one, but there are many other possible ways. Even though Envelope generators have come in many forms over the years, ADSR envelope generator is the simplest and favorite one. ADRS is the short form of Attack, Decay, Sustain and Release which combines the four DSP operations on audio input [13]. The concept of ADRS is associated with the principle that the sound output of musical instruments does not immediately build up to its full intensity nor does the sound fall to zero intensity instantaneously. That means it takes a certain amount of duration for the sound to build up in intensity and a certain amount of period for the sound to die away as well. The interval during which a musical tone is building up to some amplitude (volume) is called the "attack time" and the period required for the tone's intensity to partially die away is called its "decay time". The time of attenuation at the final stage is known as "release time". Several instruments also allow holding of a tone for certain period of time known as "sustain time". The sustain time helps to achieve various note durations in music composition [14] as it is shown in Figure 4.

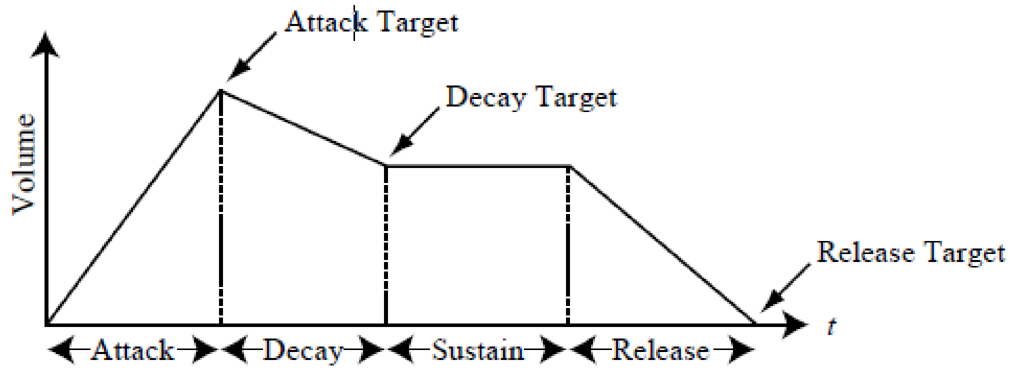


Figure 4: Classic ADSR envelope [14]

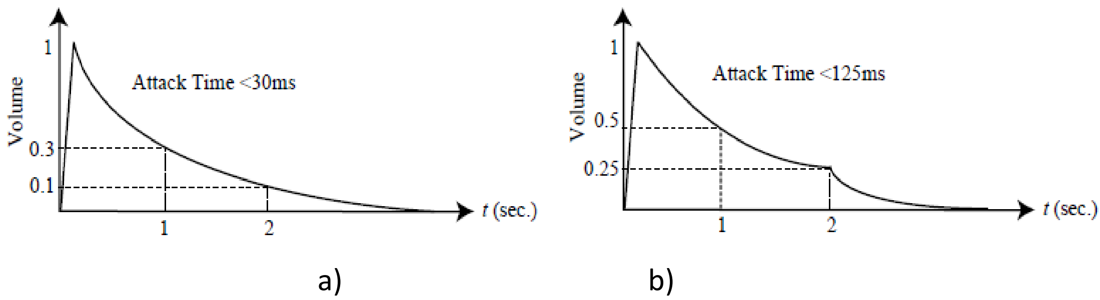


Figure 5: (a) ADSR envelopes for guitar, (b) ADSR envelopes for piano [14]

A synthesizer duplicates (increases intensity in case of Attack and decreases intensity in cases of Decay and Release) the intensity (volume) variation of the tone by multiplying (modulating) the amplitude of the sinusoid with a scale factor dictated by the ADSR envelope, a(t) as it is given in [14].

$$y(t) = a(t) * x(t) \tag{1}$$

In our plug-in development, we have used the ADSR envelope given for piano in Figure 5(b) above since piano is similar to kirar, as they both have a discrete time value and their sound pitch is basically the same.

**Design and Implementation of the Plug-in Software**

We designed our plugin in a way that it works on different DAW platforms which support the VSTi plug-in format. The “Kirar VSTi” first version got two basic features which are the SoundFont oscillator and Release DSP feature.

The features are powered with a simple graphical user interface which includes a loader button for the sound font file along with graphical slider for controlling the release DSP feature. The plugin works seamlessly on Cubase 5. The GUI of our plug-in inside the Cubase DAW is shown in Figures 6 to 8.

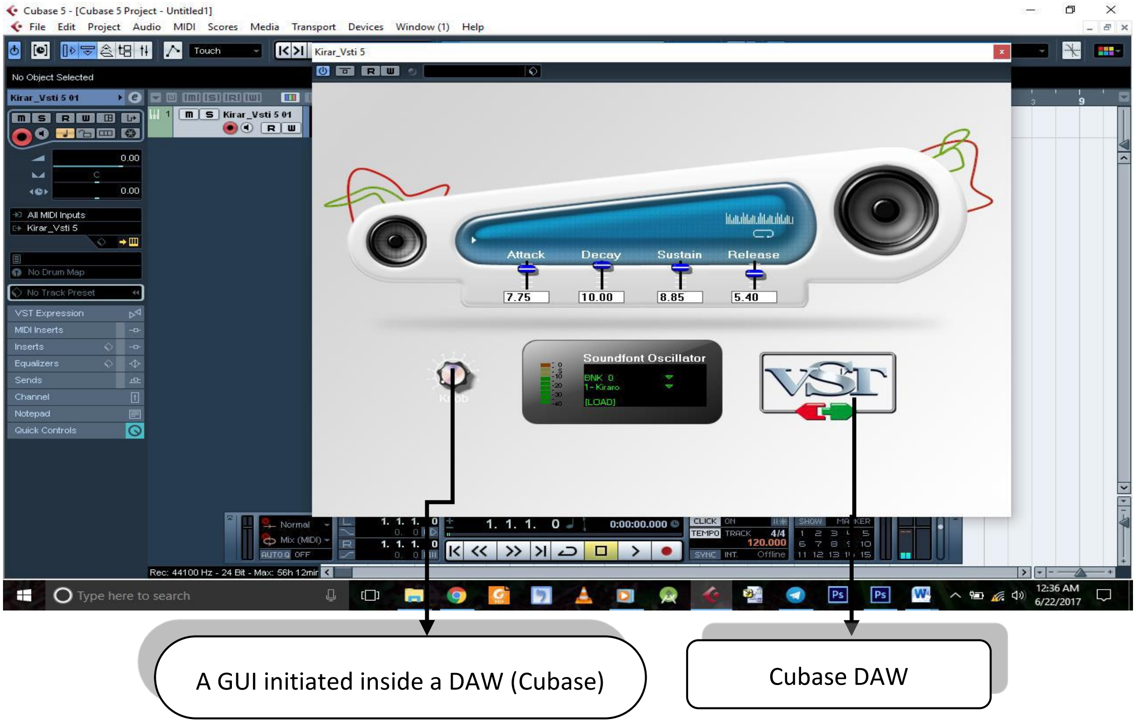


Figure 6: System Design

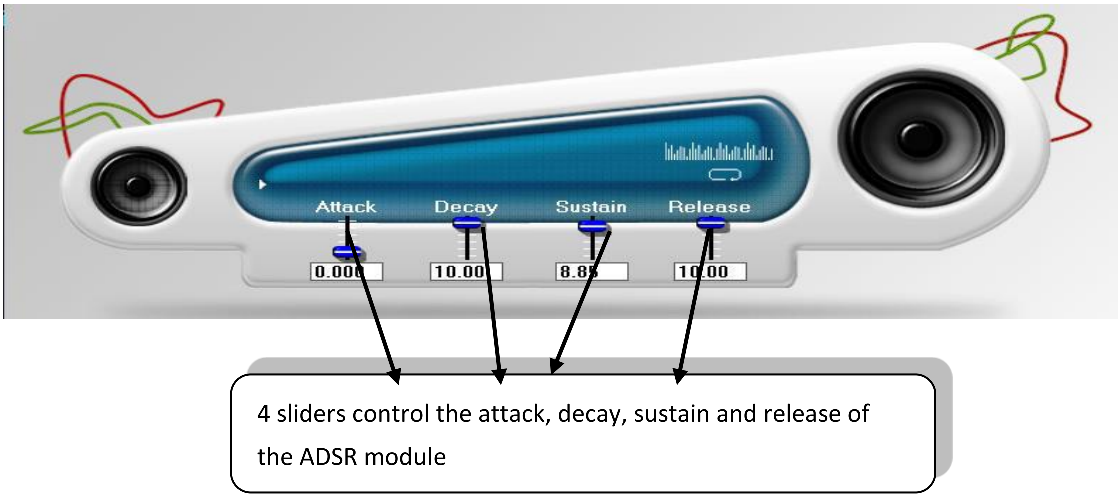


Figure 7: ADSR module

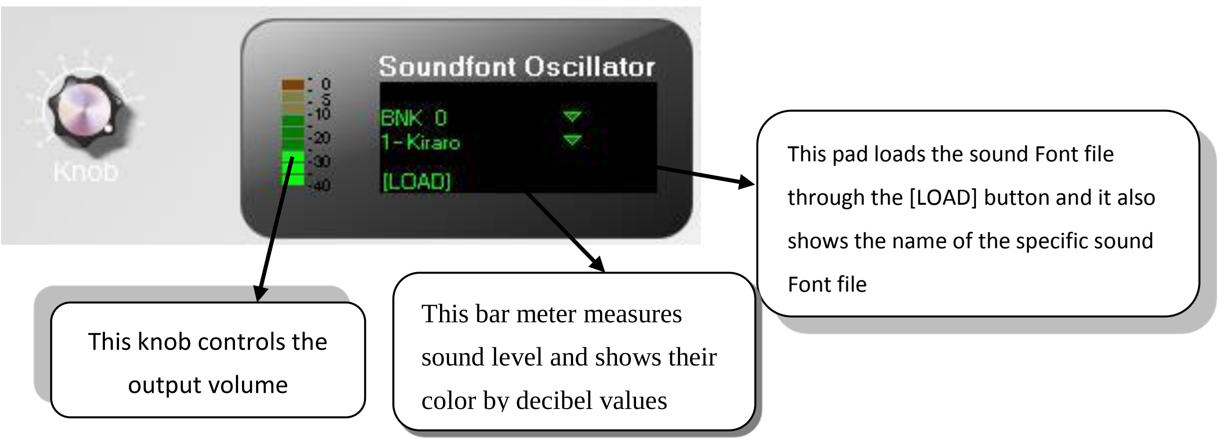


Figure 8: GUI Description

The designed plug-in has the following components:

**Keyboard module:** This module defines and identifies each of the keyboard key notes independently and it makes the system ready to be played through a computer and MIDI keyboards. Its inputs and outputs are MIDI data.

**IoMod module:** This module takes care of the inputs received from the keyboard and sends the output to the "Sound Out" module.

**Midi Filter module:** This module receives the input received through "IoMod" and filters it by root key/note and velocity and sends to the "Midi To Cv" module.

**Midi To Cv module:** After receiving a filtered input from "Midi Filter" module, this module controls the voltage and multiplexes the gate to the "Oscillator" and "ADSR" module. In addition, it sends the pitch and velocity of the input to the "Oscillator".

**Kirar Oscillator module:** After receiving a controlled volume input from "Midi To Cv" module, it generates/produces a pure tone by shaping the waveform of the input.

**ADSR module:** This module takes care of supporting the basic four VSTi standard digital signal process effects namely Attack, Delay, Sustain and Release given from number 7 to 10 below.

**String Release module:** This module controls and sets the degree of "release" working in cooperation with the "ADSR" module. With a slider supported with GUI, it increases the release from the value of [0.00 to 10.00] with a double precision.

**Attack module:** This module controls and sets the degree of "attack" working in cooperation with the "ADSR" module. With a slider supported with GUI, it increases the attack from the value of [0.00 to 10.00] with a double precision.

**Decay module:** This module controls and sets the degree of "decay" working in cooperation with the "ADSR" module. With a slider supported with GUI, it increases the decay from the value of [0.00 to 10.00] with a double precision.

**Sustain module:** This module controls and sets the degree of „sustain' working in cooperation with the "ADSR" module. With a slider supported with GUI, it increases the sustain from the value of [0.00 to 10.00] with a double precision.

**Peak Meter:** A LED Bar Graph style volume meter, calibrated in decibels. It uses colored LED bars; with green for normal volume (40dB-10dB), yellow for high volumes (10dB-5dB) and red for maximum volume (5dB-0dB).

**VCA module:** This module receives input from the "Oscillator" and "ADSR" modules and lets the DAW control the signal and the volume of the sound and sends it to the "Sound Out" module ***through IO mod*** for further process.

**Sound Out module:** This module receives the final output from the VCA through its left and right pins and handles the communication between the DAW's soundcard in order to handle playing the sounds.

**GUI module:** This module takes care of the simple GUI we managed to build for demo purposes. We have two GUI functions which are the "StringRelease" slider which helps to control the DSP process and the sound font loader button.

The procedural programming design and components are shown below on Figure 9.

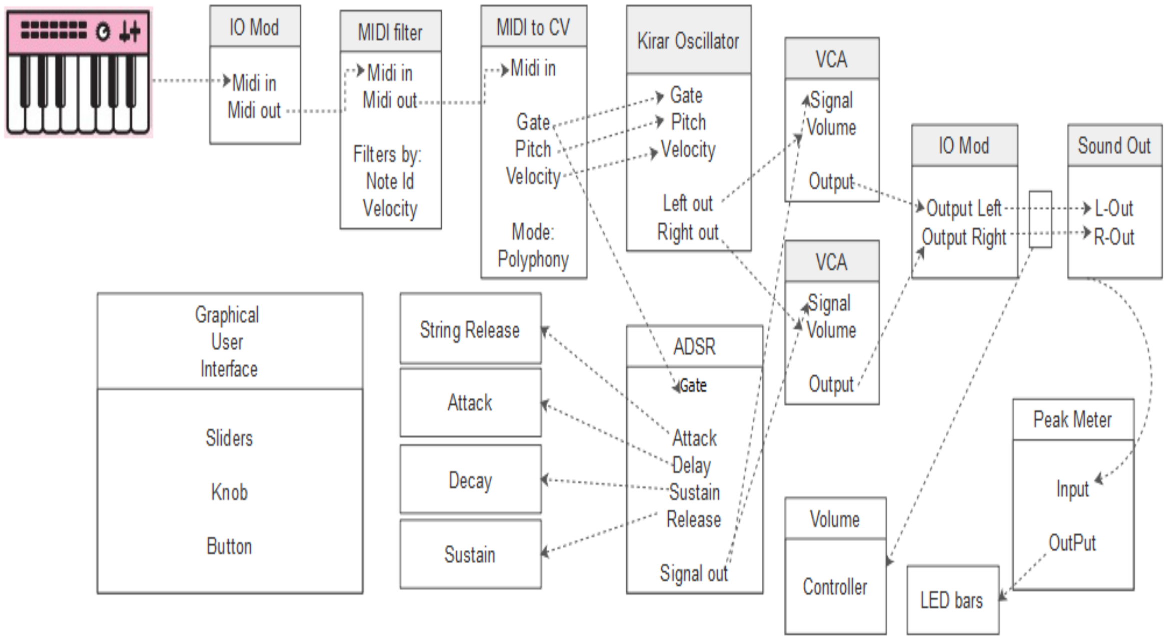


Figure 9: Procedural programming design and components diagram

## Integration and Testing in VST Systems

To integrate the code and the samples, we used Sound Font file system architecture (.sf2). This was the biggest improvement we added on our initial research project plan.

What the Sound Font file system architecture does here is that it completely separates the coding of basic classes from the file system architecture which will later let us to improve the quality of WAV samples along with recording more of them without changing the programming classes, method and the code.

The tool we used for creating the Sound Font file system (.sf2) is Vienna programming language.

Using the results we got from the sampling process, we managed to create a single Sound Font (.sf2) file, which replaces and holds all 36 samples as one.

By classifying the making process of the plug-in into main modules, we managed to create 14 independent modules, which are put together to create a system which takes a Sound Font file as an input and gives an output of an oscillated audio stream.

We have also taken care of implementing the 3-level MIDI mapping which resulted in creating an intensity based volume creation for the plugin.

Creating an appealing genuine GUI was also implemented for the plug-in so that we can get an easy and interactive program platform.

Finally a window installer .exe file was created in order to simplify the hardship of installing the plug-in.

As shown in section 4.3 above, the plug-in has been tested with Cubase 5.x as well as FL Studio DAW platforms and it worked flawlessly and was recognized as VST instrument plug-in in these platforms.

It could also initiate its own GUI in these DAW platforms.

The plug-in also managed to work seamlessly with both mouse and computer keyboard controls of the GUI.

Our plugin managed to be successfully played, recorded, re-shuffled and quantized inside the DAW.

The 3-level MIDI mapping worked to initiate intensity based sound as we tried playing it using a professional MIDI controller keyboard.

## CONCLUSIONS

We have successfully designed and implemented the plug-in for Kirar that can work in DAW platforms so that music composers can easily use the Ethiopian Kirar in their VST systems of soft music compositions.

We have collected samples for the third octave keys, made processing of audio signals and achieved the 3-level MIDI mapping. Our plug-in has been developed, integrated with Cubase 5.x and FL Studio DAW platforms and we have made a thorough test on the plug-in.

Our test result shows that our plug-in works flawlessly in these DAW platforms. We believe that our contribution in making the software models of our traditional music instruments is immense in delivering VSTi Plug-in for Kirar even though very much work is left undone in developing similar plug-ins for other Ethiopic traditional music instruments that our contribution in making the software models of our traditional music instruments is immense in delivering VSTi Plug-in for Kirar even though very much work is left undone in developing similar plug-ins for other Ethiopic traditional music instruments.

### Future Works

Even though we have addressed several challenges, our design and development has some issues which are not still addressed. These limitations of the current research project can be interesting future research directions. Some of these limitations are:

Numbers of samples are still 36 which is a lot less when we compare it to professional VSTi plugin software platforms.

This is because of the lack of equipment and standard sound proof studios which can give us more precise and quality audios.

By increasing the number of samples, the plug-in spectral diversity and hence its effects can be improved.

The sound Font files loads all of the sampled audio files altogether on the RAM, which creates problems on computers with limited RAM resources.

So by taking the average of keys a kirar player could play at a time, we limited the polyphony of the plugin to 3 keys at a time. Which means it can only play 3 notes at a certain time. By making optimizations of memory usage, all the keys can be played and used at a time.

## REFERENCES


[1]. Steinberg. VST3: New Standard for Virtual Studio Technology. Steinberg (2013), http://www.steinberg.net/en/company/technologies/vst3.html (Accessed on: June 24, 2017)

[2]. Tanev, George, and Adrijan Božinovski. "Virtual Studio Technology inside Music Production." *ICT Innovations 2013*. Springer International Publishing, 2014. 231-241.

[3]. Hsu, Mu Hsen, Timothy K. Shih, and Jen Shiun Chiang. "Real-time finger tracking for virtual instruments." *Ubi-Media Computing and Workshops (UMEDIA), 2014 7th International Conference on*. IEEE, 2014.

[4]. Tanev, George, and Adrijan Bozhinovski. "Virtual Studio Technology and Its Application in Digital Music Production." (2013): 182-186.

[5]. DeVane, Charlie, and Gabriele Bunkheila. "Automatically Generating VST Plugins from MATLAB Code." *Audio Engineering Society Convention 140*. Audio Engineering Society, 2016.

[6]. Han, Jinseung. *Digitally Processed Music Creation (DPMC): Music composition approach utilizing music technology*. Diss. Teachers College, Columbia University, 2011.

[7]. Claude Borne. The Audio Plugins, Claude Borne (2003), http://www.macmusic.org/articles/view.php/lang/en/id/62/The-Audio-Plug-ins (Accessed on: June 27, 2017)

[8]. Hitsquad. Guitar Rig 5.2.0 for Windows XP/7/Vista. Hitsquad Pty Ltd. (2013), http://www.hitsquad.com/smm/programs/GuitarRigWin/screenshot.shtml (Accessed on: June 27, 2017)

[9]. Plectra Series 4 Plug-in for Turkish Oud, https://impactsoundworks.com/product/plectra-series-4-turkish-oud/#details (Accessed on: June 27, 2017)

[10]. Physics of Music, Frequencies for equal-tempered scale, http://www.phy.mtu.edu/~suits/notefreqs.html (Accessed on June 28, 2017)

[11]. Wikibooks. Sound Synthesis Theory, Oscillators and Wavetables - Wikibooks, open books for an open world, https://en.wikibooks.org/wiki/Sound_Synthesis_Theory/Oscillators_and_Wavetables (Accessed on: June 28, 2017)

[12]. Puckette, Miller. *The theory and technique of electronic music*. World Scientific Publishing Co Inc, 2007.

[13]. De Leon, Phillip L. "Computer Music in Undergraduate Digital Signal Processing." *American Society for Engineering Education/Gulf Southwestern Region (Las Cruces, NM.)* (2000).

# MODELING AND SIMULATION OF TRACTION OF POWER SUPPLY SYSTEM CASE STUDY: MODJO-HAWASSA RAILWAY LINE IN ETHIOPIA

Getachew Biru Worku and Aseged Belay Kebede
[1]School of Electrical and Computer Engineering, Addis Ababa Institute of Technology, AAU
[2]Africa Railway Center of Excellence, Addis Ababa Institute of Technology, AAU
Corresponding Author's Email: gbiru@yahoo.co.uk

## ABSTRACT

*This paper presents the modeling and simulation of traction power supply system case study of Modjo-Hawassa railway line in Ethiopia. In this particular case a 2 × 25 kV autotransformer fed traction power supply system model is developed. The traction performance of a railway system depends on the variation of the voltage along the overhead lines. In this study, the voltage profile along the traction line has been evaluated. The system has been investigated by applying different headway distances on the trains and by increasing the number of train along the feeding section. The load flow simulation results using Matlab software show that the voltage profile in the feeding circuit differs substantially depending upon the train positions, train current, numbers of trains in the same power-feeding section and track impedance. The minimum calculated pantograph voltage and maximum percentage voltage regulation are 22.93 kV and 8.28% respectively with a maximum rail line potential of 66.2 V. These computed values are within the tolerable voltage range of the industry standard. Hence, the simulation result verified the validity of the system being adopted.*

**Keywords:** *Modeling Autotransformer, Traction power supply, Voltage profile, Simulation*

## NTRODUCTION

For more than a decade, railway system has experienced a renaissance in many countries after several years of stagnation period, including in Ethiopia. The main reasons for the renewed interest in the railway development are economic, environmental, and safety related. This has quite naturally, in turn, increased both passenger and freight transports on railway. In order to cope with this increase, large railway infrastructure expansions are expected. An important part of this infrastructure is the railway power supply system
without it, only the weaker and less energy efficient steam and diesel locomotives could be used [1]. An accurate power supply system analysis offers important information for planning, operation and design. Almost in all traction power supply system analysis or study the widely adopted trend and cost effective mechanism is simulation. In [2], widespread application which deals with many
railway power feeding system simulators were discussed. In this study, a different approach, using MATLAB, is developed.

Several alternatives analysis methods are used for designing the electrical scheme of the power supply system for electrified railways [3]. Selection of an appropriate supply system is always very dependent on the railway system objectives. Many studies show that direct linking of the feeding transformer to the overhead catenary system and the rails at each substation is relatively simple and economical. Nevertheless, there are some drawbacks to this arrangement such as high impedance of feeders with high losses, high Rail-to-earth voltage and the interference to neighboring communication circuits [2,4].On the other hand, the autotransformer feeding configuration has many advantages and solves many disadvantages of the direct feeding system. The addition of autotransformer (AT) at every 8-15 km intervals improves the voltage profile along the traction line and increases the substation distance up to 50-100 km [4]. The electromagnetic interference in an AT system is normally much more lower compared with direct feeding (1 x 25 kV) system [5]. In addition, for high power locomotive and high speed trains direct feeding system is out of choice because of this most countries are replacing 1 x 25 kV system with 2 x 25 kV [6]. In this paper, analysis, modeling and simulation of autotransformer traction power supply system is presented and a comparative analysis in terms of voltage profile along the traction network is performed.

## SYSTEM CONFIGURATION

In this system, the traction transformers are supplied from state grid, at 132 kV voltage levels. This voltage is further stepped-down to 55 kV at traction substation by using 132/55 kV transformers with center tap on the secondary side to have ±27.5 kV between the center-tap and the respective terminals. Each traction substation has two 132 kV independent power lines. The secondary terminal of the traction power transformers are selected to give a voltage of ±27.5 kV in order to compensate for any voltage drop caused by power supply line prior to the catenary system. The nominal voltage of the catenary system is considered to be 25 kV.

In addition, the system consists of center-tapped autotransformers located at every 15 km of which the outer terminals are connected between the catenary and feeder wire. The autotransformer-fed system enables power to be distributed along the system at higher than the train utilization voltage. As a nominal value, power is distributed at 55 kV (line-to-line) while the trains operate at 25 kV (line-to-ground). The system voltages for the proposed system conformed to European standards EN 50163: 2004 [7] and its values given by the above standards are as follows.

1. The nominal voltage shall be 25 kV.
2. The maximum permanent voltage allowed in the supply line shall be 27.5 kV.
3. The maximum non-permanent voltage that should be allowed for a short period of time shall be 29 kV.
4. The minimum permanent voltage shall be 19.0 kV.
5. The minimum non-permanent voltage that should be allowed for a short period of time shall be 17.5kV.

### FORCES ACTING ON THE TRAIN

Train, as a load, is on the move and considered to be one of the main problems of longitudinal rail dynamics and is governed by the Fundamental Law of Dynamics applied in the longitudinal direction of the train's forward motion [8].

$$F_t - F_{ex} = m^* a \qquad (1)$$

The term to the left of the equal sign as shown in equation (1) is the sum of all the forces acting in the longitudinal direction of the train, where "$F_t$" is the tractive or braking effort and "$F_{ex}$" is the forces that opposes the forward motion of the train. "$m^*$" is the total mass (train mass + passenger or freight mass) of the train but due to rotational inertia effect the effective linear mass of the train increases and this value varies from 5% to 15% depending on the number of motored axles, the gear ratio and the type of car construction and "a" is the longitudinal acceleration experienced by the train. Various literatures [9, 10, 11] shows different countries use different starting acceleration that ranges from $0.08\ \mathrm{m/s^2}$ to $0.25\ \mathrm{m/s^2}$ for freight trains.

**Forces against the train**

The total forces acting on a train against its direction of motion ($F_{ex}$) can be expressed mathematically as follows:

$$F_{ex} = F_r + F_{gr} + F_c \qquad (2)$$

Where $F_r$ is mechanical and aerodynamics resistance, $F_{gr}$ is gradient resistance,, and $F_c$ is curves resistance.

**Mechanical and Aerodynamic Resistance**

The force created due to mechanical and aerodynamic resistance, $F_r$ is given by:

$$F_r = A + Bv + cv^2 \qquad (3)$$

Generally $A + Bv$ is rolling resistance and $cv^2$ is aerodynamic resistance. The value of A can be approximately computed as [12]:

$$A \approx 2450 + 175 N_{axle} (\mathrm{N}) \qquad (4)$$

$N_{axle}$ is number of trailing car axle and coefficient B can be expressed as a function of total train length rather than train mass.

$$B \approx -22 + 0.58 L_T (N\, s/m) \qquad (5)$$

Where,$L_T$ is the total length of the train. The aerodynamics drag, the part which dependent upon the speed squared is usually written for no wind condition as:

$$F_D = \frac{1}{2} \rho A_f C_D v^2 = cv^2 \qquad (6)$$

Where $A_f$ is the projected cross sectional area, $C_D$ is the air drag area and ρ is the air density which is equal to $1.3\mathrm{kg/m^3}$.

**Gradient Resistance**

Gradient resistance is also the component of the train load against the direction of travel. It is positive for uphill gradients and negative for downhill gradients (i.e. pushes the train forward). Thus the gradient resistance is determined by:

$$F_{gr} = i10^{-3}mg \quad (7)$$

Where $i$the percentage gradient, m is is the mass of the train and $g$ is gravitational acceleration. For freight and passenger lines, the location where the maximum gradient needs to be used in design. Therefore, for the profile design of railway, we need to lower the maximum gradient to ensure the freight train passes through this section at no less than calculated speed.

**Curve Resistance**

Additional curving resistance $F_c$ mainly corresponds to the increased energy dissipation that occurs in the wheel rail interface, due to sliding motions (creep) and friction phenomena, at curve negotiation. It is dependent on wheel rail friction and the stiffness and character of the wheel set guidance. The resistive force produced by the curve is modeled by the following equation [12]:

$$F_c = \frac{k_e}{r}10^{-3}mg \quad (8)$$

Where $k_e$ (m) is the track gauge coefficient and r is the radius of the curve.

**Maximum Tractive Effort**

The tractive effort can be increased by increasing the motor torque but only up to a certain point. Beyond this point any increase in the motor torque does not increase the tractive effort but merely cause the driving wheels to slip. The transmitted force is limited by adhesion and the maximum force that can be transmitted can be written as [13]:

$$F_{t-max} = \mu_a . mg \quad (9)$$

Where m, $\mu_a$ are mass of the train in ton (t) and coefficient of adhesion respectively. The adhesion coefficient $\mu_a$ can be found based on Curtius and Kniffler derived adhesion curve in [14].

$$\mu_a = 0.161 + \frac{7.5}{3.6v+44} \quad (10)$$

**Power Demand of the Train**

The maximum tractive force of the locomotive multiplied by the train velocity gives the maximum power that a locomotive consumed. The mechanical tractive power of the motor is computed by [15]:

$$P_{motor} = F_{t-max}.v.(1+\xi) \quad (11)$$

Where $v$ is the speed of the train, $F_{t-max}$ is the maximum tractive force of the locomotive and $\xi$ is slippage ratio. In order to obtain more realistic results some losses and auxiliary power consumptions must be taken into account. These losses will be modeled with the parameter $\eta_{loco}$ which is the locomotive's efficiency.

$$P_D = \frac{P_{motor}}{\eta_{loco}} \quad (12)$$

The auxiliary power consumption, $P_{aux}$ will be considered as well in the calculation and includes the cooling systems, train heating and the power available for travelers (for the case of passenger train). The electrical active power demand will be:

$$P_D = \frac{P_{motor}}{\eta_{loco}} + P_{aux} \quad (13)$$

Fig. 1 shows Matlab simulation results of tractive effort and resistance force with respect to the speed of the train.

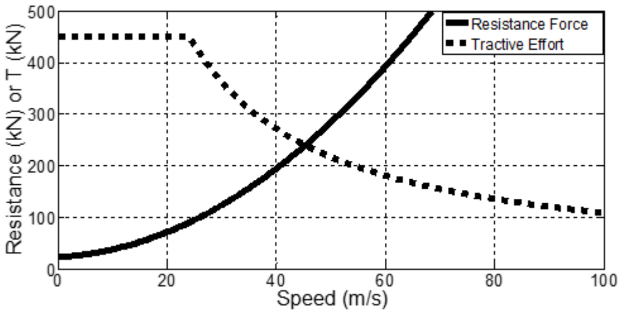


Fig. 1: Tractive effort (Resistance) Vs speed

## MODELING OF TRACTION POWER SUPPLY SYSTEM

**Mathematical Model**

Electrical power system analysis is always depends on a mathematical model which is mainly comprises a mathematical equations that defines the relationship between various electrical power quantities with the required precision. Therefore, based on the objective of the electrical power system analysis various models for a given system may be applicable. In this section, the traction power supply system mathematical model is presented.

**Train (Locomotive) Model**

In order to reduce complexity in the analysis, a constant power model is used, in which the train power and power factor are assumed constant.

$$\text{Train current} = I_{TR} = \left(\frac{S_{TR}}{V_C - V_R}\right)^{*} \quad (14)$$

$$\text{Contact line current} = I_C = I_{TR} \quad (15)$$

$$\text{Rail line current} = I_R = -I_{TR} \quad (16)$$

$$\text{Negative feeder current } I_F = 0 \quad (17)$$

$$\begin{bmatrix} I_C \\ I_R \\ I_F \end{bmatrix} = I_{TR} \begin{bmatrix} 1 \\ -1 \\ 0 \end{bmatrix} \quad (18)$$

Where $S_{TR}$, $V_R$, $V_C$ are power demand of the train, rail voltage and the contact line voltage respectively.

### Model of Substation Power Transformer

Today, there are many transformers which are used in railway power supply system such as open delta or Vv, Scott, YNd11, Wood-Bridge, single phase transformers, etc [15]. These different transformers are used in various feeding configurations, for example, in direct feeding system, Vv transformers are the best choice whereas in an autotransformer feeding arrangement, the three winding specially built single phase traction power transformer are used. In this type of transformer arrangement, the primary terminals of the transformer have a voltage rating of may be 132, 275 or 400 kV and the secondary terminal voltage is 55 kV. For the line being studied, the single phase three-winding transformer is used with the voltage designated as 132 kV/27.5 kV-0-27.5 kV. Fig. 2 illustrate such connections.

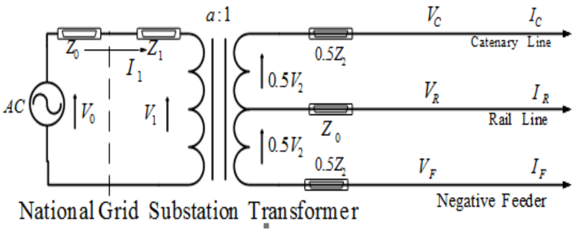


Fig. 2: Substation Transformer

For the substation power transformer, the Norton equivalent circuit in the multi-conductor model is formed as given in equation 3 defining $Z_A = Z_O + Z_1 + 6Z_2$ and $Z_B = 6Z_2 + 24Z_e$, where $Z_O$ is short circuit impedance of the high voltage grid, $Z_1$ and $Z_2$ are impedance of the primary and secondary windings respectively, $Z_e$ is impedance connected between the center tap of the second winding and the rails and a is Transformer's turn ratio. voltage respectively. In addition, $J_{SS}$ is the substation current injected model, VSS is the substation voltage and $Y_{SS}$ is the substation admittance. The short circuit impedance of the grid is assumed zero, this is equivalent to assuming the primary voltage of the substation transformer an infinite bus with a voltage of 132 kV. The no load secondary voltage between the overhead catenary system and feeder is 55 kV with a grounded center tap. The nameplate data of the substation transformer are to be 132/55 kV, 60 MVA calculated based on annual transportation demands, X/R ratio equal to 10 based on ANSI/IEEE C37.010-1979 and the impedance of the traction transformer will be 15 % based on IEC 60076 standards [16].

### Model of Autotransformer

The autotransformer has a single winding connected between the catenary and the feeder wires. The rail system (rails and grounded wires) is connected to a center point on the winding. The usual voltage rating is 50 kV supply between the catenary and feeder with a transformation ratio of 2:1 to obtain a 25 kV catenary to rail and from rail to the return feeder.

The station where the autotransformer is located is also called paralleling station because the two tracks (C wire and F wire) are connected in parallel. Thus, the admittance matrix of the autotransformer becomes:

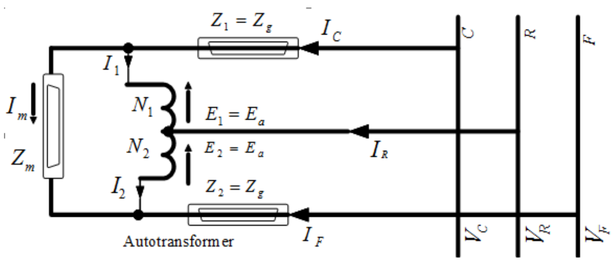


Fig. 3: Autotransformer model

$Z_1$, $Z_2$ are primary and secondary leakage impedances, $Z_m$ is magnetizing impedance, $I_m$is magnetizing current, $I_1$ , $I_2$ are primary and secondary current, $E_1, E_2$ are electromotive forces windings and N1, N2 are turns of the two windings. Assuming that $N_1 = N_2$ and $Z_1 = Z_2 = Z_g$, therefore

$$I_C + I_R + I_F = 0 \quad (27)$$

$$\left[V_F - V_C = 2E_a + Z_g(I_F - I_C) = Z_m I_m + 2Z_g(I_F - I_C)\right] \quad (28)$$

Substituting equation (27) to (28), we can easily find the following equations

$$\left[I_C = \left(\frac{1}{2Z_g} - \frac{1}{Z_m+2Z_g}\right)V_C - \frac{1}{Z_g}V_R + \left(\frac{1}{2Z_g} + \frac{1}{Z_m+2Z_g}\right)V_F\right] \quad (29)$$

$$I_R = -\frac{1}{Z_g}V_C + \frac{2}{Z_g}V_R - \frac{1}{Z_g}V_F \quad (30)$$

$$\left[I_F = \left(\frac{1}{2Z_g} - \frac{1}{Z_m+2Z_g}\right)V_C - \frac{1}{Z_g}V_R + \left(\frac{1}{2Z_g} + \frac{1}{Z_m+2Z_g}\right)V_F\right] \quad (31)$$

Thus,

$$Y_{AT} = \begin{bmatrix} \frac{1}{2Z_g} - \frac{1}{Z_m+2Z_g} & -\frac{1}{Z_g} & \frac{1}{2Z_g} + \frac{1}{Z_m+2Z_g} \\ -\frac{1}{Z_g} & \frac{2}{Z_g} & -\frac{1}{Z_g} \\ \frac{1}{2Z_g} - \frac{1}{Z_m+2Z_g} & -\frac{1}{Z_g} & \frac{1}{2Z_g} + \frac{1}{Z_m+2Z_g} \end{bmatrix} \quad (32)$$

$$\begin{bmatrix} I_C \\ I_R \\ I_F \end{bmatrix} = Y_{AT} \begin{bmatrix} V_C \\ V_R \\ V_F \end{bmatrix} \quad (33)$$

Autotransformer components are modeled by their equivalent circuits in terms of inductance, and resistance. The magnetizing impedance $Z_m$ of the autotransformer is taken as infinite and also the impedance $Z_1 = Z_2$ equal because the two windings are similar. An earthling resistance $Z_e$ is assumed to form the center-tap to remote earth. The calculated results of the AT ratings are: 50/25 kV, 10 MVA, with 7.5 % impedance and an X/R ratio of 10.

**Calculation of Impedance of Overhead Conductors**

In 1923 Carson published an impressive paper which discussed the impedance of the overhead conductor with earth return [6]. This paper has been used in many researches for the calculation of the impedance of the overhead power supply line in cases current flows through the earth especially in the railway system where significant amount of current flows via the earth to the traction substation [17][18]. In this paper Carson line model has been used for impedance calculation of the traction network. The following Carson equation is used to $I_1$ is the primary current of the transformer caused by two secondary current, the contact line current $I_C$ and the negative feeder current $I_F$ as follows.

$$I_1 = \frac{1}{2a}(-I_C + I_F) \quad (19)$$

Consider the primary-side circuit, using Kirchhoff's law, and replacing $I_1$ in equation (14), we will have,

$$V_1 = V_O - \frac{1}{2a}(Z_O + Z_1)(-I_C + I_F) \quad (20)$$

Using Kirchhoff's law on the secondary-side contact to rail line (C-R) circuit,

$$V_C - V_R + \frac{1}{2}V_2 + \frac{1}{2}Z_2 I_C + Z_e(I_C + I_F) = 0 \quad (21)$$

By defining

$$Z'_1 = Z_O + Z_1 \quad (22)$$

Based on the assumption that all currents are supplied by the substation and eventually returned to the substation, that is

$$I_C + I_R + I_F = 0 \quad (23)$$

By defining

$Z_A = Z'_1 + 6Z_2$ and $Z_B = 6Z_2 + 24Z_e$ thus,

$$[(-Z_A + Z_B)I_C + (Z_A + Z_B)I_F = 24V_F - 24V_R + 5V_O] \quad (24)$$

The above Equations (19-24) can be written in the other form as the Norton equivalent circuit as shown in equation (25)

$$\begin{bmatrix} I_C \\ I_R \\ I_F \end{bmatrix} = 2.5\frac{V_O}{Z_A}\begin{bmatrix} 1 \\ 0 \\ -1 \end{bmatrix} + \begin{bmatrix} \frac{6}{Z_A} + \frac{6}{Z_B} & \frac{12}{Z_B} & \frac{6}{Z_A} - \frac{6}{Z_B} \\ \frac{12}{Z_B} & \frac{-24}{Z_B} & \frac{12}{Z_B} \\ \frac{6}{Z_A} - \frac{6}{Z_B} & \frac{12}{Z_B} & \frac{6}{Z_A} + \frac{6}{Z_B} \end{bmatrix}\begin{bmatrix} V_C \\ V_R \\ V_F \end{bmatrix} \quad (25)$$

$$I_{SS} = J_{SS} + Y_{SS}V_{SS} \quad (26)$$

Where $I_C$, $I_R$ and $I_F$ are the contact line current, the rail line current and the negative feeder current and $V_O$, $V_C$, $V_R$ and $V_F$ are the nominal voltage, contact line voltage, rail line voltage and negative feeder voltage respectively. In addition, $J_{SS}$ is the substation current injected model, VSS is the substation voltage and $Y_{SS}$ is the substation admittance. The short circuit impedance of the grid is assumed zero, this is equivalent to assuming the primary voltage of the substation transformer an infinite bus with a voltage of 132 kV. The no load secondary voltage between the overhead catenary system and feeder is 55 kV with a grounded center tap. The nameplate data of the substation transformer are to be 132/55 kV, 60 MVA calculated based on annual transportation demands, X/R ratio equal to 10 based on ANSI/IEEE C37.010-1979 and the impedance of the traction transformer will be 15 % based on IEC 60076 standards [16].

**Model of Autotransformer**

The autotransformer has a single winding connected between the catenary and the feeder wires. The rail system (rails and grounded wires) is connected to a center point on the winding. The usual voltage rating is 50 kV supply between the catenary and feeder with a transformation ratio of 2:1 to obtain a 25 kV catenary to rail and from rail to the return feeder.

The station where the autotransformer is located is also called paralleling station because the two tracks (C wire and F wire) are connected in parallel. Thus, the admittance matrix of the autotransformer becomes:

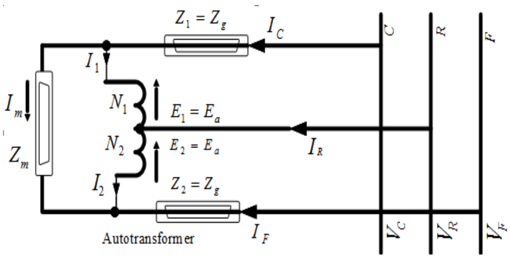


Fig. 3: Autotransformer model

$Z_1$, $Z_2$ are primary and secondary leakage impedances, $Z_m$ is magnetizing impedance, $I_m$is magnetizing current, $I_1$ , $I_2$ are primary and secondary current, $E_1, E_2$ are electromotive forces windings and N1, N2 are turns of the two windings. Assuming that $N_1 = N_2$ and $Z_1 = Z_2 = Z_g$, therefore

$$I_C + I_R + I_F = 0 \tag{27}$$

$$[V_F - V_C = 2E_a + Z_g(I_F - I_C) = Z_m I_m + 2Z_g(I_F - I_C)] \tag{28}$$

Substituting equation (27) to (28), we can easily find the following equations

$$\left[I_C = \left(\frac{1}{2Z_g} - \frac{1}{Z_m+2Z_g}\right)V_C - \frac{1}{Z_g}V_R + \left(\frac{1}{2Z_g} + \frac{1}{Z_m+2Z_g}\right)V_F\right] \tag{29}$$

$$I_R = -\frac{1}{Z_g}V_C + \frac{2}{Z_g}V_R - \frac{1}{Z_g}V_F \tag{30}$$

$$\left[I_F = \left(\frac{1}{2Z_g} - \frac{1}{Z_m+2Z_g}\right)V_C - \frac{1}{Z_g}V_R + \left(\frac{1}{2Z_g} + \frac{1}{Z_m+2Z_g}\right)V_F\right] \tag{31}$$

Thus,

$$Y_{AT} = \begin{bmatrix} \frac{1}{2Z_g} - \frac{1}{Z_m+2Z_g} & -\frac{1}{Z_g} & \frac{1}{2Z_g} + \frac{1}{Z_m+2Z_g} \\ -\frac{1}{Z_g} & \frac{2}{Z_g} & -\frac{1}{Z_g} \\ \frac{1}{2Z_g} - \frac{1}{Z_m+2Z_g} & -\frac{1}{Z_g} & \frac{1}{2Z_g} + \frac{1}{Z_m+2Z_g} \end{bmatrix} \tag{32}$$

$$\begin{bmatrix} I_C \\ I_R \\ I_F \end{bmatrix} = Y_{AT} \begin{bmatrix} V_C \\ V_R \\ V_F \end{bmatrix} \tag{33}$$

Autotransformer components are modeled by their equivalent circuits in terms of inductance, and resistance. The magnetizing impedance $Z_m$ of the autotransformer is taken as infinite and also the impedance $Z_1 = Z_2$ equal because the two windings are similar. An earthling resistance $Z_e$ is assumed to form the center-tap to remote earth. The calculated results of the AT ratings are: 50/25 kV, 10 MVA, with 7.5 % impedance and an X/R ratio of 10.

**Calculation of Impedance of Overhead Conductors**

In 1923 Carson published an impressive paper which discussed the impedance of the overhead conductor with earth return [6]. This paper has been used in many researches for the calculation of the impedance of the overhead power supply line in cases current flows through the earth especially in the railway system where significant amount of current flows via the earth to the traction substation [17][18]. In this paper Carson line model has been used for impedance calculation of the traction network. The following Carson equation is used tocompute mutual impedance ($Z_{ad^1}$) and self-impedance ($Z_{aa}$) of the Catenary system.

$$r_d = \pi^2.10^{-4}.f\ ohm/km \tag{34}$$

The self-impedance ($Z_{aa}$) of wire a with earth return can be expressed as:

$$Z_{aa} = (r_d + r_a) + j2\omega k\ ln\left({}^{D_{ad}}/_{r_o}\right)\Omega/L \tag{35}$$

Where $r_o$ is the radius of the conductor (m) and $D_{ad}$ is equivalent conductor at depth. Also, $k = 2.10^{-7}$,$\boldsymbol{\omega} = 2\pi f$ finally, the mutual impedance ($Z_{ad^1}$) is stated as:

$$Z_{ad^1} = j\omega k(ln\left({}^{1}/_{D_{sa}}\right))\ ohm/L \tag{36}$$

The quantity $\mathbf{D_{ad}}$ is a function of both the earth resistivity $\rho_e$ and the frequency **(f)** and is defined by the relation

$$D_{ad} = 1.309125 \times \delta \tag{37}$$

$$D_{ad} = 658.87 \times \sqrt{\frac{\rho_e}{f}}\ m \tag{38}$$

If no actual earth resistivity data is available, it is a common practice or a thumb rule to consider $\rho_e$ **as** 100 ohm-meter. The earth resistivity $\rho_e$ depends on the nature of the soil.

1. **Contact wire (C)**: Part of the overhead contact line system which establishes contact with the current collector. To avoid errors, the impedances of the messenger and the contact wire are calculated independently.
2. **Messenger wire (M)**: Parts of the overhead contact line system used to support the contact wire.
3. **Rails (R)**: The two rails in the same track are also treated as an independent conductor. They are connected to autotransformers at the center tap.
4. **Negative Feeder (F)**: Besides the catenary, another outer tap of the autotransformer is connected to the feeder wire..

The conductor configuration or arrangement of the overhead line is based on the industry standards conductor clearances. According to IEC the minimum electrical clearances of the conductor must be maintained under all line loading and environmental conditions. Since the actual sag clearance of conductors on overhead contact line is seldom monitored, sufficient allowance for this clearance (safety buffer) must be considered in the process of the initial design.

Minimum horizontal and vertical distances from energized conductor ("electrical clearances") to ground, other conductors, vehicles, and objects such as buildings, are defined based on three parameters. Clearances are defined based on the transmission line to ground voltage, the use of ground fault relaying, and the type of object or vehicle expected within proximity of the line. The IEC 270 Rules cover both vertical and horizontal clearances to the energized conductors [19].

The electric static clearance, which is the minimum distance required between the live parts of the overhead wire equipment and structure or the earthed parts of the overhead wire equipment under 25 kV must be at the minimum 320 mm as per IEC 270. The minimum electrical clearance to earth or another conductor is 150 mm under adverse condition and the minimum clearance between 2 parallel wires in open overlaps is 250 mm but may be reduced to 150 mm absolute minimum under the worst case.

The international standards covering most conductor types are IEC 61089 (which supersedes IEC 207, 208, 209 and 210) and EN 50182 and EN 50183[20][21]. In this paper, for all negative feeder wire, earth wire and messenger wire aluminum conductor steel reinforced (ACSR) has been used. ACSR has been widely used because of its mechanical strength, the widespread manufacturing capacity and cost effectiveness. Hard Copper wires are used for the overhead contact lines, which has a very high strength, corrosion resistance and is able to withstand desert conditions under sand blasting.

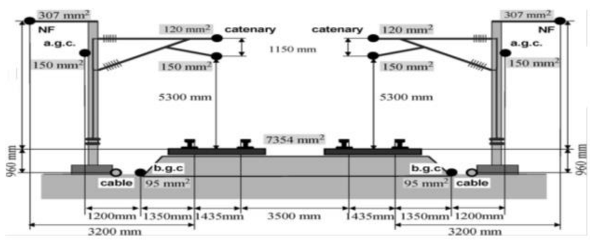


Fig. 4: Configuration of the catenary system

## Modeling Using Matlab Autotransformers

Matlab software does not have an autotransformer model in its library for this reason a two winding linear transformer as shown below in figure 5 connected and used as autotransformer [7].

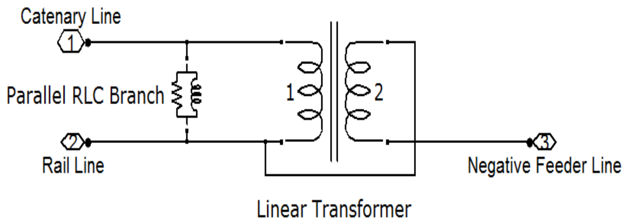


Fig. 5: Autotransformer model using two winding transformer

## Power Transformer Model

In this section the traction substation power transformer model as shown on the figure 5 below is presented. The Matlab Simulink library does not have an exact substation transformer that have seen in the mathematical modeling section but the linear transformer which has three windings, the primary winding at the input side and two secondary winding is appears to the perfect match. The secondary windings are connected in such a way as shown in Fig. 6 to form the center tap.

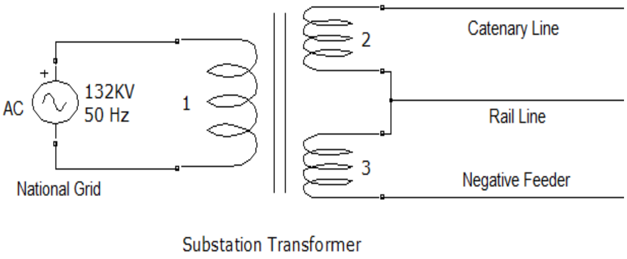


Fig. 6: A Substation transformer model

## Overhead Catenary System Model

To model the catenary system MATLAB/ Simulink mutual inductance element which is shown in the Fig. 7 below is used. As explained earlier the traction power supply system uses five conductors, which give 25 full impedance matrixes, from which five of them are self-impedance and twenty of them are mutual impedance as shown in Table 1.

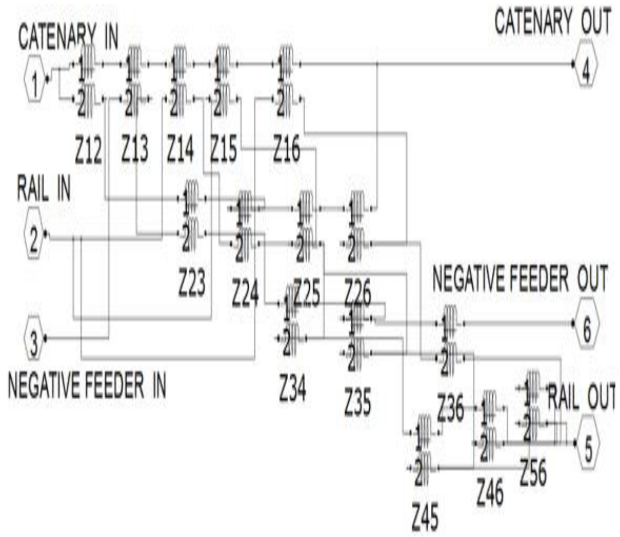


Fig. 7: The catenary system model

The six input line as shown in fig. 7 are connected in such a way to form to a six output line where the six input and output line combined to form three input and three output wire. These sets are appropriately called Catenary, Rail, and Feeder.

## SIMULATION RESULT AND ANALYSIS

The purpose of this simulation is to evaluate the designed autotransformer-fed power supply system for Modjo-Hawassa railway line corridors. Since voltage profile and voltage regulation along the line are the most important parameters to evaluate the system performance, a computer-aided steady state load-flow simulation in terms of voltage were performed. The analysis is done for two different cases.

The performance of the traction power system has been investigated by applying different headway distances on the trains and by increasing the number of train along the feeding section. Tables 2-4 shows simulation findings based on a single locomotive which is moving along the 55 km long feeding section and results were taken one at a time at points 15 km, 30 km and 55 km from the traction substation. Table 5-7 shows simulation results based on three consecutive locomotives which are moving at the same time along feeding section at a distance of 15 km, 30 km and 55 km (end of the feeding section) from the traction substation.

Note that in Tables SS means substation and the first (AT1), the second (AT2), the third (AT3) and the fourth (AT4) autotransformers are located at a distance of 15 km, 30 km , 45 km and 55 km away from the traction substation respectively.

Note that in Table 1, C (C1, C2) means contact line wires, M (M1, M2) messenger wires, F (F1, F2) Negative feeders and R(R11, R12, R21, R22) one of the four rail line on the double track configuration.

Table 1: Ten by ten impedance matrix of the overhead catenary system

| | C1 | M1 | F1 | C2 | M2 | F2 | *R11* | *R12* | *R21* | *R22* |
|---|---|---|---|---|---|---|---|---|---|---|
| *C1* | *0.218+j0.77* | *0.049+j0.42* | *0.049+j0.34* | *0.049+j0.33* | *0.049+j0.327* | *0.049+j0.29* | *0.049+j0.32* | *0.049+j0.32* | *0.049+j0.31* | *0.049+j0.30* |
| *M1* | *0.049+j0.42* | *0.239+j0.75* | *0.049+j0.34* | *0.049+j0.33* | *0.049+j0.329* | *0.049+j0.29* | *0.049+j0.31* | *0.049+j0.31* | *0.049+j0.29* | *0.049+j0.29* |
| *F1* | *0.049+j0.34* | *0.049+j0.34* | *0.152+j0.72* | *0.049+j0.29* | *0.049+j0.292* | *0.049+j0.27* | *0.049+j0.29* | *0.049+j0.29* | *0.049+j0.28* | *0.049+j0.27* |
| *C2* | *0.049+j0.33* | *0.049+j0.33* | *0.049+j0.29* | *0.218+j0.77* | *0.049+j0.420* | *0.049+j0.34* | *0.049+j0.31* | *0.049+j0.30* | *0.049+j0.32* | *0.049+j0.32* |
| *M2* | *0.049+j0.33* | *0.049+j0.33* | *0.049+j0.29* | *0.049+j0.42* | *0.239+j0.745* | *0.049+j0.34* | *0.049+j0.29* | *0.049+j0.29* | *0.049+j0.31* | *0.049+j0.31* |
| *F2* | *0.049+j0.29* | *0.049+j0.29* | *0.049+j0.27* | *0.049+j0.34* | *0.049+j0.342* | *0.152+j0.72* | *0.049+j0.28* | *0.049+j0.27* | *0.049+j0.29* | *0.049+j0.29* |
| *R11* | *0.049+j0.32* | *0.049+j0.31* | *0.049+j0.29* | *0.049+j0.31* | *0.049+j0.297* | *0.049+j0.28* | *0.073+j0.61* | *0.049+j0.41* | *0.049+j0.33* | *0.049+j0.31* |
| *R12* | *0.049+j0.32* | *0.049+j0.31* | *0.049+j0.29* | *0.049+j0.30* | *0.049+j0.294* | *0.049+j0.27* | *0.049+j0.41* | *0.073+j0.61* | *0.049+j0.35* | *0.049+j0.33* |
| *R21* | *0.049+j0.31* | *0.049+j0.29* | *0.049+j0.28* | *0.049+j0.32* | *0.049+j0.312* | *0.049+j0.29* | *0.049+j0.33* | *0.049+j0.35* | *0.073+j0.61* | *0.049+j0.41* |
| *R22* | *0.049+j0.30* | *0.049+j0.29* | *0.049+j0.27* | *0.049+j0.32* | *0.049+j0.312* | *0.049+j0.29* | *0.049+j0.31* | *0.049+j0.33* | *0.049+j0.41* | *0.073+j0.61* |

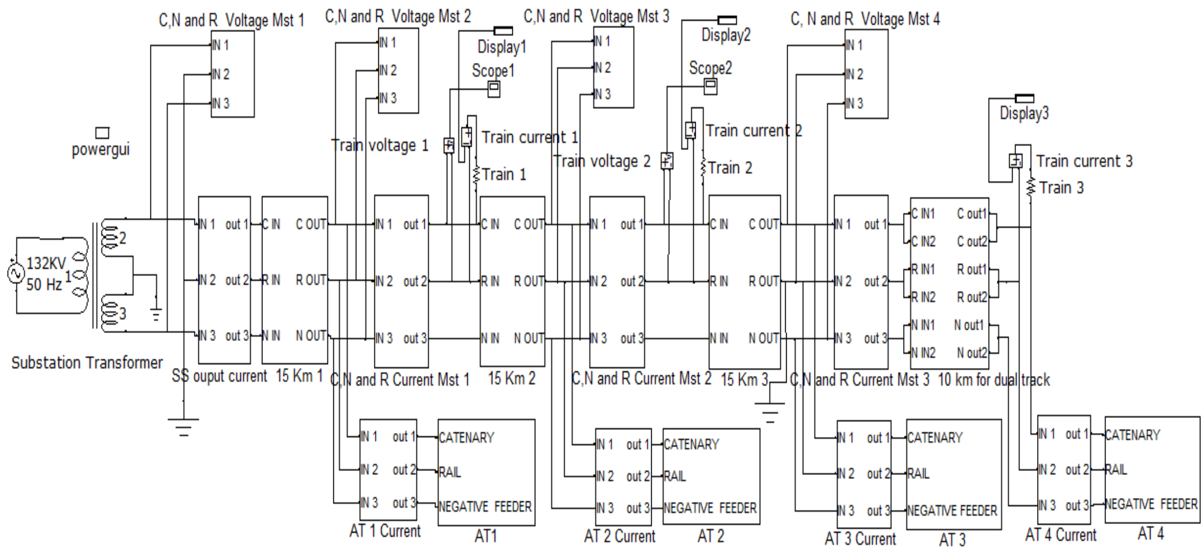


Fig. 8: Simulated power supply system having 2 x 25 kV AT, 2 conductors and a return wire

In this study, the train voltages will be the potential at the train's current collector (pantograph) or elsewhere on the catenary, measured between the catenary and the rail return circuit and also the train current is the current measured at the pantograph.

| Train position | SS output voltage | Train voltage |
|---|---|---|
| 15 km | 27.41 kV | 26.67 kV |
| 30 km | 27.38 kV | 25.47 kV |
| 55 km | 27.36 kV | 24.78 kV |

Table 2**:** Train position and voltage profile in the case of single train

Table 2 shows that the train voltage decreased from 26.67 kV to 24.78 kV as the train position changed from 15 km to 55 km along the feeding section, which shows that as the train distance increases relative to the traction substation, the impedance of the traction network lifts up which in turn leads to reduction in voltage profile across the catenary system.

Table 3: Train position and current in the case of single train

| Train Position | Substation output Current (A) | Train Current (A) |
|---|---|---|
| 15 km | 592.86 | 587.82 |
| 30 km | 577.63 | 574.28 |
| 55 km | 573.85 | 559.61 |

Table 3 indicates the train current decreases when the distance from the substation increases, this is because as the trains distance increases, small amount of current flows in different circuits such as autotransformers that does not have train in between (theoretically this current should not flow into this autotransformers but practically that is not the case because it only works for ideal autotransformers) and cause the current to return to the substation via the return conductors and it is found that the train current decreases from 587.82 A to 559.61 A along the feeding section.

Table 4: Train position and AT voltages in the case of single train

| Train position | AT Terminal | AT 1 kV | AT 2 kV | AT 3 kV | AT 4 kV |
|---|---|---|---|---|---|
| 30 km | C | 26.72 | 26.08 | 25.47 | 25.54 |
| | R | 0.000 | 0.056 | 0.000 | 0.00 |
| | N | 26.82 | 26.37 | 26.05 | 25.79 |
| 55 km | C | 26.69 | 26.06 | 25.47 | 24.77 |
| | R | 0.000 | 0.030 | 0.000 | 0.000 |
| | N | 26.72 | 26.16 | 25.67 | 25.26 |

Table 4 indicates that as the train distance with respect to the traction substation increases the autotransformer voltage decreases this is because when the distance increases the impedance of the traction network rises which in turn increase the voltage drop and o the maximum observed rail line potential for this case becomes 56.35 V.

Table 5: Train positions and voltage profiles in the case of three trains

| Train Position | SS Output Voltage | Train Voltage | % Voltage regulation |
|---|---|---|---|
| 15 km | 27.08 kV | 24.89 kV | 0.64 % |
| 30 km | 26.96 kV | 23.85 kV | 4.60 % |
| 55 km | 26.95 kV | 22.93 kV | 8.28 % |

Table 5 shows that the voltage at 15 km is 24.89 kV and at 55 km is 22.93 kV. The train voltage at 15 km and at 55 km are reduced by 6.67 % and 7.46 % respectively compared with previous case of single train shown in Table 2. This is because as the number of train increases, the current flowing through the traction catenary network increases as presented in Table 6, which leads to a higher voltage drop. This higher voltage variation across the line causes the percentage voltage regulation to rise from 0.64 % to 8.28 %.

Table 6: Train positions and current in the case of three trains

| Substation output Current (A) | Train Position | Train Current (A) |
|---|---|---|
| 1590.3 | 15 km | 548.61 |
| | 30 km | 524.04 |
| | 55 km | 514.25 |

As shown in Table 6 the train currents decreases for the case three consecutive trains compared to a single train as shown in Table 3, this is due to the fact small amount of the autotransformer current returned to the substation via the rail. This reduction of current decreases the performance of the train or decreases the speed of the train because the speed of the train directly depends on the current that the train motor receives.

Table 7: AT voltage in the case of three trains

| AT Terminals | AT 1 kV | AT 2 kV | AT 3 kV | AT 4 kV |
|---|---|---|---|---|
| C | 24.89 | 23.81 | 23.42 | 23.34 |
| R | 0.000 | 0.066 | 0.000 | 0.000 |
| N | 25.57 | 24.66 | 24.05 | 24.06 |

Table 7 show the reduction of the voltage at autotransformer terminals with the increase of the number of trains along the given feeding section. The conclusion is that both the number of train and train distance affects the autotransformers voltage profile.

The following simulation results are found based on a model developed using Matlab as shown in Fig.8.

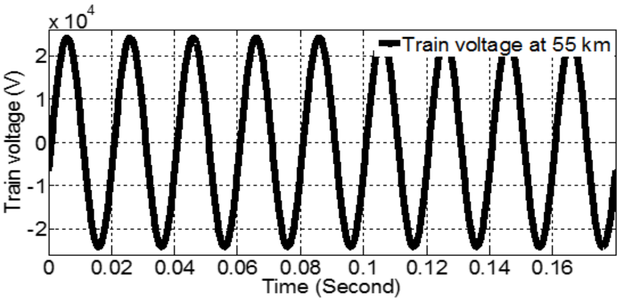


Fig. 9: Voltages of a single train on the same feeding section

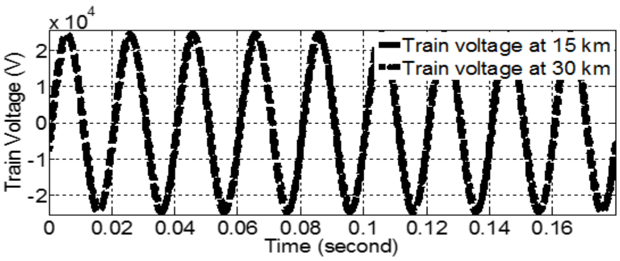


Fig.10: Voltage of two consecutive trains on the same feeding section

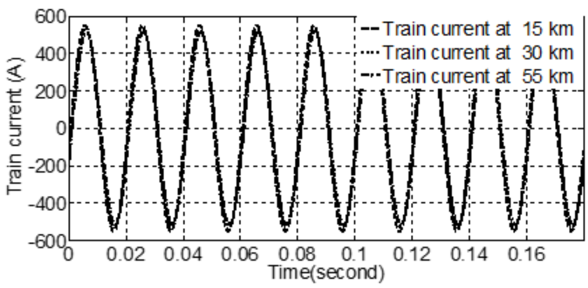


Fig. 11: Train currents of three consecutive trains on the same feeding section

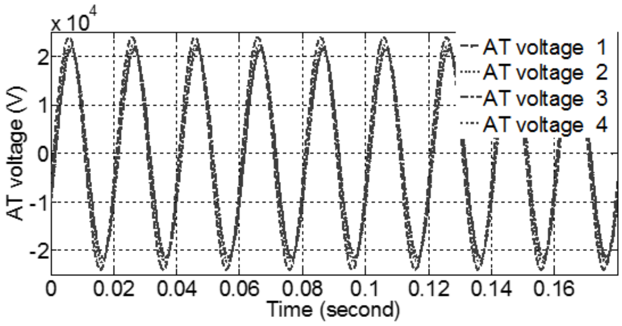


Fig.12: AT voltages of three consecutive trains on the same feeding section

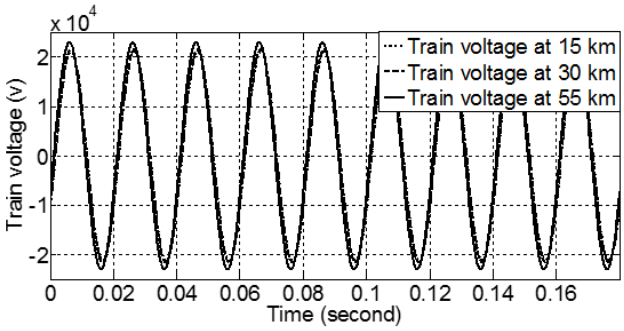


Fig. 13: Voltages of three consecutive trains on the same feeding section

## CONCLUSIONS

In this paper, modeling of major components of traction power supply system has been done for autotransformer traction power supply system arrangement using Matlab and simulation of the supply system with variation of distance of electric locomotive and the number of train across the line has been conducted.

From the results obtained, it can be concluded that the magnitude of the train voltage decreases with increase in distance of locomotive from the traction substation and also decreases with increasing the number of train along the feeding section.

The minimum computed pantograph voltage for the train is 22.93 kV, which is within the tolerable voltage fluctuation range of BS EN 50163:2004 of overhead contact lines [22] and also the maximum rail line potential becomes 66.2 V which is also within the recommended limit of BS EN 50122-1 (IEC 62128-1) [23]. In addition, the maximum percentage voltage regulation is found to be 8.28 % with respect to the nominal voltage which is within the standard limit described by IEC 61000-2-2 [24].

Finally, the results obtained from the model confirm with the industry standards and this clearly indicates the successful use of developed mathematical model for simulating traction power supply system.

## REFERENCES

[1].Kulworawanichpong T., "Optimizing AC Electric Railway Power Flows with Power Electronics Control", PhD thesis, University of Birmingham, November 2003.

[2].Belay Tibeb Mintesnot, “Modeling and Simulation of AC traction power Supply system” MSc thesis, Southwest Jiao tong University, November, 2013.

[3]. T. K. Ho, Y. L. Chi, J. Whang, K. K. Leung, L. K. Siu, and C. T. Tse, “Probabilistic load flow in AC electrified railways,” IEE Proc.-Electr. Power Appl., vol. 152, pp. 1003–1013, May 2005.

[4].P. Lukaszewicz, “Energy Consumption and Running Time for Trains”, PhD thesis, Division of Railway Technology, KTH, Stockholm, Sweden, 2000.

[5].B. Boullanger, “Modeling and simulation of future railways,” Master’s thesis, Royal Institute of Technology (KTH), Mar. 2009.

[6]. Wagner C. F., and Evans R. D., “Symmetrical components”, New York, McGraw-Hill, 1933.

[7].Jesus Serrano, Carlos A. Platero, Maximo Lopez-Toledo and Ricardo Granizo “A Novel Ground Fault Identification Method for 2 × 25 kV Railway Power Supply Systems” Technical University of Madrid, Spain, 2016.

[8].Sanjay Y. Patel “Special Design Auto-Transformers” Smit Transformers, Ohio, September 2004.

[9].Mariscotti A., Pozzobon P., and M. Vanti, "Simplified Modeling of 2 x 25-kV AT Railway System for the Solution of Low Frequency and Large-Scale Problems", IEEE Transactions on Power Delivery, vol. 22, pp. 296 — 301, January 2007.

[10]. Andrew J. Gillespie P.E and H. Ian Hayes P.E, “Practical Guide to Railway Engineering”, AREMA committee- 24, USA, 2003.

[11].White R.W. , “AC supply systems and protection”, Fourth Vocation School on Electric Traction Systems, IEE Power Division, April 1997.

[12].Courtois C., “Why the 2x25 kV alternative?”, Half-day Colloquium on 50 kV Auto-transformer Traction Supply Systems The French Experience, IEE Power Division, pp. 111-114, November 1993.

[13].Mariscotti A., Pozzobon P., and Vanti M., "Distribution of the Traction Return Current in AT Electric Railway Systems," IEEE Transactions on Power Delivery, vol. 20, no. 3, July 2005.

[14]. Hill R. J., Cevik I. H., "On-line Simulation of Voltage Regulation in Autotransformer-Fed AC Electric Railroad Traction

Networks", IEEE Transactions on Vehicular. Technology, vol. 2, no. 3, August 1993.

[15]. Carson J. R., "Wave propagation in overhead wires with ground return," Bell System Tech Journal, 1926.

[16].Glover J.D., Sarma M. S., Overbye T. J., Power Systems Analysis and Design, 4th ed.Thomson Engineering, May 2007.

[17]. Varju G., Simplified method for calculating the equivalent impedance of an AT system. Technical report, Technical University of Budapest/Innotech Ltd, 1996.

[18].T. K. Ho, Y. L. Chi, J. Wang, and K. K. Leung, "Load flow in electrified railway," in Proceedings of the second International Conference on Power Electronics, Machines and Drives, vol. 2, pp. 498 –503, 2004.

[19].Vinod Sibal, "Traction power supply system for California high speed train project", California, America, 2011

[20].Kiessling F., Piff R., Schmieder A., and Scheneider E., "AC 25kV 50 Hz traction power supply of the Madrid-Seville line" in Contact Lines for Electrical Railways: Planning-Design-Implementation-Maintenance, SIEMENS, August 2009.

[21].Pilo E., Ruoco L., and Fernandez A., "Catenary and autotransformer coupled optimization for 2x25kV systems planning. In Computers in Railways X: Computer System Design and Operation in the Railway and Other Transit Systems", Prague, Czech Republic, 2006.

[22].Shenoy U.J., Senior Member, IEEE, K.G.Sheshadri, K. Parthasarathy, Senior Member, IEEE, H.P.Khincha, Senior Member, IEEE, D.Thukaram, Senior Member,IEEE,´´ MATLAB Based Modeling and Simulation of 25KV AC Railway Traction System-A Particular Reference to Loading and Fault Condition," 2009.

[23]. Abrahamsson, L., Kjellqvist, T. &Ostlund, S., HVDC Feeder Solution for Electric Railways. IET Power Electronics, 2012. Accepted for publication.

[24].Shahnia F., and Tizghadam S., "Power distribution system analysis of Rural electrified railways" University of Tabriz, Iran,

# ENHANCED ENERGY DETECTOR USING ADAPTIVE WIENER FILTER IN COGNITIVE RADIO

Benyam Hailegnaw[1], Mohammed Abdo[2]
[1] UNDP/UNDSS, Addis Ababa
[2] School of Electrical and Computer Engineering, AAiT, AAU

## ABSTRACT

The rising demand in wireless services and applications bring channel constraint on the existing frequency spectrum allocation scheme. By addressing the concept of cognitive radio technique (CR), it is possible to mitigate the scarcity of spectrum channel and underutilization of spectrum efficiencies. Various techniques and methods have been used to maximize the probability of detection (Pd) in CR system. Energy detector spectrum sensing is one of the transmitter based techniques, which detects the presence of primary user in cognitive system. However performance indicator metrics show that the energy detector algorithm has poor performance when the received SNR value is too low as compared to the system threshold value. In this paper the performance of conventional and enhanced energy detector (using adaptive Wiener filter) is examined based on Receiver Operating Curve (ROC) and Complementary Receiver Operating (CROC). Simulation results are plotted for different threshold values, false alarm probability, detection probability and the received SNR. Results for AWGN and Rayleigh flat fading channel models are presented. The Simulations results in Rayleigh flat fading channel show that, the insertion of adaptive Wiener filter in conventional energy detector has improved the probability of detection by 8% and reduce the probability of miss detection by same amount.

***Keywords*** *adaptive Wiener filter: Cognitive radio, energy detector, false alarm and detection, performance metrics (ROC, CROC), probability spectrum sensing, threshold value.*

## INTRODUCTION

Technological advancement of wireless communication in this century brings a variety of wireless products/devices that can be used for a wide range of application. Devices in wireless environments operate on specified licensed spectrum. This operational frequency range should be designed, allocated and properly administrated by governmental institution such as ETA of Ethiopia, FCC of USA. The assigned frequency range can be used in cellular network, FM radio, TV broadcasting service etc. [1,2].

Study at FCC shows that the spectrum usage is highest specifically in cellular network (GSM), TV bands, fixed radio system and FM radio channel. But significant amount of the spectrum remains underutilized [3]. It also shows that the spectrum usage in the band below 3 GHz has utilization efficiencies of 15% to 85% [4,5]. As new service and wireless application are continuously added the system channel will be fully occupied and consequently it creates congestion and channel scarcity. To mitigate this problem, I. Mitola proposed the concept of cognitive radio system in his doctoral dissertation. [6]. Cognitive radio can be defined as a radio system that can adaptively and dynamically allow user(s) to use the spectrum in the opportunistic way [5-8].

This paper deals with enhancement of the performance of conventional energy detector using adaptive Weiner filter. Focus is made on how the performance metrics are improved at low SNR signal.

## THEORETICAL BACKGROUND

The concept of energy detector was developed by Urkowitz [9]. In his concepts signal is passed through band pass filter of the bandwidth W and integrated over time interval, the output of the block of integrator is compared to predefined threshold. The value of threshold can be set to variable or fixed based on condition of channel. The blind signal detector is another name for energy detector because it ignores the signal structure i.e., it estimates the presence of signal by comparing the energy received with known threshold from the statistics of the noise. The value of signal to be analyzed should be deterministic, pass through a flat band limited power density spectrum of Gaussian noise with known mean and variance Applying sampling theorem, it can be approximated by the sum of squares of statistically independent random variables having zero mean and unity variance. The resulting sum will have a chi-square distribution and reduces to a simple identification problem of binary hypothesis model. Based on this assumption, the transfer function of the deterministic signal under AWGN in the time domain is a Sinc function having the transfer function [9,10]

$$H(f) = \begin{cases} \frac{2}{\sqrt{N}} & |f - fo| \leq W \\ 0 & \text{Otherwise} \end{cases} \quad (1)$$

where N is the one side noise power spectral density of the Sinc signal, $f_0$ and W are the center frequency and the band width of band pass filter (BPF), respectively. The analytical representation of the signal in binary hypothesis is expressed as [8-11]

$$s(k) = \begin{cases} n(k) \ \ldots\ldots\ldots\ldots\ldots & H_0 \\ hx(k) + n(k) \ldots\ldots\ldots & H_1 \end{cases} \quad (2)$$

where $h_x(k)$ and n(k) represent the signal and noise, respectively.

The test hypothesis is used to decide the presence of primary user (PU) in the system/channel. From Eqn. (2) , the output can be represented by two logical states $H_0$ (absence or null hypothesis) and $H_1$ (the presence of PU signal information [9,10]. Therefore a decision rule can be stated as: $\mathbf{H_0}$……if $\boldsymbol{\varepsilon < \upsilon}$ and $\mathbf{H_1}$**……**if $\boldsymbol{\varepsilon > \upsilon}$, where $\boldsymbol{\varepsilon} = |\mathbf{E_s(k)}|^2$ is the estimated energy of the received signal and $\upsilon$ is chosen to be the noise variance. It is known that for an input signal x(t), the Fourier transform is X(ω) and $t_2$-$t_1$ the time period over which the input sample is observed. The threshold voltage value is related to the probability of false alarm and the noise power. It can be computed as follows [14]:

Energy spectrum of a signal is:

$\{x(t)\} = |X(\omega)|^2 (t_2 - t_1)$

(3)

$$V_1T = \sqrt{(2\ \sigma_1 n \uparrow 2(\log(\ 1/P_1 fa\ )}$$

(4)

where $V_T$ is the threshold voltage,

$$V_T(\omega) = \int_{t_1}^{t_2} V_T e^{-i\omega t} dt$$

(5)

$$= |V_T(\omega)|^2 = \frac{V^2}{\omega^2}(t_2 - t_1)$$

(6)

and $P_{fa} = 10^{\frac{V_T}{\sigma_n{}^2}}$

(7)

### Conventional Energy Detector

Energy detection is a non-coherent detection method that detects the presence of the primary signal based on the received energy level. Figure 1 shows the discrete version of conventional energy detector block diagram.

When the signal is analyzed in frequency domain, the fast Fourier transforms (FFT) based method is used in process.

The resulting signal fed into the integrator which will be compared to a predetermined receiver threshold value to check whether PU exist or not. For detection purpose the measured signal is always higher than that of the energy threshold value [7].

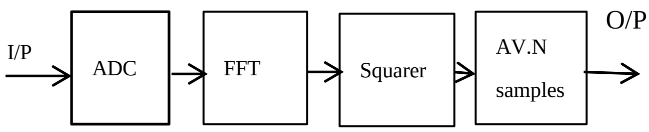


Figure 10: Block diagram of energy detector [7]

Though the energy detection method is the simplest technique, it become too difficult to measure the noise variance accurately at weak SNR and the performance of energy detector becomes poor [7, 14, 15].

**The Enhanced Energy Detector**

In this method an attempt is made to enhance the performance of energy detector by inserting an adaptive Weiner filter on the front side of conventional detector. The block diagram is depicted in Figure 1. By adaptive filter we mean that Wiener coefficients are updated recursively until they reach an optimum value. Moreover, the Recursive Least Square Algorithm (RLS) filter is an adaptive formulation of the Wiener filter. Especially for stationary

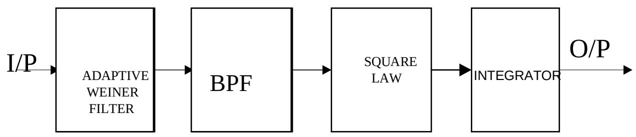


Figure 2: Enhanced energy detector spectrum sensing block diagram.

signals, the RLS algorithm converges to the same solution as the Wiener filter. Thus Recursive Least Square algorithm becomes the solution to optimize the performance of Wiener filter.

**Performance Metrics Measurement**

The performance of the spectrum sensing technique can be quantified by the performance metric values. These values determine the correctness of the presence of the spectrum hole or channel in the system [14]. The following parameters are used to check the performance of energy detector:

- Probability of detection.
- Probability of false alarm.
- Probability of miss detection.
- The receiver operating characteristics curve (ROC),
- The Complementary receiver operating characteristics curve (CROC),

The performance metrics ROC curve measures the sensitivity of the detector. It can also be used along with binary hypothesis model. The signal detection and estimation capabilities of the detector is represented by the graphical plot of $P_d$ or $P_m$ versus $P_{fa}$ as the threshold varies. Generally speaking the ROC curve can be given as $P_d = f(P_{fa})$ and shows the tradeoff between detection probability and false alarm rate for an optimum threshold.

It also shows the trade-off between detection probability and false alarm rate for an optimum threshold [11].The higher the area under the $P_d$ v s$^{P_{fa}}$ curve, the best is system detection response. Likewise the CROC curve is the complement of ROC curve. As the value of CROC become lower so does the system detection. It measures the area under the curve $P_m$ vs $P_{fa}$[12,13,14,15]

## Simulation Results and Discussions

The simulation parameters used in this work are listed in Table 1

**Table 2: Simulation Parameters**

| Simulation | Type and values |
|---|---|
| Cognitive user | Single user |
| Transmitted Signal | BSK and QPSK |
| Detector Type | Energy Detector |
| Propagation channel model | Flat Mode channel |
| Initial update =lambda | 0.99 |
| Number of Monte Carlo simulation | 100000 |
| FIR Filter Order | 32 |
| Transmitted Signal SNR values | -5dB and 5 dB |
| Modulation Index | 4 |
| Probability of false alarm | 0.01 |
| Number of samples | 10 and 1000 |
| Mean and Variance (noise) | 0 and 1 |
| Channel | AWGN and Rayleigh |

**Simulation Results and Discussions for AWGN Channel**

This section assesses the performance of conventional and enhanced energy detector algorithms based on the performance metrics. Figure 3 depicts the conventional (the broken curve) and enhanced energy detector (the solid curve). Setting the value of false alarm probability equal to 0.01, the plots are generated when 1000 sample of QPSK signals are received. It is observed that as the SNR increase from -20dB to -4dB with step increment of 0.5dB, so does the detection probability. The result plot shows the detection values at lower SNR are too low, for SNR values higher than -12dB the detection value of the receiver start to rise. This can be seen from the Table 2.

Table 2: $P_d$ vs SNR comparison table

| | Conventional | | | Enhanced | | |
|---|---|---|---|---|---|---|
| $P_{fa}$ | 0.001 | | | 0.001 | | |
| No of QPSK samples | 1000 | | | 1000 | | |
| $P_d$ | 0.8 | 0.5 | 0.15 | 0.8 | 0.5 | 0.15 |
| SNR(dB) | -9.4 | -10 | -11.8 | -4.3 | -5.6 | -3 |

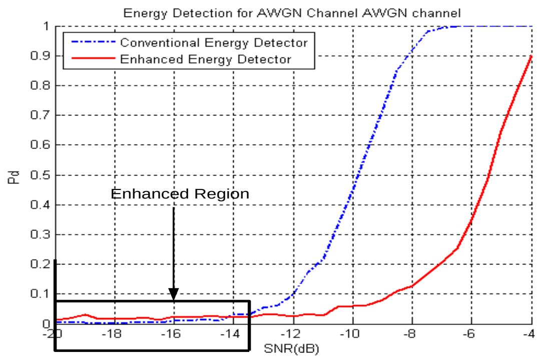


Figure 11: Conventional and enhanced energy detector Probability of detection Vs Signal

Table_2 of the result shows that by setting the probability of detection value for receiver equal to 0.8, the corresponding SNR signal value at the conventional detector is -9.4dB. Whereas, the SNR value of enhanced detector is -4.3dB. This enhanced value is 45.75% higher than the conventional response value. Likewise, when the probability detection value of the receiver equal to 0.5, the corresponding SNR signal value at the conventional detector is -10dB, while, the SNR value of enhanced detector is -5.6 dB.

This enhanced value is 56% higher than the corresponding conventional response value. Therefore under constant value of detection probability at the receiver, the signal SNR at enhanced detector is higher than conventional energy detector.

Thus the insertion of adaptive Weiner filter on the front end of conventional energy detector can improve the detection performance values of the conventional energy detector.

Figure 4 depicts the relation between $P_{fa}$ Vs the system threshold values when 10 sample BSK signals with SNR value of -5dB is transmitted. As can be seen from Table 3, when the $P_{fa}$ value of receiver is equal to 0.1, the threshold value of the conventional energy detector will be 1.4 whereas for enhanced energy detector the threshold value is 0.275. In this case the enhanced energy detector lower than the conventional threshold by 19.64%

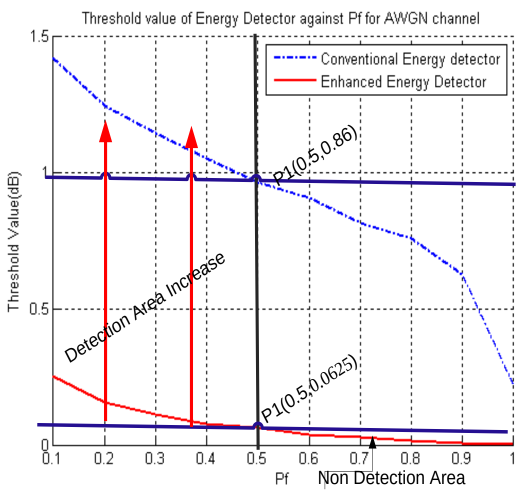


Figure 12: False alarm probabilities Vs the system threshold values.

Similarly, when the $P_{fa}$ value of receiver is equal to 0.7, the threshold value of the conventional energy detector will be 0.8, whereas for enhanced energy detector the threshold value is 0.025.In this case the enhanced energy detector threshold is lower than the conventional threshold by 39.28%. Therefore under constant value of $P_{fa}$ at the receiver, the threshold value of the receiver for the enhanced energy detector is lower than that of conventional energy detector.

Table 3 $P_{fs}$ vs Threshold comparison table

| | Conventional Energy Detector | | | Enhanced Energy Detector | | |
|---|---|---|---|---|---|---|
| No of BSK Samples | 10 | | | 10 | | |
| SNR(dB) | -5 | | | -5 | | |
| $P_{fa}$ | 0.1 | 0.7 | 1 | 0.1 | 0.7 | 1 |
| Threshold value | 1.4 | 0.8 | 0.3 | 0.275 | 0.025 | ≈0 |

Thus the sensitivity of the conventional energy detector improved as adaptive Weiner filter is inserted. For conventional energy detector as the value of $P_{fa}$ increased toward 1, the corresponding threshold values decrease toward 0.2, whereas the threshold value reach below 0.0625 for the enhanced detector. Specifically when the $P_{fa}$ value is set to be 0.5, the corresponding threshold value for conventional and enhanced detector is 0.86 and 0.0625 respectively (Figure.4). Let P1 (0.5, 0.86) and P2 (0.5, 0.0625) be these points. Both point P1 and P2 divide the region into four parts. Point P1 is an intersection point for the broken (conventional response curve) and heavy black line. Similarly point P2 is the intersection of heavy black line and solid curve (enhanced curve).The whole region is divided into four sections, but the region of interest is the most upper and lower left (detection area section) which is created by the union of both curves. Under constant false alarm probability value of 0.5, the detection area obtained by the enhanced system is much higher than that of detection area obtained by conventional detector. Thus the insertion of adaptive Weiner filter increases detection area of conventional energy detector.

Table 4: ROC comparison table
Sample_data_1: Conventional Energy detector

| Pf | 0.0025 | 0.0049 | 0.0081 | 0.0121 |
|---|---|---|---|---|
| Pd_Simu | 0.942434 | 0.951381 | 0.957675 | 0.962455 |
| Pd_Approxm | 0.894764 | 0.926457 | 0.945921 | 0.958905 |

Sample_data_2: Enhanced energy detector table.

| Pf | 0.0025 | 0.0049 | 0.0081 | 0.0121 |
|---|---|---|---|---|
| Pd_Simu | 0.997188 | 0.998481 | 0.99909 | 0.99942 |
| Pd_Approxm | 0.996067 | 0.996934 | 0.99749 | 0.997896 |

Figure5 and 6 depict the simulation response of Receiver Operating Curve (ROC) for both conventional and enhanced energy detector receiver. The plots are generated when the received signal SNR is -5dB.The comparisons of the two plots are supported by the tabular data given as Sample_Data_1 and Sample_Data_2 which are assigned as Table 4. The Pd_Simu is the simulated value of detection probability for each value of false alarm probability and was found using Montecarlo simulation. It is obtained when computational technique in probability detection

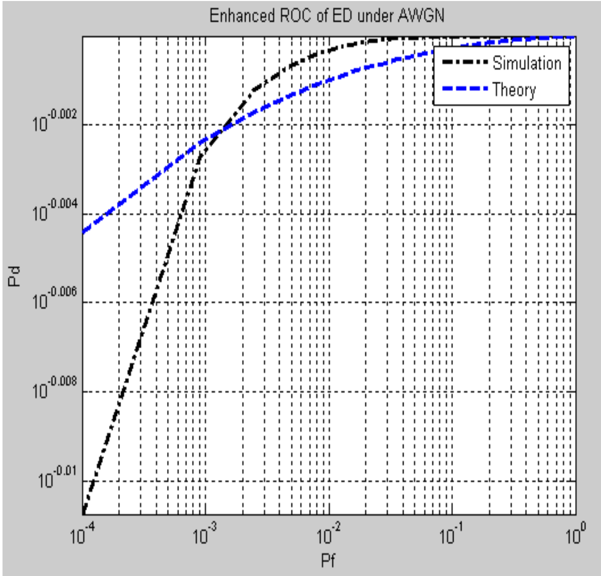


is used while Pd_Approx. is obtained when the

Figure 14: ROC curve of enhanced energy detector.

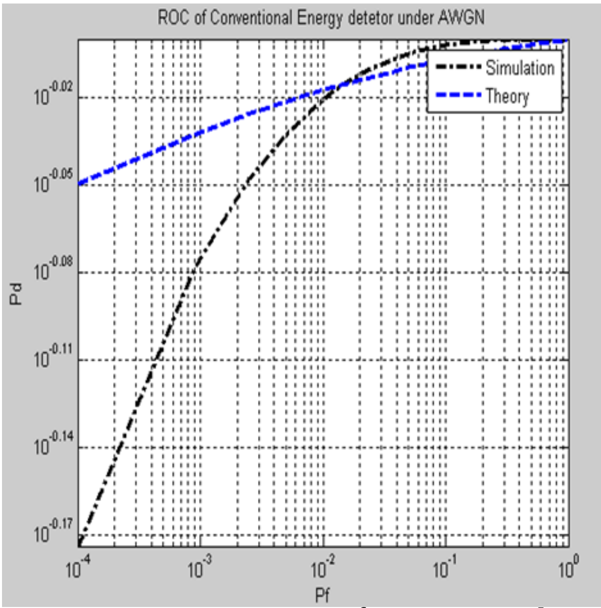


Figure 13: ROC curve of Conventional energy detector

theoretical values of probability detection are assumed [11]. It is applicable when the chi square probability density Sample_Data_1 and Sample_Data_2 for the same value of false alarm probability it was found function for an index value of $m \geq 100$ is considered. Analytically, taking two sample values that Pd_Simu and Pd_Approx. in Sample_Data_2 are higher than those of values in Sample_Data_1 (Table 4). This shows that the insertion of adaptive Weiner filter on the front end of the energy detector increased the operational area of receiver operating curve. Figure 7 and 8 are CROC response of conventional and enhanced energy detector respectively. They are simulated when the received signal SNR is 5dB and the order of filter is 32. Table 5 shows tabular data given as Sample_Data_3 and Sample_Data_4, which were generated from Figures 7 and 8.

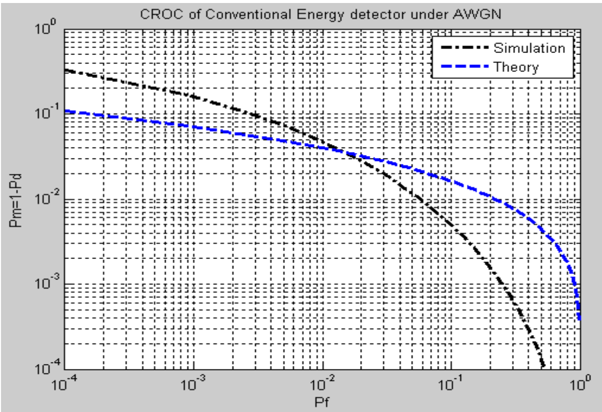


Figure 7: CROC curve for Conventional energy detector

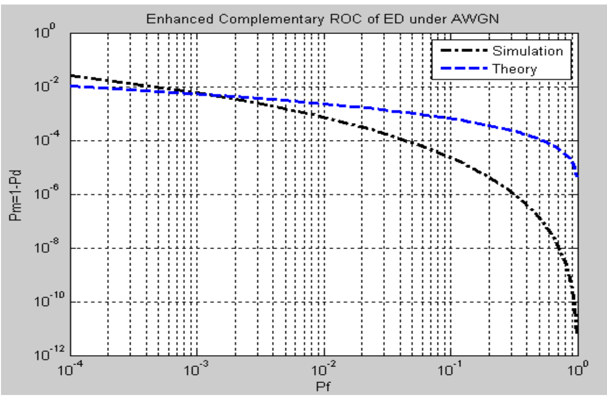


Figure 8: CROC curve for Enhanced energy

Table 5: CROC comparison table

Sample_data_3: Conventional Energy Detector for N=32

| Pf | 0.0025 | 0.0049 | 0.0081 | 0.0121 |
|---|---|---|---|---|
| Pm_Simu | 0.10523 | 0.07354 | 0.05407 | 0.04109 |
| Pm_Approxm | 0.05756 | 0.04861 | 0.04232 | 0.03754 |

Sample_data_4: Enhanced Energy Detector for N=32

| Pf | 0.0025 | 0.0049 | 0.0081 | 0.0121 |
|---|---|---|---|---|
| Pm_Simu | 0.002812 | 0.001519 | 0.000909 | 0.00058 |
| Pm_Approxm | 0.003933 | 0.003066 | 0.002504 | 0.002104 |

The CROC curve results which are depicted as Sample_data_3and Sample_data_4 in Table 5 show that for same value Pf the corresponding value of Pm is the complement of Pd on the ROC curve. Interestingly the CROC graph is an inverted version of ROC curve or it is the complement of ROC.

The values of miss detection in both samples are calculated using $P_m = 1 - P_d$. For the same value of $P_f$, if the values of Pm_Simu and Pm_Approx are compared on Sample_Data_3 and Sample_Data_4 of Table 5, the results show that Pm_Simu and Pm_Approx. in Sample_Data_4 are lower than the values in Sample_Data_3.

Thus, the insertion of adaptive Wiener filter in conventional energy detector lowers the miss detection values. Consequently, the adaptive Wiener filter in the front end of energy detector has improved the system performance of energy detector by minimizing the area under CROC curve.

## Simulation Results and Discussion for Rayleigh Channel

Based on the simulation parameters given in Table 1, this section discusses result of energy detector spectrum sensing when flat fading Rayleigh channel model is considered. Figure 9 depicts the simulation result of ROC curve of Rayleigh channel model. The plot shows the relation between the false alarm values with that of the corresponding detection probabilities value when the signal received SNR is -5dB.

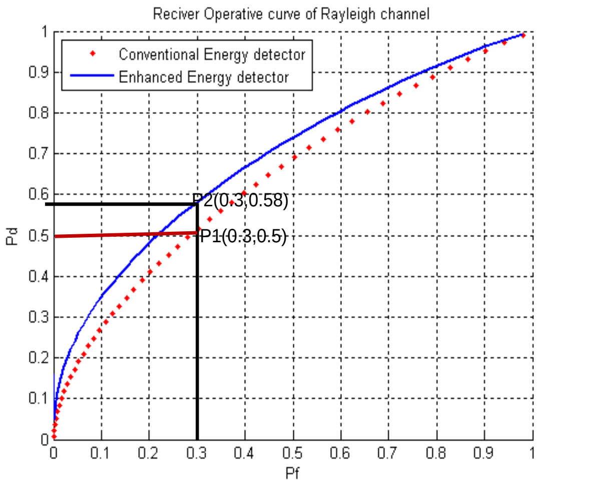


Figure 9: ROC curve for Conventional and Enhanced Energy Detector Rayleigh channel

Result shows that as the signal SNR value is increased, the detection probability values will become higher and the ROC curve achieves the maximum value of area under curve (AUC) which equal to one. Considering points P1 (0.3, 0.5) on the conventional and P2 (0.3, 0.58) on the enhanced ROC curve, one observes that for constant $P_f$ value of 0.3, point P1 corresponds to 50% of detection probability whereas point $P_2$ (for the enhanced detector), the detection probability is 58%. Moreover the area under curve obtained by enhanced curve is higher than that of area obtained from conventional detector. Thus the insertion of adaptive Wiener filter enhanced the system performance by 8 %. Accordingly the insertion of adaptive Wiener filter increases the area curve of (ROC) energy detector system.

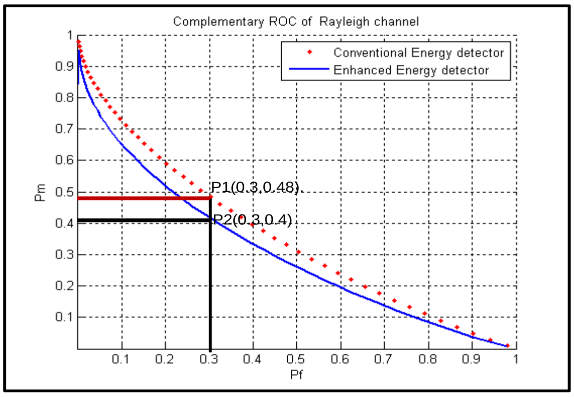


Figure 10: CROC curve for Conventional and Enhanced Energy Detector Rayleigh channel

Figure10 shows the complementary receiver operating curve (CROC) of the conventional (the broken curve) and enhanced detector (the solid curve).It shows the relation between probabilities of false alarm Vs the probability of miss detection. This graph is an inverse (complement) version of Figure 9. Generally speaking, system response (i.e, CROC) whose area under the curve is minimum as compared to others will have an improved detection performance than others. As the value of $P_f$ gets closer to 1 on the right side, the value *Pm* decreases towards 0. Considering points P1 (0.3, 0.48) and P2 (0.3, 0.40) on figure 10, the miss detection probability value is 0.48 at point P1, which is to 48% of miss detection probability. on the other hand for the enhanced detector the response at $P_f$ value of 0.3 the miss detection probability is 0.40 which is 40%. Moreover the discussion is same for all value of Pf on figure 10. Thus the insertion of adaptive Wiener filter reduces the miss detection probability value by 8%.Consequently; under constant false alarm probability value the insertion of adaptive Wiener filter in the front end of energy detector enhanced the performance of CROC by reducing the miss detection value.

## CONCLUSIONS

In this paper, the response of conventional energy detector when adaptive Wiener filter is inserted on the front end of energy detector has been analyzed. The simulation results were done for AWGN and Rayleigh fading channels. For both cases, simulation results showed that the insertion of adaptive Wiener filter on the front end of energy detector has improved all the performance metrics indicators considered in this study (i.e. ROC, CROC, threshold value, false alarm and detection probability). Moreover at lower values of signal SNR the performance of energy detector has improved.

## REFERENCES


[1] Shahzad.A, "Comparative Analysis of Primary Transmiter Detction Based Spectrum Sensing Technique in Cognitive Radio Systems," Australian Jornal Of Basic and Applied Science, vol. 4, no. 9, pp. 4522-4531, 2010.

[2] Axell E.,Leus G.,E.Larsson G. "Poor Spectrum Sensing for Cognitive Radio Sytem State of the art and Recent Advanced," IEEE Signal Processing Magazine, vol. 291, no. 3, pp. 101-116, 2012.

[3] Tevifik Yucek,Hu Seyin Arslan, "A Survey of Spectrum Sensing Algorithim for Cognitive Radio Application," IEEE Communications Survey &Tutorial, vol. 11, no. 1, pp. 116-130, Firist Quarter 2009.

[4] Communication F., "Spectrum Policy Task Force," REP.ET Docket, pp. 2-135, 2002.

[5] Akyildiz I. F. , Won-Yeol, L., C. V. Mehmet,M. Shantidev, "Next Generation Dynamic Spectrum Acess Cognitive Radio Wirless Network," A Survey Computer Networks, vol. 50, no. 2, pp. 2127-2159, 2006.

[6] Joseph.I.Mitola, "Cognitive Radio An Integrated Agent Architecture for Software Defined Radio," PhD Thesis,Royal Institute of Technology Stockholm, 2000.

[7] Mohamood A. Abdulasattar, Zahir A.Hussien, "Energy Detection Technique for Spectrum Sensining in Cognitive Radio : A Survey," International Journal Of Computer Networks & Communication(IJCNC), vol. 4, no. 5, 2012.

[8] Nisha Yadav, Uman Rathi, "Spectrum Sensing Technique: Research, Challange and Limitation," JECT, vol. 2, no. 4, 2011.

[9] Urkoitz H., "Energy Detection of Unknown Deterministic Signals," Proceedings Of IEE, vol. 55, no. 4, pp. 523-531, 1967.

[10] Murray R Spiegel ,John J. Schiller, R. Alu Srinivasan, Probability and Statistics 2nd edition ., Schaum's Outline Series.

[11] Omar Altrad ,Sami Muhidat, "A New Mathematical Analysis of the Probability of Detection in Cognitive Radio over Fading Channels," EURASIP Journal on wireless communication and Networking, vol. 159, 2013.

[12] AbhijeetA.Chincholkar,Ms.Chaitali H.Thakare Yavatmal, "Matlab implementation of Spectrum Sensing Methods in Cognitive Radio," Global Journal of Engineering Science and Research Management Chin holkar, vol. 1, no. 2, pp. 2349-4506, 2014.

[13] Fawecett T., "An Introduction to ROC Analysis," Pattern Recogntion Letters, vol. 27, pp. 861-874, 2005.

[14] Saman Atapattu, Chintha Tellambura, Hai Jiang, "Energy Detection Based Cooperative Spectrum Sensing in Cognitive Radio Networks," IEEE Transaction on Wireless Communication, vol. 10, no. 4, 2011.

[15] Fadel F. Digham, Mohamed Slim Alouini, Marvin K. Simon., "Energy Detection of Unknown Signals Over Fading Channels," IEEE Transactions on Communications, vol. 55, no. 1, pp. 21-24, 2007.